CHANDRAN, RAKKIYAPPAN, PhD. Bio-Mimetic Multimodal Nanostructured Surfaces Fabricated with Self-Assembling Biopolymer and Its Applications (2017)
Directed by Dr. Dennis R. LaJeunesse. 125 pp.

Nanotechnology will revolutionize the industrial world in 21st century. Almost every country has invested in research to unfold the mysteries of nanomaterials and for their applications. A major driving force of nanomaterial research is through the imitation of living system and materials, also known as biomimetics. Polymeric biomaterials have a critical role in the advancement of medicine and sustainable green materials. In this dissertation I demonstrate the roles that the polysaccharide biopolymer chitin has as the major structural component of the arthropod cuticle and the potential that chitin has as a versatile component to novel biomaterial applications. Chitin is a polysaccharide that is a polymer of N-acetylglucosamine, chitin is the second most abundant biopolymer on the planet and a primary component of insect, arthropod and fungal exoskeletons/cuticles. Various factors contribute to the mechanical properties of an insect cuticle including cuticle thickness and composition. In my dissertation research I have also shown that nanoscale chitin polymer alignment may be another factor that contributes to the optical, surface, and mechanical properties of a cuticle. Purified chitin self-assembles into 20 nm chitin nanofibers that serve as the foundation for all higher order chitin structures in the cuticles of insects and other arthropods via interactions with structural cuticle proteins. In addition to this I have also demonstrated that purified chitin and its deacetylated form of chitosan have great potential as a substrate for many nanofabrication technique and thus provide a new and novel material in place of traditional synthetic polymers. In my dissertation is shown that the chitin and chitosan have great potential as the substrate for

nanosphere lithography for the production of the generation of flexible antimicrobial and antifogging nanostructured surfaces. Metal nanoparticles are critical for many application and industrial processes, however the methods needed for their synthesis often are energy intensive and environmentally unfriendly. I demonstrate that chitin and chitosan are powerful tools for the green synthesis of metal nanoparticles. While arthropod cuticles are traditional examples for bio-mineralization and bio-metalization, I have found that a primary component of these process is due in fact to chitin and I use chitin to develop a novel class of composite nanomaterial which has important implications for a broad range of applications including antimicrobial surfaces, bioremediation, and cell scaffolds for biomedical engineering and regenerative medicine.

BIO-MIMETIC MULTIMODAL NANOSTRUCTURED SURFACES FABRICATED WITH SELF-ASSEMBLING BIOPOLYMER AND ITS APPLICATIONS

by

Rakkiyappan Chandran

A Dissertation Submitted to
the Faculty of The Graduate School at
The University of North Carolina at Greensboro
in Partial Fulfillment
of the Requirements for the Degree
Doctor of Philosophy

Greensboro
2017

Approved by

_____
Committee Chair

To My Family,Friends And All My Well-Wishers – Who Have Supported My Endeavours.

APPROVAL PAGE

This dissertation written by Rakkiyappan Chandran has been approved by the following committee of the Faculty of The Graduate School at The University of North Carolina at Greensboro.

Committee Chair

Dennis R. LaJeunesse

Committee Members

Daniel Herr

Jianjun Wei

Christopher Kepley

Date of Acceptance by Committee

Date of Final Oral Examination

TABLE OF CONTENTS

Page

LIST OF TABLES

Page

LIST OF FIGURES

Page

CHAPTER I

INTRODUCTION

The goal of my research was to characterize the nanoscale chitin organization in arthropod cuticles and determine the mechanisms that control self-assembly of chitin nanofibers, and how nanoscale chitin organization impacts higher order self-assembly in both natural and synthetic materials, especially in nanosale chitin-based biometalization. Long-range goals of this project are to utilize these foundational mechanisms to control and determine chitin self-assembly. This knowledge will assist the design of novel bio-materials that have nanoscale structures, which will have tailored mechanical, physical and chemical properties. These materials will have many applications especially in bio-medical industry, biosensing, and tissue engineering, and because these materials are bio-degradable and natural they will provide a new sustainable platform for the development of future advanced materials.

1.1 Why Natural Polymers for Biomimetic

The term biomimetics was coined by Otto H Schmitt and involves the study and imitation of natural methods, mechanisms and processes. Biomimetics is also known as bionics, biognosis, or biomimicry, and implements concepts and principles from nature to create new materials, devices, and systems. Biomimetics and the adaptation of methods and systems found in nature to form synthetic constructs takes advantage of millions of

years of evolution that has driven natural systems to become highly optimized and efficient in specific processes in conditions that are often less energetically costly as synthetic process. All biological system contains some form of a biopolymer. Natural polymers are abundant and have been used by mankind in various forms, such as paper and wood (i.e. cellulose) for generations. Because biological polymers are so abundant and renewable, they are economically important and because they can be grown and harvested they are environmentally and economically sustainable; however, as complex and sophisticated as these polymers have been used by man in the past, the potentials as demonstrated by their use in nature systems has not been approached.. Natural polymers are a major component of biomimetic research and have important roles in either bottom up and top down strategies for the generation of new biomaterials especially in the area of tissue engineering and regeneration (Fig 1-2).

Tissue engineering and regeneration is an interdisciplinary and multidisciplinary research field that aims at the advancement of biological substitutes to repair, maintain, or improve tissue function [1]. All biological materials have a hierarchical structure that spans from the nanoscale to the macroscale and it is this hierarchical structure that controls and determine the broad range of mechanical and physical properties of that biological material, For instance, vertebrate bone and arthropod cuticles have an amazing range of mechanical properties, possess incredible mechanical strength per density, and can self-repair [2]. One goal of biomimetic research is use this type of information about biomaterial structure to identify and develop alternatives to harvested tissues for transplantation. To accomplish the diverse needs in tissue engineering, various synthetic materials

have been exploited as scaffolds for tissue regeneration. Though certain metals are excellent choice for medical implants due to their mechanical properties, these synthetic constructs are disadvantageous for some scaffold applications because of their lack of degradability in a biological environment [3]. Synthetic and natural inorganic, ceramic materials such as hydroxyapatite or calcium phosphates have a good osteo-conductivity and are being used as a mineralized tissue engineering substrate, but still have problems due to the inability to generate these materials that into highly porous structures that also maintain mechanical integrity. The emergence of a biomimetic biopolymer technology has an enormous and immediate application in tissue regeneration. As a scaffolds made of biodegradable biopolymer will control and define the microenvironment for the differentiation of regenerative stem cells by supporting cell attachment, proliferation, and the mechanical environment of those cells.

Polymeric nanomaterials that are used in tissue regeneration and regenerative medicines are will be used in one of two distinct approaches: a bottom-up approaches that uses nanotechnology as a strong tool for synthesis of novel materials that functions differently in bulk compared with their nanoscale versions or, a top-down approach that involve nanoscale modifications of existing polymers and materials to fabricate nano-engineered systems, such as nano-patterned substrates to provide structures that influence cell behavior and subsequent tissue formation. In either approach polymeric biomaterials will play a vital role as scaffolds to stipulate three-dimensional templates and synthetic extracellular matrix (ECM) environments for tissue regeneration [4]. Further scaffolds formed by various polymers have the property that can mimic certain advantageous char-

acteristics of the natural ECM and are often beneficial for various purposes. Thus, the chemical composition, physical structure, and biologically functional moieties are all important characteristics to include in the design of new and novel biomaterials that will be used in tissue engineering. Thus, in conclusion, the polymer nano-structured biomaterials are a very breathtaking and rapidly expanding research area, and will provide new enabling technologies for various applications.

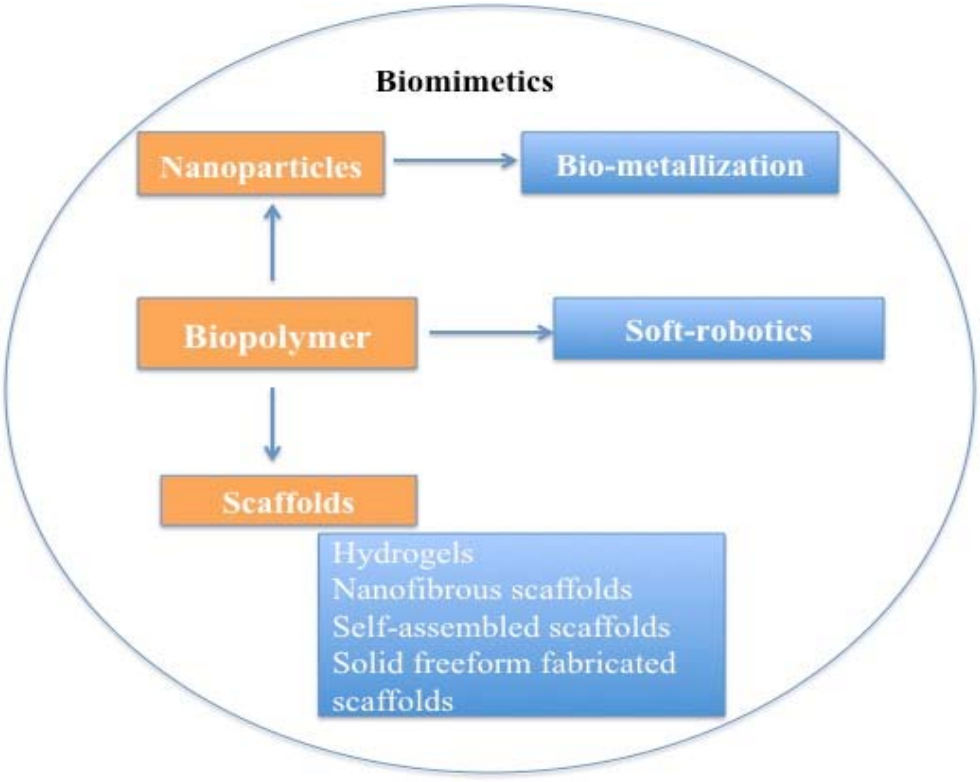

Figure 1. Schematic of Biomimetics Based on Polymer and Nanoparticles

1.2 Bottom – Up and Top – Down Approach for Biomimetic

The nanoscale topography has a significant effect on cellular behavior and tissue regeneration. The synthesis of various materials from atomic or molecular species via chemical reactions, allowing for the precursor particles to grow in size is bottom-up approach. The assembling of monomeric forms of polymer to create desired structure and the addition of inorganic nanomaterial plays a significant role in biomimetic. Biomimetic polymeric matrices should be designed to have structural similarity to native material in a nanoscale range. Thus top-down approaches involve nanoscale modifications of existing polymers and materials to imitate nano-scaled patterns that may precisely direct formation of appropriate functional material. Hence, it is required to fabricate polymeric biomaterials using nano-engineered systems. Figure 2 and 3. Shows the illustration of various bottom-up and top-down approaches used in nanotechnology [1].

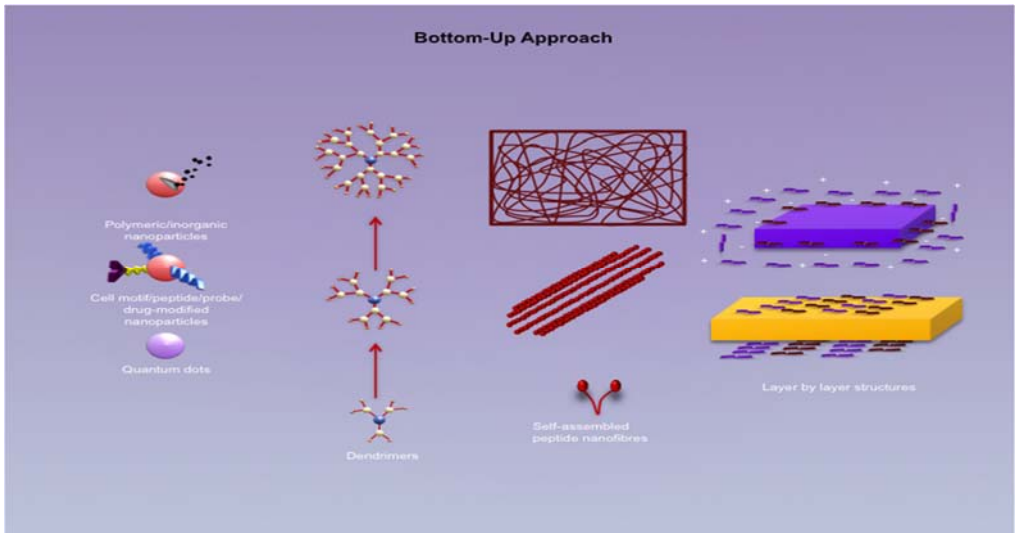

Figure 2. The Illustration Of Various Bottom-Up Nanotechnology Approaches.

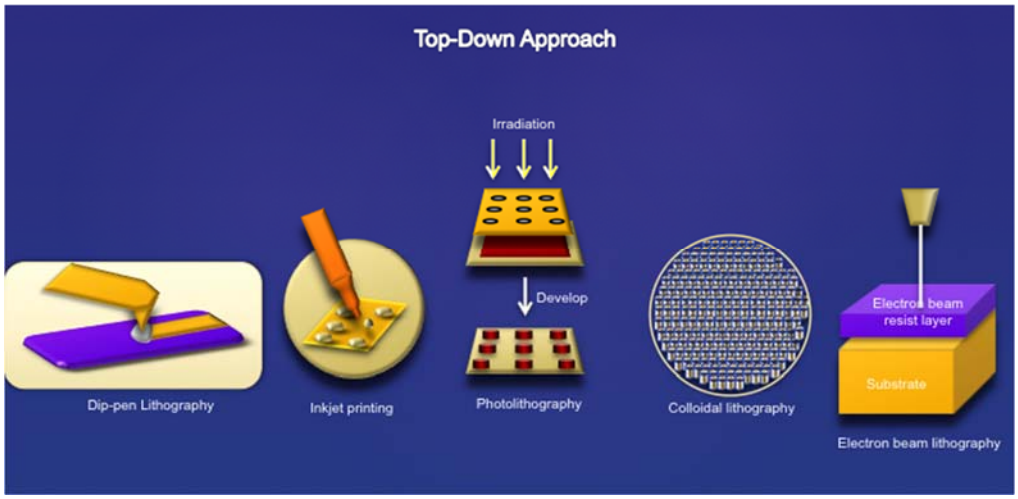

Figure 3. The Illustration of Various Top-Down Nanotechnology

CHAPTER II

LITERATURE REVIEW

2.1 Overview of Polymer Nanofibers in Arthropod Cuticle

Natural biological structural materials [5, 6] such as bone, tooth, wood, arthropod cuticle [7, 8], crustacean exoskeleton [9], and mollusk shell are inspiration for sustainable structural composites [10-12]. In these materials, the intimate assembly of biological materials creates a complex hierarchical structure that results in outstanding and sometime-unexpected mechanical and chemical properties. Among many biodegradable polymers, chitin is a biomaterial that holds enormous potential in the field of nanoscience and tissue engineering, due to a number of characteristics, including its polyelectrolyte and cationic nature, the presence of reactive groups within the polymer, high adsorption capacities, and inherent bacteriostatic and fungistatic activity. Due to these properties chitin has been used in variety of biomedical applications including wound dressing and sutures [13, 14]. Insect and arthropod cuticles are remarkable materials that play multiple critical mechanical roles in the life of an insect or crustacean and therefore, assume a variety of morphologies and configurations [15-23]. Depending on the type and function, the insect cuticle displays an extraordinarily broad range of physical and mechanical properties with some of the strongest, toughest, and hardest natural materials in the

biological world; the cuticle of some appendages like stingers and mandibles are hard, while the cuticle in the joints of the appendages or in larvae the cuticle is flexible [15, 18, 22, 24, 25]. Cuticle composed of two layers, a thin waxy water-resistant epicuticle, and an inner bilaminate procuticle which is composed of an outer exocuticle and an inner endocuticle [19-21, 24]. The exocuticle is hard and pigmented, while the endocuticle contains higher water content and is more flexible [25]. The balance between the thickness, arrangement and specific composition of the cuticular layers determines the properties of a given cuticle. Larval cuticles and other soft cuticles have a thinner, less sclerotized exocuticle, while in the cuticle of the mandibles and carapace (elytra) of beetles the exocuticle is more developed and very hard [19, 20, 22, 24]. The cuticle is a natural composite material made of chitin nanofibers embedded in a proteinaceous matrix [19]. Purified chitin self-assembles into 20 nm chitin nanofibers that serve as the foundation for all higher order chitin structures in the cuticles of insects and other arthropods via interactions with structural cuticle proteins [19]. Chitin nanofibers undergo several levels of higher reorganization and arrangement into fiber bundles and then into layers forming helicoidal stacks of material that resist stresses in all directions [19, 22, 24-26]. This organization is mediated through the activity of several chitin-binding proteins, although the exact role that each chitin binding protein plays in this organization remains unclear [27-29] and the extent of nanoscale organization of chitin in cuticular structures of insect and other arthropod exoskeletons remains unclear [27-29] and the extent of nanoscale organization of chitin in cuticular structures of insect and other arthropod exoskeletons remains unclear.

Insect and arthropod cuticles are remarkable materials that play multiple critical mechanical roles in the life of an insect or crustacean and therefore, assume a variety of morphologies and configurations [15-22]. Depending on the type and function, the insect cuticle displays an extraordinarily broad range of physical and mechanical properties with some of the strongest, toughest, and hardest natural materials in the biological world; the cuticle of some appendages like stingers and mandibles are hard, while the cuticle in the joints of the appendages or in larvae the cuticle is flexible [15, 18, 22, 24, 25]. Cuticle composed of two layers, a thin waxy water-resistant epicuticle, and an inner bilaminate procuticle which is composed of an outer exocuticle and an inner endocuticle[19-21, 24]. The exocuticle is hard and pigmented, while the endocuticle contains higher water content and is more flexible [25]. The balance between the thickness, arrangement and specific composition of the cuticular layers determines the properties of a given cuticle. Larval cuticles and other soft cuticles have a thinner, less sclerotized exocuticle, while in the cuticle of the mandibles and carapace (elytra) of beetles the exocuticle is more developed and very hard [19, 20, 22, 24]. The cuticle is a natural composite material made of chitin nanofibers embedded in a proteinaceous matrix [19]. Purified chitin self-assembles into 20 nm chitin nanofibers that serve as the foundation for all higher order chitin structures in the cuticles of insects and other arthropods via interactions with structural cuticle proteins[19]. Chitin nanofibers undergo several levels of higher reorganization and arrangement into fiber bundles and then into layers forming helicoidal stacks of material that resist stresses in all directions [19, 22, 24, 25]. This organization is mediated through the activity of several chitin-binding proteins.

2.2 Chitin/Chitosan Based Polymer for Biomimetic

Unlike many biopolymers, chitin is mechanically stable but biodegradable, non-toxic, and physiologically inert [30]. Most of the chitin (N-acetylglucosamine) containing biological materials is found in complex structural interactions between the chitin polysaccharide polymer and specific chitin binding/cuticle proteins, that define the specific properties of a cuticle structure, for instance the high strength to mass ratio of insect cuticles, crustacean shells, and mollusk nacre [31]. Despite these desirable properties, artificial bioinspired mimetic composites based on chitin nanofibers have been difficult to produce due to chitin's insolubility in most aqueous and organic solvents [32]. More work has been done with the more soluble but chemically distinct deacetylated chitin derivative, chitosan [32]. chitosan which is β-(1-4)-linked D-glucosamine (deacetylated unit) and *N*-acetyl-D-glucosamine (acetylated unit) has been used for many applications [33] . Chitosan is approved by the U.S. Food and Drug Administration (FDA) for wound dressings[34]. biocompatible, biodegradable, and non-toxic, and are anti-microbial and hydrating agents [35], Other important application of chitin/chitosan are implemented in filtration [36], Biosensors [37], Tissue engineering [38], Drug delivery [39]. In addition to its chemical composition, a major difference between chitin and chitosan is that, chitosan does not form nanofibers, because it lacks chitin's acetylamide groups that contribute to hydrogen bonding between chitin polymer chains during the chitin nanofiber self-assembly process [40]. Many researchers have strived to engineer bioinspired materials with synthetic components that reproduce the unique properties of natural structures [15], including insect cuticle [15] but it is difficult to work with chitin because of its low solu-

bility. This major difference in form between the two biopolymer suggests that control of the nanoscale organization of chitin has more potential for the development of new materials that are distinct from chitosan-based materials. Below figure 4 shows the various applications and properties of chitin/chitosan.

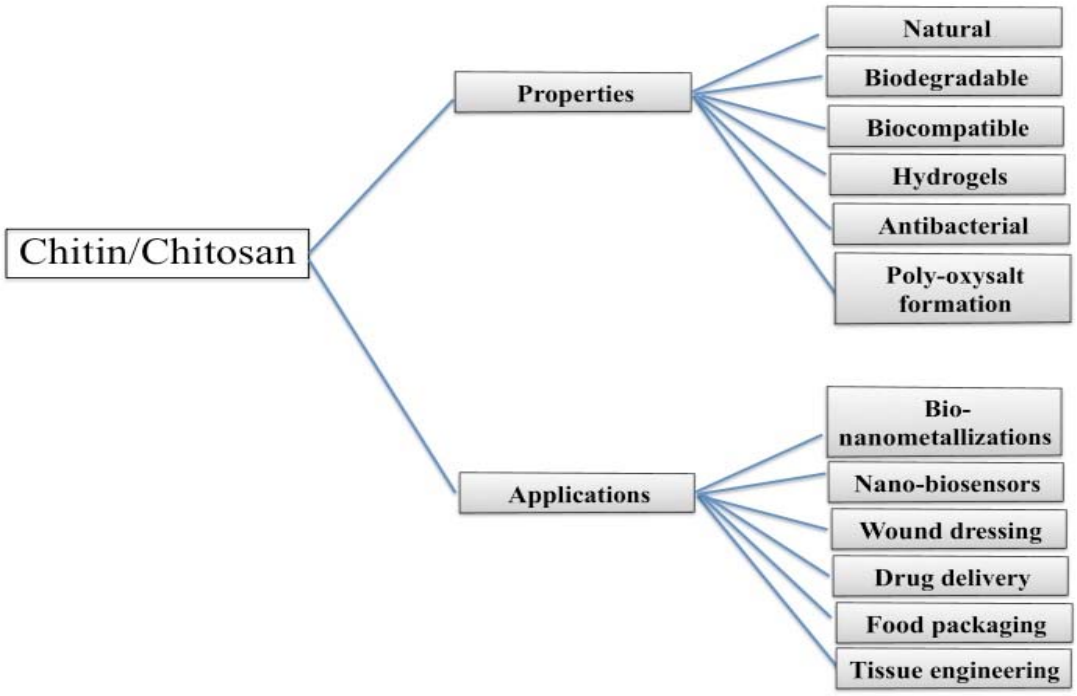

Figure 4. Various Properties And Application Of Chitin/Chitosan

2.2.1 Chemical Structure of Chitin / Chitosan

The chitin structure is composed of repeating units of N-acetyl-D-glucosamine. However, free amino groups are also present in the natural chitin material obtained through isolation processes. Chitin is considered to be a co-polymer of N-acetyl-D-glucosamine and glucosamine. When the percentage of N-acetyl-glucosamine unit in the whole polymer chain is above 50%, the material is termed chitin. Further, the structure of

chitin is similar to cellulose, except that the C2-hydroxyl group of celluloses is replaced by an acetamide group in chitin. Due to this similarity in structure, they also reflect similar roles in nature, both acting as structural materials. The presence of amino and acetamide groups in the chitin structure could be the basis for many additional substitution reactions that make chitin more promising than cellulose as a candidate for functionaling materials from nature. Figure 5. Shows the chemical structure of chitin/chitosan.

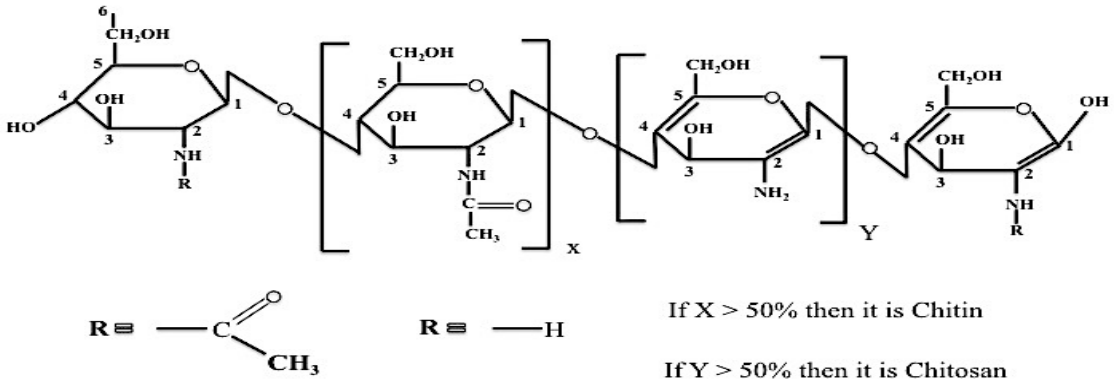

Figure 5. Chemical Structure Of Chitin/Chitosan

2.2.2 Degree of N-Acetylation (D.A.)

The Degree of Acetylation (D.A.) is defined as the percent of N-acetyl-D-glucosamine unit in the chitin polymer chain. The D.A. of commercial chitin depends on the origin of the shells and the isolation method. Most commercial chitin has a D.A. ranging between 85% and 95%. Many methods have been developed to determine the D.A. because of its great influence on the physical and chemical properties of the chitin material. The most fundamental and widely used method is elemental analysis (E.A.). Although the results are generally not precise due to the large molecular weight.

2.3 Polymer Nanofiberes Self-Assembly Mechanisms

Self-assembly is a process in which a disordered system of pre-existing components forms an organized structure as an effect of certain specific, local interactions among the components themselves, without any external directions [41]. When the constitutive components are molecules, the process is termed molecular self-assembly [41]. It can be classified as either static or dynamic. In static self-assembly, the ordered state forms as a system approaches equilibrium, reducing its free energy whereas in dynamic self-assembly, patterns of pre-existing components organized by specific local interactions are not commonly described as self-assembled but are better described as self-organized.

Molecular self-assembly takes place without guidance or management from an outside source. There are two major types of molecular self-assembly, intramolecular self-assembly and intermolecular self-assembly. Intra-molecular self-assembling molecules are often complex polymers with the ability to assemble from the random coil conformation into a well-defined stable structure (secondary and tertiary structure) [42]. Thus, molecular self-assembly is a key concept in supramolecular chemistry since assembly of the molecules is directed through non-covalent interactions (e.g., hydrogen bonding, metal coordination, hydrophobic forces, van der Waals forces, π-π interactions, and/or electrostatic as well as electromagnetic interactions).Few common examples include the formation of micelles, vesicles, liquid crystal phases, and Langmuir monolayers by surfactant molecules [41].

A self-assembling system is identified by three parts: an order systems, the interactions that control the assembly process and the components of the process. In all self-assembling systems, the final product of the self-assembled process has a higher order than the isolated components; this is true whether the product is a the process or or a structured material [41]. There is a key role of weak intermolecular interactions in all self-assembling processes; especially in biological systems, for example weak interactions control control processes like protein folding and self-assembly and structure of biological membranes. The components of a self-assemblying system span a wide range of nano and mesoscopic structures, with different chemical compositions, shapes and functionalities. Researchers have used self-assembly mechanisms in a variety of capacities including biometallization [43], RNA nanotechnology [44] , proteins [45], enzymes [46] , and metal based mesoporous materials [47], microfluidic particle crystals [48]. Self-assembled materials exist as zero, one, two and three dimensional materials. 2D self-assembled materials have been made via a range of different molecular systems that self-assemble, forming ordered, monomolecular structures by the coordination of molecules to surfaces. Self-assembled monolayers (SAMs) [49] are have been used in various technologies and the mechanism are reasonably well understood. SAMs are a molecular self-assembly that exists on the nanometer scale and are also the first of the self-assembled systems to move into technology transfer in Nanotechnology.

2.4 Layer-by-Layer Systems for Biomimetic

Langmuir–Blodgett deposition and self-assembled monolayers (SAMs) have great potential for applications in the fields of biology and medicine [50]. These techniques exhibit capability for the immobilization of proteins and cells and subsequent application in biocatalysis, drug delivery, and tissue engineering [51, 52]. However, both methods have some disadvantages: Langmuir–Blodgett deposition requires expensive instrumentation and long fabrication periods for preparation of the biomolecule films and SAMs have limited capacity for loading of biological components into the thin films and this process is compatible with limited number of substrate [52].

An alternative to Langmuir–Blodgett deposition and SAMs is layer-by-layer (LBL) assembly, which is a technique of depositing multilayers on materials surface.[53]. The preparation principles and procedures of LBL [54] assembly involves the immersion of a substrate into an oppositely charged polymer solution and alternating adsorption of complementary multivalent species onto the substrate via electrostatic interactions such as hydrogen bonding [55], covalent bond [56], charge transfer [57] or other secondary interactions.

The LBL has some advantages over other surface modification technologies such as: ease of preparation, versatility, capability of incorporating high loadings of different types of biomolecules in the films, fine control over the materials structure, and robustness of the products under ambient and physiological conditions [52]. Due to this, researchers have extended LBL assembly to include the deposition of not only water-

soluble linear charged-polymers, but also viruses, proteins, silica colloids, metal nanoparticles, dyes, metal oxides, amphiphiles, clays and polystyrene nanospheres [58]. The ability of LBL films to incorporate a broad range of drugs while retaining drug activity is particularly enabling and may open the door to new therapeutic approaches in modified implants, wound healing and remediation, cardiovascular stents, and passive or actively triggered microscale release to localized regions [59]. Recently, some authors have focus in apply this method to tissue regeneration. He et al. showed applicability of LBL assembly on surface modification of a novel biodegradable polyurethane that was synthesized with aliphatic L-lysine ethyl ester diisocyanate (LDI), poly-caprolactone diols (PCL-diol) and dianhydro-d-sorbitol (isosorbide), serving as a hard segment, soft segment and chain extender, respectively. Type I collagen and chondroitin sulfate were selected as building blocks to create a cellular microenvironment mimicking chondrogenic environment [60]. Gadiere et al. reported a unique combined effect of substrate chemistry controlled by native, non-crosslinked chondroitin sulfate A - Polycationic – polyelectrolyte multilayer films and substrate stiffness in the relevant range modelling polymeric biomaterials that are eligible for bone tissue engineering [61]. Catros et al. evaluated the influence of the three-dimensional organization of MG63 cells and PCL electrospun scaffolds on cell proliferation *in vitro* and *in vivo*, using a layer-by-layer sandwich model of assembly [62]. Figure 6. Shows the layer by layer assembly of poly cations and poly anions.

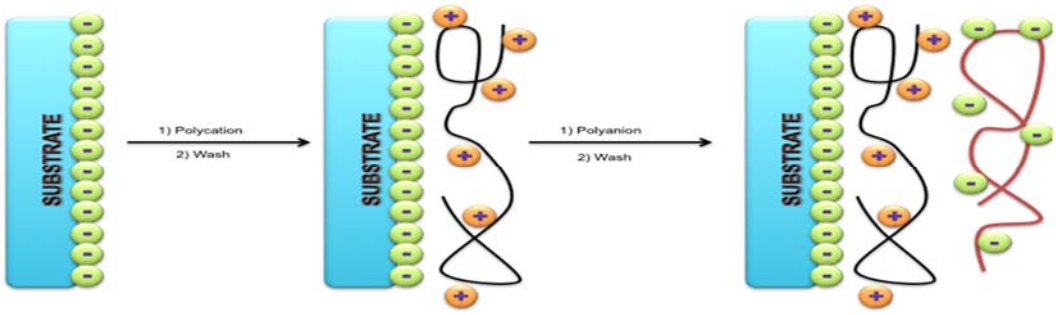

Figure 6. Layer By Layer Assembly Process of Polycations And Polyanions

2.5 Bio-Nanometallization

Polymerbased nanocomposite plays a major role in in the field of nanotechnology. Nanocomposites are hybrid materials can are defined as a two-phase system, where at least one dimension of the reinforcing filler is on the nanometre scale. Metallic nanoparticles are often incorporated in polymeric matrices to make nanocomposites scaffolds to mimic the native structure. The use of nanoparticles in a nanocomposite,especially those used in biomedical application, raises the need of a comprehensive understanding of their secondary effects and cytotoxicity [63]. The large surface area of nanoparticles makes them very reactive in the polymer. Using metal nanoparticles as additional additives in polymer matrices generates a wide range of potential applications. The efficiency and potential of the polymer nanomaterial facing the intended applications depends both on the nature of metal nanoparticle and content and on the metal particles dispersion state on to the polymer surface [64, 65]. The presence of metal nanoparticles in a sufficient

amount at the material surface will theoretically alter and define changes in the material properties of the composite such as optics/reflectivity, bactericidal properties, or barrier properties. Surface metallization of various substrates has been then accomplished and chemical, physical or sputtering deposition techniques have been widely used. Ceramic nanomaterials have been used as a major filler material to improve the characteristics of conventional polymers, such as increased modulus, strength, fracture toughness, and impact resistance [66].

The interaction between nanomaterial and polymer matrix is the basis for enhanced mechanical and functional properties of the polymers [67]. Recently, the nanocomposite approach has emerged as an efficient strategy to upgrade the structural and functional properties of synthetic polymers through the combination of polymers and organic/inorganic fillers [68]. In particular, the novel bio-nanocomposites allow both local and bulk modulation of the material mechanical properties [69, 70]. The use of nanocomposites has emerged as an efficient strategy to upgrade the structural and functional properties of natural and synthetic polymers.

Polymers nanomaterial based on its nature could be god electrical and thermal insulator or could be good conducting material, further they can be either hydrophobic or hydrophilic in nature, mechanically hard, plastic or rubbery. Depending on the nano-scale structure, metal nanoparticles have unique physical and chemical properties (optical, electronic, magnetic, catalytic and antimicrobial). Metal polymer nanocomposites not only combine the advantageous properties of metal nanoparticles and polymers but also exhibit new multifunctional and high performance polymer characteristics.

The incorporation of metal nanoparticles into polymer matrices can be achieved either by *in situ* or *ex situ* method [71-76]. Nanoparticles are first produced by the reduction of metal ions following by the distribution of the preformed metal nanoparticles into a polymer solution or monomer solution to polymerize. The *in-situ* technique involves the production of nanoparticles inside the polymer matrix. Monomers are polymerized in solution containing metal salts, then metal nanoparticles are generated by reducing metal ions through a reduction process [77]. Further, in the recent days there is a growing need to develop eco-friendly processes, which do not use toxic chemicals in the synthesis protocols. Green synthesis approaches include mixed-valence polyoxometalates, polysaccharides, tollens, biological, and irradiation method, which have advantages over conventional methods involving chemical agents associated with environmental toxicity [78]. Selection of solvent medium and selection of eco-friendly nontoxic reducing and stabilizing agents are the most important issues, which must be considered in green synthesis of NPs [79].

2.6 Synthesis of Metal Nanoparticle and Nanowires

2.6.1 Polyol Synthesis

The most common method of synthesis of metallic nanoparticles is the polyol method,which is an excellent method for the synthesis of submicrometer-sized metallic nanoparticles [80]. The polyol method mainly concerns the preparation of metallic powders by reduction of inorganic compounds in liquid polyols. It essentially applies to most of the metal precursors such has silver, god, cobalt, nickel, copper and precious metals. A

general reaction on model has been established with a reaction via the solution. Dissolution of the solid precursor, which leads to reduction in solution then homogeneous nucleation and growth of the metallic phase from the solution. The polyol method has become widely used by many research groups for the synthesis of metal nanostructures like Xia et al. and other groups synthesized Ag nanowires with higher aspects ratios by injection of ethylene glycol solutions of AgNO3 and PVP, added drop-by-drop, at a constant solution temperature of 160 °C [81, 82]. In this polyol process, the introduction of an exotic reagent is considered to be the key factor that leads to the formation of wire-like structures. In their experiments, Ag nanowires are generated using a self-seeding process and EG acts as both solvent and reducing agent. By controlling the injection rate, multiple-twined particles (MTPs) formed at the initial stage of the reduction process could serve as seeds for the subsequent growth of silver nanowires, which is the so-called self-seeding process. At a lower precursor concentration, it is possible to reduce the chemical potential to a relatively low level so as to make MTPs thermodynamically stable because it is bound almost entirely by the lower energy {111} facets. This is one of the most common methods followed by many researchers to synthesis metallic nanowires.

2.6.2 Salt Mediated Polyol Method of Synthesis

Based on the PVP (polyvinylpyrrolidone) assisted polyol method, Xia and coworkers developed a salt-mediated polyol process to prepare silver nanowires [82]. In this method, salts (NaCl, $Fe(NO)_3$, $CuCl_2$ and CuCl) play a major role in seeding and influence the morphology of the final metal products[82] . This salt-mediated synthesis

strategy is a simple and effective method for the mass synthesis of silver nanowires and nanoparticls [83]. however, the conditions for this synthesis method are somewhat energy intensive, as the process for the synthesis of silver nanowires in high yields through the reduction of $AgNO_3$ with ethylene glycerol requires heating to 148 °C in the presence of PVP and a trace amount of NaCl. Furthermore, oxygen must be removed from the reaction solution in the presence of Cl^- anions in order to obtain silver nanowires. The concentration of NaCl strongly affects the final shapes of products; low concentration of NaCl (0.12 mM) favors of the formation of cubes and bipyramids, whereas a higher concentration of 0.3 mM is the best condition for the formation of NaCl nanowires [84]. These results demonstrate the role that solvent conditions and distribution of charged groups in the solvent have in the stabilization and growth of the metal nanomaterials.

Stable silver nanoparticles were synthesized using chitosan function as both reducing and stabilizing agent without using any toxic chemicals [85]. In this synthesis like other silver nanoparticle synthesis reactions, the reaction was carried out in an autoclave at a pressure of 15 psi and 120 ^{0}C temperature. The influence of different parameters such as time, change of concentration of silver nitrate, concentration of the salts and concentration of chitosan controlled the type and crystallinity of the silver nanoparticles generated by this method [86]. Raspberry-shaped multi-hollow polymer microspheres were prepared by seeded swelling polymerization and decorated with silver nanoparticles (AgNPs) in the presence of polyvinylpyrrolidone (PVP), which acted as both reducing and stabilizing agent. The formation mechanism of the raspberry-like multi-hollow microsphere involved water absorption of sulfonated groups in the seeded swelling

polymerization (REF). Effects of weight ratio of sodium 4-vinylbenzenesulfonate to styrene (NaSS/St) of the seed particles, the concentration of PVP and $[76]^{+}$ ions on the properties of polymer/Ag nanocomposite [76].The shape and size controlled synthesis of silver nanoparticles using Aloevera plant extract and their antimicrobial activity is studied by Logaranjan K et.al. Biogenic synthesis of silver nanoparticles (AgNP) was performed at room temperature using Aloevera plant extract in the presence of ammoniacal silver nitrate as a metal salt precursor. and this method can be one of the easier ways to synthesis anisotropic AgNP, in which the plant extract plays a vital role to regulate the size and shape of the nanoparticles [87].

The synthesis of gold nanoparticles through the polymer, which play a major role in size and shape control [88-90]. Responsive polymers and polymer-coated nanoparticles have many potential bio-applications with the crucial parameter being the exact temperature where the transition occurs. Chemical modification of hydrophobic/hydrophilic or ligand binding sites has been widely explored as a tool for controlling this transition, but requires the synthesis of many different components to achieve precise control. Co-operative transitions of responsive-polymer coated gold nanoparticles and precision tuning and direct evidence for co-operative aggregation is performed. One such study reports an extensive investigation into the use of blending as a powerful tool to modulate the transition temperature of poly (*N*-isopropylacrylamide) (PNIPAM) coated gold nanoparticles. By simply mixing two nanoparticles of different compositions, precise control over the transition temperature can be imposed. This was shown to be flexible to all possible

mixing parameters (different polymers on different particles, different polymers on same particles and different sized particles with identical/different polymers)[88].

2.6.3 Seed-Mediated Growth Synthesis

The seed mediated method of synthesis of silver nanoparticles and nanowires are also been followed by many researchers.The salt of sodium and calcium etc acts as seed to support the growth of specific nanoparticles like the reduction of gold proceeds via direct reduction on the surface of seeds [91]. The large-scaled preparation of silver nanowires and nanoparticles with uniform diameter by seed-mediated growth approach in a rod-like micellar media. In principle, two steps were necessary in order to achieve the formation of nanowires. Ag nanoseeds with an average diameter of 4 nm were prepared by chemical reduction of $AgNO_3$ by $NaBH_4$ in the presence of trisodium citrate. Then $AgNO_3$ was reduced by ascorbic acid in the presence of Ag seed obtained in the first step, the micellar template cetyltrimethylammoniun bromide (CTAB), and NaOH in order to synthesize nanorods and nanowires with various aspect seed. The seed-mediated growth approach is prone to form silver nanorods and nanowires of controllable aspect ratio [92]. It is well documented that Ag nanowires were one of the earliest twinned Ag nanostructures reported and now have become an active area of research in Ag nanoparticles,although it is great challenge to achieve control over the length and width of Ag nanorods and nanowires. Seed generated silver nanorods and nanowires with pentagonal cross-section have been proposed to come from the evolvement of decahedra. Kitaev et al. has synthesized monodisperse size-controlled faceted pentagonal silver nanorods by

thermal regrowth of decahedral silver nanoparticle in aqueous solution at 95 °C, and used these Ag nanoparticles to synthesis monodisperse size-controlled faceted pentagonal silver nanorods. The width of the silver nanorods was determined by the size of the starting decahedral particle, while the length was varied from 50 nm to 2 mum by the amount of new silver added to the growth solution [93].

A facile method for the preparation of silver nanoparticles of various sizes and morphologies, including dodecahedra, nanorods, and nanoplates, has been developed [94]. This method involves using the absorbance properties of the spherical silver nanoparticles and irradiating a selected light emitting diode by which they controlled the morphology and optical properties of silver nanoparticles. These thermal routes to anisotropic AgNPs give particles with high polydispersity, limiting their applications in single molecule spectroscopy and surface plasmon resonance spectroscopy [94].

Although silver nanoparticles are commonly made via tis method, other metallic nanoparticles have also been synthesized using a seed-mediated method. Size-controlled synthesis and growth mechanism of monodisperse tellurium nanorods and size-controlled synthesis of uniform nanorods of trigonal tellurium (t-Te) by a surfactant-assisted method [95]**.** . Te-nanorods were grown from a colloidal dispersion of amorphous Te (a-Te) and t-Te nanoparticles at room temperature, which was first formed through the reduction of (NH4)2TeS4 by Na2SO3 in aqueous solution at 80 °C. Te nanorods were also obtained in mixed surfactants, where the different surfactants were used to selectively control the growth rates of different crystal planes [95]. Researchers have also synthesized metal nanoparticles having metal has a seed. Like, gold nanostars have been synthesized with a

silver seed mediated growth method. The physical, chemical and optical properties of nano-scale colloids depend on their material composition, size and shape. There is a great interest in using nano-colloids for photo-thermal ablation, drug delivery and many other biomedical applications. Gold is particularly used because of its low toxicity. The researchers have synthesized star shaped colloidal gold, also known as star shaped nanoparticles or nanostars. This method is based on a solution containing silver seeds that are used as the nucleating agent for anisotropic growth of gold colloids [96].

2.6.4 Seedless and Surfactant Assisted Synthesis

Surfactant assisted synthesis is one of the important methods for soft-template processes. Chelating-template-assisted *in situ* encapsulation of zinc ferrite inside silica mesopores for enhanced gas-sensing characteristics. A facile in situ approach has been designed to synthesize zinc ferrite/mesoporous silica guest-host composites. Chelating surfactant, N-hexadecyl ethylenediamine triacetic acid, was employed as structure-directing agent to fabricate mesoporous silica skeleton and simultaneously as complexing agent to incorporate stoichiometric amounts of zinc and iron ions into silica cavities [97]. A novel anionic surfactant-templated synthesis of ZnO/mesoporous silica nanocomposites has been carried out by using N-hexadecylethylenediamine triacetate (HED3A), a triprotic surfactant, as the structure-directing agent. In this method fabrication and photoluminescent properties of ZnO/mesoporous silica composites is templated by a chelating surfactant. Here, the variation of the zinc ion concentration in the initial template solution induces an evolution of the silica mesophase, presumably due to the change in electro-

negativity of the HED3A headgroup caused by the chelating effect [98]. Similarly, a novel one-step method for synthesis of nickel oxide/silicon dioxide (NiO/SiO(2)) mesoporous composites by using N-hexadecyl ethylenediamine triacetate (HED3A) as structure-directing agent where it play a role in directing the mesophase formation, the anionic surfactant also functions as a chelating agent that binds nickel ions. Thus, template-induced encapsulation of NiO cluster in mesoporous silica via anionic surfactant-templated route is one such research experiment where surfactant plays a major role in synthesis and stabilization [99].

2.7 Biomimetic Polymer/Apatite Composite Nanomaterials

The major inorganic component of bone mineral is a biological apatite with dimensions typically on the order of tens of nanometers in length and several nanometers wide which might be defined as non-stoichiometric and ion substituted calcium deficient HAp $Ca_{10-x}(HPO_4)_x(PO_4)_{6-x}(OH)_{2-x}$ [100].One of the main characteristics of apatites is that many ionic substitutions can occur in the crystal lattice which mean the composition of apatite in bone is not fixed and the chemical variations may occur according to the number of available elements in the body. Among the substituting ions that are found in bone, include calcium, potassium, carbonate, magnesium, strontium, chloride or fluoride [101]. Ionic substitutions changes the crystal lattice and morphology of apatites as well as physical properties as solubility, dissolution rate, hardness, brittleness, strain, and surface energy, [100]. HAp [102], $Ca_{10}(PO_4)_6(OH)_2$, has chemical similarity to the inorganic component of bone matrix and exhibits osteoconductivity, bioactivity, and biocompati-

bility with soft tissues [103]. For this reason, HAp scaffolds have been advocated for use in bone tissue engineering. The interdependence of mineral's composition, structure, and properties is particularly important in the improvement of the ceramic scaffolds. For example, it have been observed that the behavior of osteoblastic cells at the surface of HAp and carbonated apatite is greatly influenced by the polar interaction energy emphasizing the important role of surface energy for the attachment of bone cells on biomaterial [104]. It has been postulated that dimension scale of the particles and their specific topography is of great importance for the interaction with cells. Various shapes and sizes of nano-HAp have been obtained and their bioactivities are investigated. Scaffold coated with needle-shaped HAp nanoparticles showed the strongest osteoblast differentiation profile compared with rod and spherical shaped nanoparticles [105].

The excellent bioactivity of nano-HAp makes them useful as bone substitutes and coatings that promote cell adhesion and bone in-growth. Nano-HAp exhibits improved sinterability and enhanced densification due to greater surface area, which may also improve fracture toughness, as well as other mechanical properties [106]. Nano-HAp/polymer composites have beendeveloped for bone fixation and bone repairing applications with some attractive properties (large specific surface area, improved biodegradability and biological activity). Thus, the introduction of nano-HAp forming HAp/polymer greatly increased the mechanical properties of the polymer composite scaffold and improved the protein adsorption capacity [107].

Nanocomposite biomaterials play a pivotal role as scaffolds to provide three-dimensional templates and synthetic ECM environments for tissue regeneration. It is of-

ten beneficial for the scaffolds to mimic certain advantageous characteristics of the natural ECM, or developmental or repair and regeneration processes. The current biomimetic materials approach in tissue regeneration include synthesis to achieve certain compositions or properties similar to those of the ECM, novel processing technologies to achieve structural features mimicking the ECM on various levels, approaches to emulate cell-ECM interactions, and biologic delivery strategies to recapitulate a signaling cascade or developmental/wound healing program [108, 109]. The rapid restoration of tissue biomechanical function represents a great challenge, highlighting the need to mimic tissue structure and mechanical behavior through scaffold designs. For this reason, several biodegradable and bioresorbable materials, as well as technologies and scaffold designs, have been widely investigated from an experimental and/or clinical point of view [110]. It is recognized that successful biomaterials and structures for tissue engineering are those that closely mimic the composition chemistry and hierarchical structure of the native tissues to be replaced and regenerated, including the possibility of adaptation to the biological changes during the healing process, and which exhibit specific mechanical and biological functions to enable rapid new tissue regeneration. Nanocomposite 3D scaffolds based on biodegradable polymers have been developed by using different nano-structures and processing methods. These techniques mainly include solvent casting and particulate leaching, gas foaming, emulsion freeze-drying, electrospinning, rapid prototyping and thermally induced phase separation [111]. Below shows various ceramic nanomaterials and metal nanoparticles composites for various applications.

Table 1. Ceramic Nanomaterials and Metal Nanoparticles Composites for Various Applications

Nanomaterial	Chemical Formula	Composite material	Ref
Alumoxane	$[Al(O)_x(OH)_y(O_2CR)_z]_n$	PPF/PPF-DA	[112-115]
Hydroxyapatite	$Ca_{10}(OH)_2(PO_4)$	PLGA PLLA PVA PCL	[107] [116] [117] [118]
Calcium phosphates	$Ca_x(PO_4)_y$	PCL PLA PLLA/PLGA	[119] [120] [121]
Silica	SiO_2	PEG PCL PLLA	[122] [123] [124]
Silicates	SiO_4^{4-}	PEO PEG PLLA	[125] [126] [127]

DFA, dimmer fatty acid; PPF, poly (propylene fumarate); PPF-DA, propylene fumarate-diacrylate; PLLA, poly(l-lactic acid); PET, poly(ethylene terephthalate); PDLLA, poly(D,L lactid acid); PVA, polyvinyl alcohol; PEO, poly(ethylene oxide); PEG, Poly-ethylene glycol.

The interaction between nanoparticles and polymer matrix represents the basis for enhanced mechanical and functional properties of the polymers. Recently, the nanocomposite approach has emerged as an efficient strategy to upgrade the structural and functional properties of synthetic polymers, by the combination of polymers and organic/inorganic fillers. In particular, the novel bio-nanocomposites allow both local and bulk modulation of the material mechanical properties [69, 70]. The use of nanocomposites has emerged as an efficient strategy to upgrade the structural and functional properties of synthetic polymers, especially for bone tissue engineering applications. This is because bone itself is a nanocomposite with organic and inorganic phases, made up of bone-forming cells, bone resorption cells, ECM and inorganic bone mineral [128]. Various fibrous and particulate nanocarriers have been tried as scaffolds or combined with other materials such as ceramics to form nanocomposites for fulfilling the requirements of an ideal tissue-replacement support [109]. Electrospun scaffolds hold promise for the regeneration of dense connective tissues, given their nanoscale topographies, provision of directional cues for infiltrating cells and versatile composition. Synthetic slow-degrading scaffolds provide long-term mechanical support and nanoscale instructional cues; however, these scaffolds suffer from a poor infiltration rate. Alternatively, nanofibrous con-

structs formed from natural biomimetic materials (such as collagen) rapidly infiltrate but provide little mechanical support [109, 129]. Below are the few potential nanofabrication methods and its applications in tissue engineering and regeneration where polymer and metal nanoparticles play a major role.

Table 2. Few Potential Nanofabrication Methods and Its Applications in Tissue Engineering and Regeneration.

Nanofabrication process	Polymer material	Organic/Inorganic or Natural/ Synthetic	Potential application	Ref
Electro spinning	PLGA	Synthetic	Neural tissue	[130]
	PLGA/ Chitosan	Synthetic/Natural	Controlled release, Scaffolds	[131, 132]
	PLGA/elastin / gelatin	Synthetic/Natural/Natural	Vascular tissue	[133]
		Synthetic	Cartilage tissue	[134]
	PCL	Synthetic/Natural	Neural tissue	[135]

	PCL/gelatin PLLCL/collagen	Synthetic/Natural	Skin tissue	[136]
Self-assembly	Peptide Peptide Amphiphile	Synthetic Synthetic	Controlled release, neural tissue, bone tissue, Bone-tissue, vascular tissue	[137-141] [142-144]
Phase separation	PPC/chitosan PLLA	Syntetic/Natural Synthetic	Bone-tissue Neural and tendon tissue	[145] [146]

PLGA,poly(lactide-co-glycolide);PLLCL, poly(l-lactic acid)-co-poly(3-caprolactone);

PPC, poly(propylene carbonate).

CHAPTER III

SEM CHARACTERIZATION OF ANATOMICAL VARIATION IN CHITIN ORGANIZATION IN INSECT AND ARTHROPOD CUTICLES

The cuticles of insects and arthropods have some of the most diverse material properties observed in nature, so much so that it is difficult to imagine that all cutciles are primarily composed of the same two materials: a fibrous chitin network and a matrix composed of cuticle proteins. Various factors contribute to the mechanical and optical properties of an insect or arthropod cuticle including the thickness and composition. In this paper, we also identified another factor that may contribute to the optical, surface, and mechanical properties of a cuticle, i.e. the organization of chitin nanofibers and chitin fiber bundles. Self-assembled chitin nanofibers serve as the foundation for all higher order chitin structures in the cuticles of insects and other arthropods via interactions with structural cuticle proteins. Using a technique that enables the characterization of chitin organization in the cuticle of intact insects and arthropod exoskeletons, we demonstrate a structure/function correlation of chitin organization with larger scale anatomical structures. The chitin scaffolds in cuticles display an extraordinarily diverse set of morphologies that may reflect specific mechanical or physical properties. After removal of the proteinaceous and mineral matrix of a cuticle, we observe using SEM diverse nanoscale and

micro scale organization of in-situ chitin in the wing, head, eye, leg, and dorsal and ventral thoracic regions of the periodical cicada Magicicada septendecim and in other insects and arthropods. The organization of chitin also appears to have a significant role in the organization of nanoscale surface structures. While microscale bristles and hairs have long been known to be, chitin based materials formed as cellular extensions, we have found a nanostructured layer of chitin in the cuticle of the wing of the dog day annual cicada Tibicen tibicens, which may be the scaffold for the nanocone arrays found on the wing. We also use this process to examine the chitin organizations in the fruit fly, Drosophila melanogaster, and the Atlantic brown shrimp, *Farfantepenaeus aztecus*. Interestingly many of the homologous anatomical structures from diverse arthropods exhibit similar patterns of chitin organization suggesting that a common set of parameters, govern chitin organization.

3.1 Introduction

Chitin is a polymer of N-acetylglucosamine, the second most abundant biopolymer; and a primary component of insect, arthropod and fungal exoskeletons/cuticles. The insect cuticle is a natural composite material composted of a chitin network embedded in a matrix of proteins and lipids. Various factors contribute to the mechanical properties of a cuticle including the thickness and composition. In this paper we also identified another factor that may contribute to the optical, surface, and mechanical properties of a cuticle, i.e. the nanoscale organization of chitin. Purified chitin self-assembles into 20 nm chitin nanofibers that serve as the foundation for all higher order chitin structures in the

cuticles of insects and other arthropods via interactions with structural cuticle proteins. We have developed a technique that enables the characterization of chitin nanofibers organization in the cuticle of intact insects and arthropod exoskeleton that allows structure/function correlation of nanochitin organization with anatomy. Using this technique we characterize the structural organization of cuticle chitin nanofibers using FE-SEM, FTIR, and XRD, and demonstrate that the nanoscale chitin scaffolds display extraordinarily diverse morphologies that reflects a range of physical/chemical properties. After removal of the cuticles' waxy proteinaceous matrix, we observe nanoscale organization of in-situ chitin nanofibers in the wing, head, eye, leg, and dorsal and ventral thorasic regions of the periodical cicada *Magicicada septendecim.* We also use this technique to examine chitin nanostructure in other insects and arthropods finding a new conical nanochitin layer in the wing of the dog day annual cicada *Tibicen tibicen.* We also examined chitin nano cuticles of the fruit fly, Drosophula melanogaster, and the Atlantic brown shrimp*, Farfantepenaeus aztecus* and show similar patterns of chitin nanofibers organization. Flies mutant for the CPR51A gene exhibit gross defects in thoracic chitin nanofibers organization and demonstrate the role that cuticle protein contributes to this organization.

In this work I present a new technique for the *in situ* examination of nanoscale organization of cuticle chitin in the periodic Brood II seventeen year cicada *Magicicada septendecim.* We observe a broad range of chitin nanofibers organization in different cuticle structures in the periodic cicada that suggests ordering of chitin nanofibers is critical component to these structures. Moreover, this technique also has facilitate the discovery

novel chitin based structures as components of epicuticle nanoscale structures such as the nanoknobs of the noise generating tymbal membrane and conical nanoscale arrays of the wings of the dog day cicada *Tibicens tibicens*. I also show that this technique can be used to examine smaller insect cuticles and non-insect arthropods. Using this technique on the fruit fly *Drosophila melanogaster* we observe chitin nanofiber organization in the fruit fly *Drosophila melanogaster* and the Atlantic brown shrimp. In the dorsal thorax of the fruit fly and the head of the brown shrimp we observe a woven nano-chitin pattern similar to those seen in the cicadae. Moreover, the woven chitin nanofiber organization in dorsal thorax is disrupted in fruit flies mutant for the cuticle bind protein Cpr51A, which demonstrates the role that cuticle proteins play in chitin nano-fiber organization.

3.2 Methods and Materials

3.2.1 Insect and Arthropod Species Used in this Study

Insect cuticles for these experiments were from the periodic 17 year cicada Brood II *Magicicada septendecim* collected locally in Greensboro, North Carolina during the June 2013 emergence, the annual dog day cicada *Tibicens tibicens* collected locally in Greensboro, North Carolina during the summer of 2013, the fruit fly *Drosophila melanogaster*, from the Bloomington stock center, wild type strain Oregon R (Bloomington Stock Number 5) and the Cpr51A mutant strain (Bloomington Stock Number 18821) and crustacean the Atlantic brown shrimp *Farfantepenaeus aztecus* purchased at a local sea food market.

3.3 Cuticle and Bulk Chitin Preparation

Whole insects/arthropods were either left whole or dissected; wash three times in dH_2O and then processed using the following method shown in (Figure 6). Dissected parts where subjected to an acid wash treatment in 1M HCL overnight at 65^0C in test tubes, followed by a basic wash treatment of 1M NaOH solution and place them into oven at 65 ^{0}C, overnight. The samples were dehydrated in an ethanol series 20%, 50% 70% 84%, 90%, 95% for 10-15 minutes and into 100% ethanol overnight and then allowed the solvent to evaporate. For bulk chitin preparations used to control for purity of *in situ* chitin preparations. Whole insects were powdered in a mortar and pestle in ethanol slurry. The crude powdered cuticle was dried overnight at 70º C. The cuticle powder processed as described above for the *in-situ* chitin cuticle prep with centrifugation/ washes after acid and basic treatments. After the final wash, the purified chitin cuticles and lyophilized chitin powder analyzed by FT-IR and X-Ray Diffraction and compared to commercially purchased chitin (Sigma, C9752) as a control.

3.4 SEM/EDS Imaging SEM Sample Preparation

Samples (either the prepared or native cuticles) were washed three times in dH2O. After drying, the samples had a 10 nm gold layer applied using a Leica EM ACE200 with real time thickness monitoring using a quartz crystal microbalance (QCM). Scanning electron micrographs were obtained using a Zeiss Auriga FIB/SEM. Scale bars were added using ImageJ software. Scanning electron-microscopy (SEM) combined with energy

dispersive X-ray spectroscopy (EDS) analysis was used to morphologically and chemically characterize the cicada wings using an electron beam of 7.0 KV.

3.5 Quantifying Alignment with Image J Oval Profile Plugin

SEM micrographs, 1024 X 768 pixels, were sub-divided to five sections of 250 X 250 pixels. A Fast Fourier Transform (FFT) was performed on each sub-division of the image to render a frequency domain image. An oval selection of radius 50 pixels was then used to select the central region of the FFT image. The oval profile was plotted using a division of n = 360 and "Radial Sums" plotting mode. The sums are taken about a 180-degree section of the oval selection, since the fibers can be approximated at straight.

3.6 Results

3.6.1 *In Situ* Chitin Purification

Chitin is a major structural component of insect and arthropod and observing its organization within the cuticle is challenged by the lack or reagents to directly label chitin at the ultramicroscopic level. Historically chitin has been observed in cuticles via TEM by negative permanent stain of the surrounding matrix, and some SEM imaging of chitinaceous structures has been performed in large crustaceans to characterize large scale chitin organization[147], however little work has been done to detect and characterize nanoscale chitin organization. Industrial preparation of chitin involves acidic treatments to demineralize and deproteinate followed basic treatments to remove more protein and lipid cuticle components [148-150]. We have modified this preparation to generate a

simple and fast technique that enables the preservation of nanoscale chitin structure in the context of gross anatomy (Figure 7). The process results in a clear, structurally intact exoskeleton exact that is devoid of pigments (compare Figure 7B with 7C). The chitin within the cuticle displays a purity that is comparable to commercial available chitin samples and bulk preparations as determined by Fourier transform infrared spectroscopy).

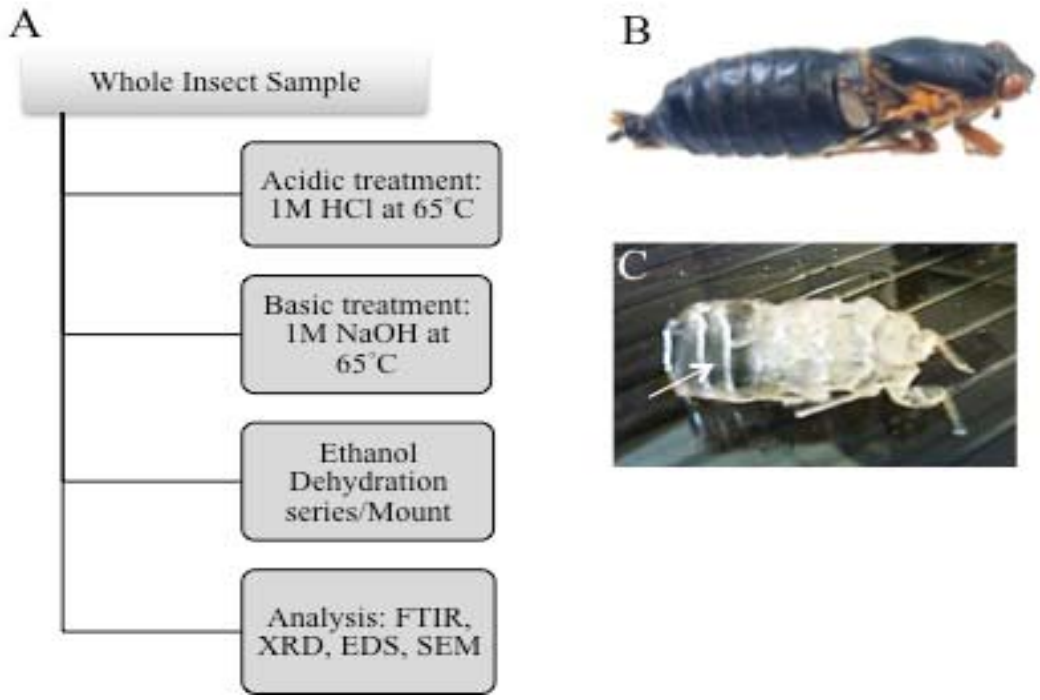

Figure 7. Schematic of in situ Cuticle Chitin Preparation.

A) A flow chart outlining the steps in the process as used in this publication. B) Whole cuticle of the periodic cicada *Magicicada septendecim* prior to the procedure (note: wings have been removed). C) The thoracic and abdominal section of the period cicada after in situ chitin preparation, note the preservation of the overall anatomy but the lack of pigment and the cleared portions of the cuticle (arrow).

FTIR analysis of chitin samples show a similar set of characteristic peaks that are indicative of bond stretching within the chitin monomer. In all sample we observed the characteristic transmission peaks that represent the amide bonds of chitin Amide I ($_{C=O}$) at 1660 and 1627, Amide II ($_{C-N}$) at 1558 and amide III ($_{C-N}$) at 1312; the amide absorbance at 1660/1627 demonstrate differences in hydrogen bonding within the chitin show that the chitin present is alpha [151]. The transmission peaks between 3102 to 3400 cm-^{1} also show a pattern similar to alpha chitin with strong transmission for hydroxyl groups ($_{OH}$) at □3479 and □ 3448 and amines ($^{as}_{NH}$ and $^{s}_{NH)}$ respectively (Figure 8)[151].

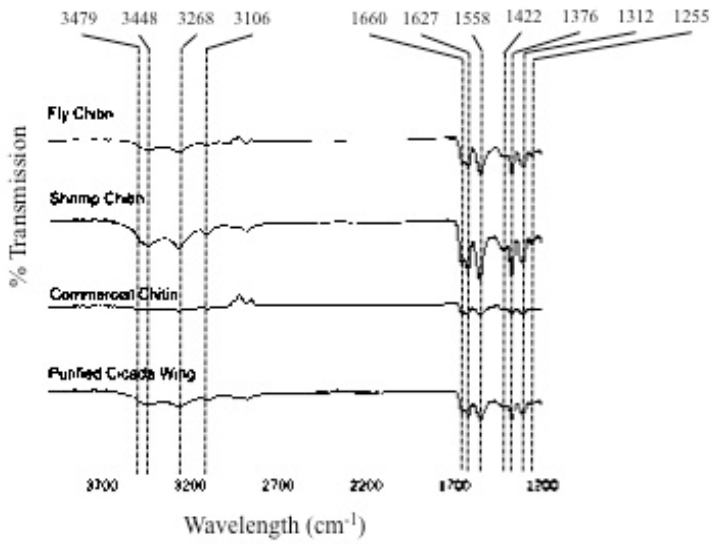

Figure 8. FTIR Analysis of Chitin Samples.

FT-IR data was collected to compare and contrast the quality of chitin obtained from different sources. Similar transmission profiles from all samples demonstrating the presence of characteristic transmission peaks for vibrational information at hydroxyl bonds □3479 and □3426, amines □3290 and □3106 as well as hydrogen bonding in am-

ides □1660, □1627 (Amide I), □1558 (Amide II) and □1312 Amide III. Demonstrates that the in-situ chitin preparation results in an alpha type chitin with structure and purity to other bulk chitin preparation both in house and commercially available.

XRD analysis of chitin samples also demonstrates that the predominance of purified alpha chitin all samples with 2□ degrees peaks at 9.2° signifying the (020) crystal lattice, 12.7° signifying the (101) lattice, 19.1° signifying the (040) and (110) lattices, a minor bump at 23.2° denoting the (130) lattice, a 2□ peak at 26.1 denoting the (013) lattice (Figure 9) [151]. The EDX study of cicada wing was based on selecting characteristic elements of interest such as (C, O and Ca). There was a reduction in the quantity of calcium content (Ca) after the chitin purification process.

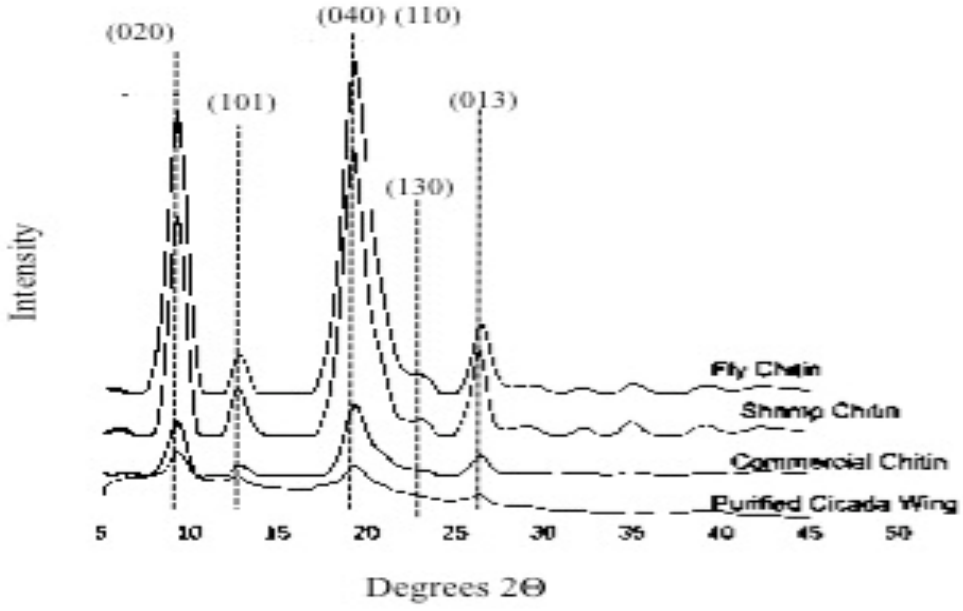

Figure 9. XRD Analysis of Different Chitin Samples.

XRD also shows a pattern of 2Q degrees and crystallinity similar to previously described alpha type chitins 2□ degrees peaks at 9.2°, (020) crystal lattice, 12.7°, (101) lattice, 19.1°, (040) and(110) lattices;, a minor bump at 23.2° for the (130) lattice, a 2^0 peak at 26.1 denoting the (013) lattice. The chitin profile from the *in-situ* cicada wings which contains significantly less material but similar arrangement of peaks.

3.6.2 Differential Chitin Nanofibers Organization in Cicada

Using this technique, we examine the cuticle of the periodic cicada using SEM before and after cuticle extraction. The results show striking diversity in the organization nanofibers chitin in the cuticle that is characteristic to specific anatomical structures with some structures, e.g. dorsal thorax and leg, having very organized chitin nanofibers while others displaying less, e.g. wing and eye (Table 3; Figure 10). We observe highly organized chitin nanofibers in the dorsal thorax (Figure 10A), the head (Figure 10B) and the femur of the foreleg (Figure 10C) of the periodic cicada; while the nanochitin in the eye (Figure 10D) and wing blade are less organized.This organization is distinct in each of these areas and can be quantified as the deviation from the mean and the radial sums of the after a FFT analysis using the ImageJ Oval Profile Plugin (ref; Table 3).

Table 3. Chitin Nanofibers Alignment in Different Anatomical Structures

Structure	**# Images (n)**	**Deviation from high mean angle**	**Difference in Radial Sums**	**Alignment**	**Alignment relative to A/P body**

		direction			axis*
Wing	5	±36.23	211.82	Low/no alignment*	NA
Dorsal head	5	±6.12	685.12	Highly Aligned**	orthogonal
Dorsal Thorax	5	±6.66	850.26	Highly Aligned**	orthogonal
Eye	5	±58.25	247.44	Low/non Aligned**	NA
Femur	5	±12.12	459.02	Aligned*	parallel

*Proximal/distal axis for leg and wing ** anterior/posterior

In general, the more organized the chitin nanofibers network, the lower the standard deviation from the mean high angle was determined for each image (n=5) and the smaller the difference in the radial sums after FTT. The magnitude of alignment can be determined by the difference between the maximum radial sum value and the minimum radial sum value.

Beyond the general organization, there are qualitative differences in chitin nanofibers patterns. The dorsal thorax of the periodic cicada is composed of a finely woven pattern of nanofibers that form braids of material (Figure 10A, thin arrows) that are

roughly parallel to the body anterior/posterior body axis (Figure 10A, double headed arrow).

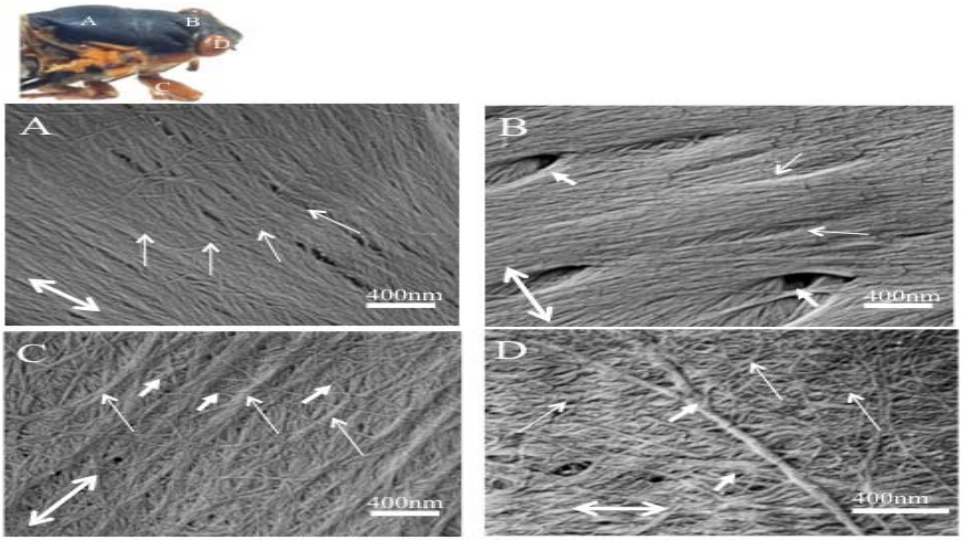

Figure 10. Anatomical Variation of 20nm Chitin Nanofiber Organization.

The image of the cicada in the upper left hand portion depicts the location of each high imagination image.

A) Dorsal thorax, the nanoscale fiber bundles are "woven' into larger organization that is directly aligned with the body axis (small arrows) thick; double headed arrow showing the orientation of the image relative to the anterior/posterior body axis; scale bar 400nm.
B) Dorsal Head region between the eyes, nanoscale fibers are also organized into higher order structures that are thicker than that seen in the dorsal thorax (thin arrows), oval voids in this organized chitin are also present (thick short arrows),

however this organization is somewhat orthogonal to the main anterior/posterior body axis - double headed arrow showing anterior/posterior body axis; scale bar 400nm.

C) Foreleg femur segment, nanoscale order of the chitin is represented by thicker tightly organized bundles of chitin (50nm-100nm wide; thin arrows) that are cross-linked to one another (thick arrow) and that align along the length of the leg, double headed arrow showing proximal/distal axis of leg with the proximal towards the upper right; scale bar 400nm.

D) Eye, the chitin underlying the eye of the periodic cicada is organized along any axid and exhibits a net-work of thin nanoscale chitin fibers (thin arrows), that are sometimes punctuated by thicker filaments (thick arrow); double headed arrow showing proximal/distal axis of leg with the proximal towards the upper right; scale bar 400nm.

The region of the head of the periodic cicada between the eyes although composed of the same 20nm chitin nanofibers has a thicker “braid (Figure 10B, thin arrows) that is orthogonal to the same anterior/posterior body axis (Figure 10B, double headed arrow) and which has a series of oval voids ranging in size from 100-150nm in width. In the femur of the foreleg of the periodic cicada, exhibits an entirely different pattern of chitin nanofibers (Figure 10C) in which thicker band of chitin nanofibers (Figure 10C, thin arrows), which extend along the length of the leg (Figure 10C, double headed arrow) are connected by thinner fibers (Figure 10C, thick arrows). However, some anatomical

structures exhibit little or no directionality to the chitin nanofiber organization. The cuticle in the eyes has a majority of the chitin nanofibers organized in an evenly distributed (Figure 10D, thin arrows) with an occasional thick fiber (Figure 10D, thick arrow).

3.6.3 Epicuticle Organization and Nanoscale Chitin

The nanochitin organization in the cuticle features does not necessarily reflect the distribution of epicuticle nanoscale structures as shown in figure 11. The cicada eye has a defined nanostructured surface with hemispherical/conical structures that resemble other insect (Figure 11A) but do not show any relationship to the nanoscale chitin (Figure 10D). Moreover, the surface of the foreleg femur of the periodic cicada is decorated by nanoscale pits (Figure 11D) that do not follow the same distal to proximal alignment as the nanoscale chitin fiber (Figure 10B).

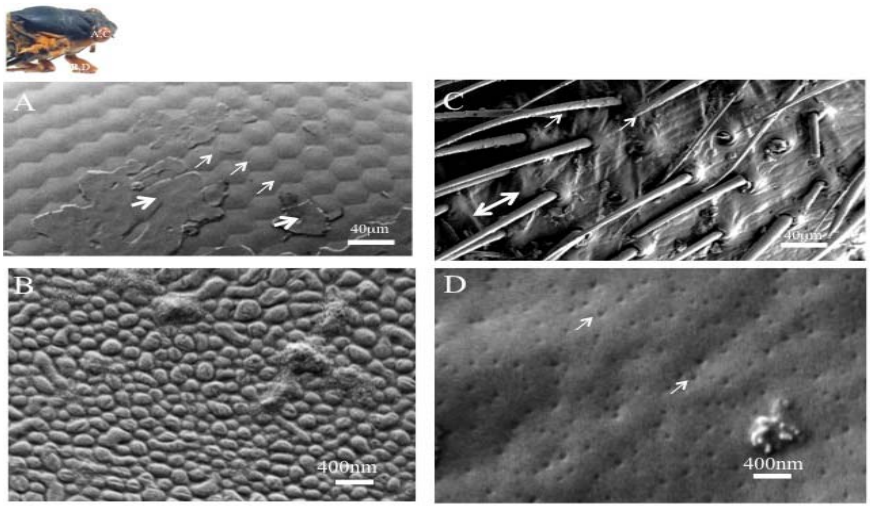

Figure 11. Epicuticle Nanoscale Structures of the Eye and Leg from Periodic Cicada.

Magicicada septendecim. A, B) compound eye; C, D) leg. A and B) low magnification images, scale bar 40□m; C,D) high magnification images, scale bar 400nm. A) The compound eye of *Magicicada septendecim* is composed of hexagonal ommatidia (thin arrows) and a thin layer of electron desne material that obscure some of the ommatidia (thick arrow). B) high magnification of the surface of the ommatidia reveals a field of irregular low aspect ratio structures (thin arrows) that vary in shaped and size, scale bar 400nm; C) a low magnification image of the femur of the foreleg showing bristles (thin arrows) oriented and aligned along the distal/proximal axis (double headed arrow, distal toward lower left corner), the sockets of damaged bristles are also present (thick arrow), scale bar 40mm; D) high magnification of the area between bristles shows a field of fine 50-70nm pits (thin arrows), scale bar 400nm.

However, some nanoscale epicuticle structures have a chitin nanofibers basis. Cicada wings have well characterized arrays of conical nanostructures that vary in size, shape and distribution from species to species and which control the optical and surface chemistry properties of the wing's surface ([152-154]). The surface of the periodic cicada wing is covered with low aspect round hemispherical cones (Figure 12C), while the wings of the dog day cicada (*Tibicens tibicens*) has a nanostructured surface that is composed of higher aspect ratio nanocones (Figure 12B)[154].

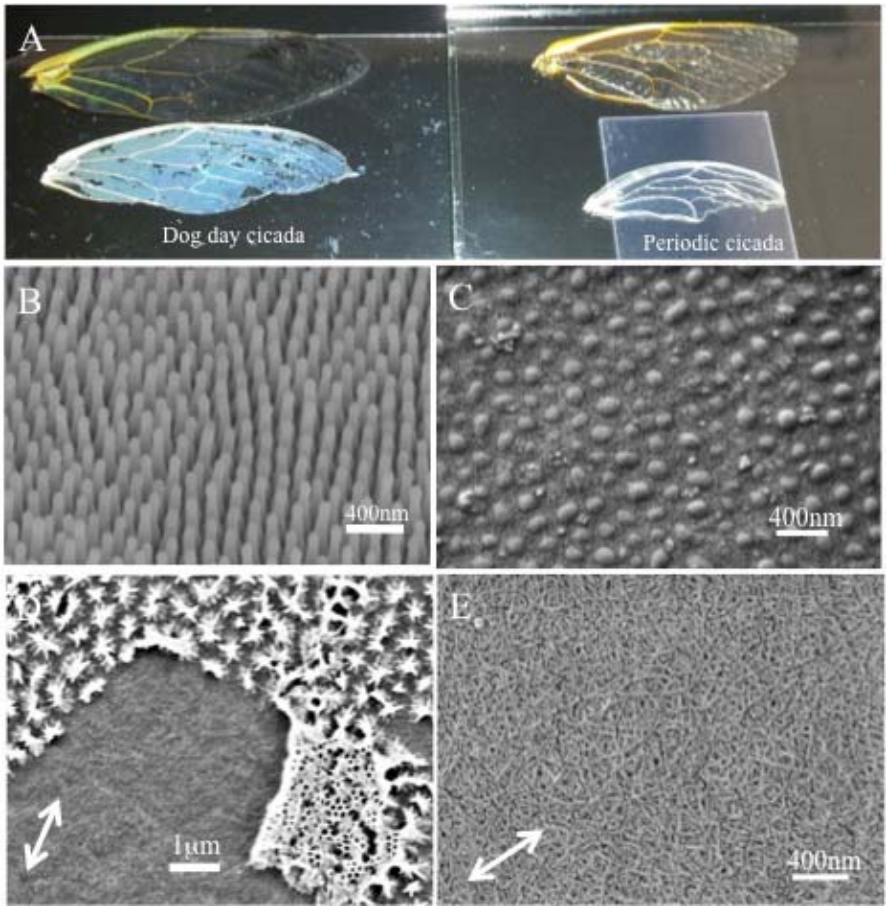

Figure 12. Comparison of Chitin Nanoscale Organization in Periodic and Annual Cicada Wing.

A) Images of whole cicada wing before and after protein/lipid extraction. On the left are the wings of the annual dog day cicada (*Tibicen tibicen)*, top unprepared wing distinguished by a flat//nonglossy appearance and the brown/yellow pigmentation in the vein material; directly below is a prepared wing exhibiting a loss of pigmentation in the vein material and a bluish cast to the intervein space (arrow), not the fine areas without bluish cast (thin arrow). On the right are wing from the periodic cicada *Magicicada septendecim,* note the glossy/shiny appearance of the wing and yellow/orange pigmentation

in the vein, directly below is a prepared wing exhibiting loss of pigment and clear/non-shiny intervein material. B) high magnification micrograph of the unprepared dog day cicada wing which exhibits an array of nanocones, scale bar 400nm; C) high magnification micrograph of the unprepared periodic wing showing irregular low aspect ratio hemispherical nanoscale structures, scale bar 400nm; D) high magnification micrograph of a prepared dog day cicada wing from a region in which the bluish cast is broken. The area has two layers a top layer with conical chitin structures (thin arrows) and a base layer that exhibits a meshwork of chitin nanofibers (asterisk), scale bar 1 □m; E) a highmagnification micrograph of a periodic cicada wing has no nano-conical chitin layer, only the mesh work of chitin nanofibers; double headed arrow shows postion relative to proximal/distal axis of the wing, distal towards the upper right; scale bar 400nm.

We have found that the underlying structure of the high aspect ratio nanocone array is due to the presence of a thin layer which contains chitinous nanoscale cones (Figure 12D, thin arrows) that sits on top of an underlying cuticle nanochitin layer (Figure 12D, asterisk), which is similar in organization and structure to that of the periodic cicada (Figure 12E). This layer is tangible at the macroscopic level during the chitin preparation. After the preparation, dog day cicada wing have a bluish/white layer in the intervein regions of the wing (Figure 12A, arrow), this layer fractures and floats off the wing during the preparation.

3.6.4 Tymbal Membrane Contains Elaborate Nanoscale Structures

We observe a similar connection between epicuticle nanoscale structures and chitin nanoscale organization in the tymbal membrane. The tymbal membrane is the primary component of the sonic apparatus of the cicada and is located at the junction of the abdomen and the thorax (Figure 13A, arrow, 13B close-up). The tymbal membrane is a thin, ribbed structure. Low power characterization of the surface of the tymbal membrane reveals a netted pattern across the surface of the tymbal ribs (Figure 13C, arrow). More detailed inspection of this netter pattern reveals a distinct nanoscale arrangement of nano-knobs or pegs, one connected set that generates the network proper (Figure 13D, thin arrows) which than surrounds another independent set of non-connected knobs (Figure 13D, thick arrow). Further inspect shows that the nanoscale knobs that compose the netted areas reside on a ridge (Figure 13E, thin arrows), while the nested nanoscale knobs are a clustered, non-connected ridge (Figure 13E, thick arrow). The pegs themselves are 400nm wide structures (Figure 13F, arrow).

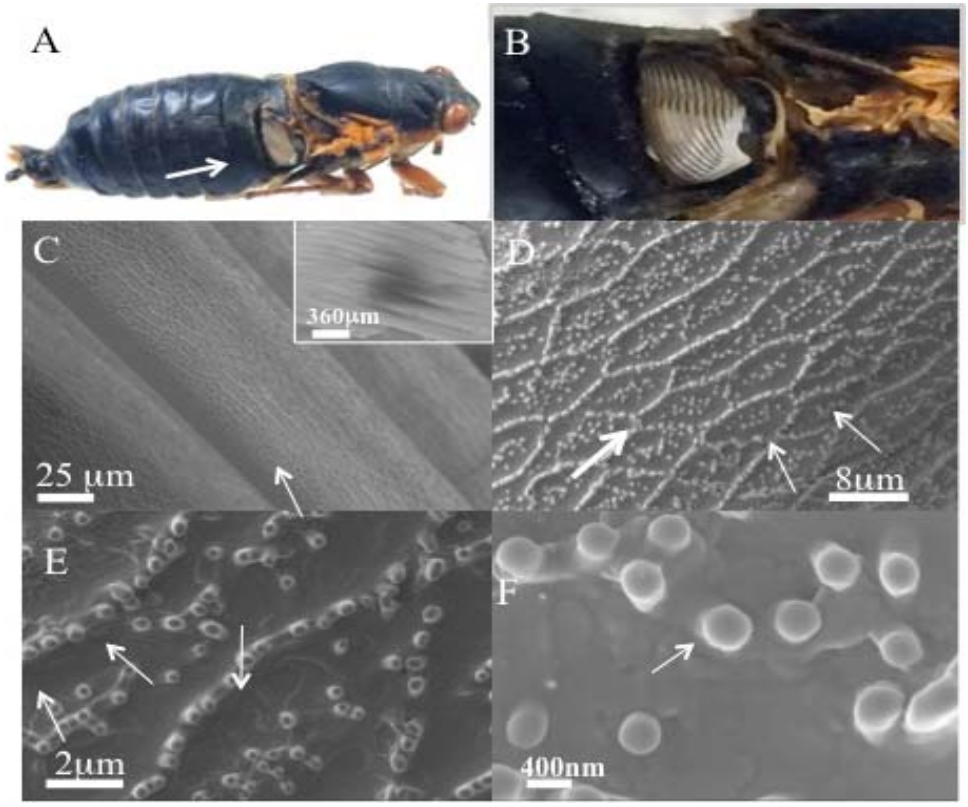

Figure 13. Nanoscale Surface Structures on the Tymbal Membrane of the Periodic Cicada.

Magicicada septendecim. A) photograph of an intact (minus wings) periodic cicada indicating the location of the tymbal membrane (arrow). B) A more detailed image of the tymbal membrane in situ within the upper abdomen of the cicada. C) low magnification SEM micrograph of the tymbal membrane, showing the striated band structure of the tissue and the netted/patterned structure of its surface (arrow), scale bar 25□m; inset, a lower magnification SEM of the entire tymbal membrane, scale bar 360□m; D) higher magnification of the netted patterned surface which is composed of both connected lattices (thin arrows) that enclose unconnected punctate knob nanostructures (thick arrow, scale

bar 8□m; E) detail of an individual netted cell of this pattern showing a combination of nano pegs and knobs some incorporated into ridges that generate the closed cells (thin arrows) and other independent peg (thick arrows), scale bar 2□m; E) high magnification SEM micrograph of a cluster of 400nm nanoknobs (thin arrow), scale bar 400nm.

After, the chitin preparation/removal of the netted surface figure 14A, a underlying pattern of nanochitin that shows some directional organization along the length of the tymbal ribs is apparent (Figure 14B, thin arrows), as well as larger thicker chitin fiber connections between the highpoints of the ribs (Figure 13, asterisk) and the lower inter-rib areas (Figure 14B, thick arrow). Chitin nano-balls appear as small flecks at low magnification (Figure 14B) are revealed across the surface of the chitin network of the tymbal membrane (Figure 14C thin arrows); these structures are between 80-100nm in diameter and may be the basis for the nano-knob structures observed on the native tymbal surface.

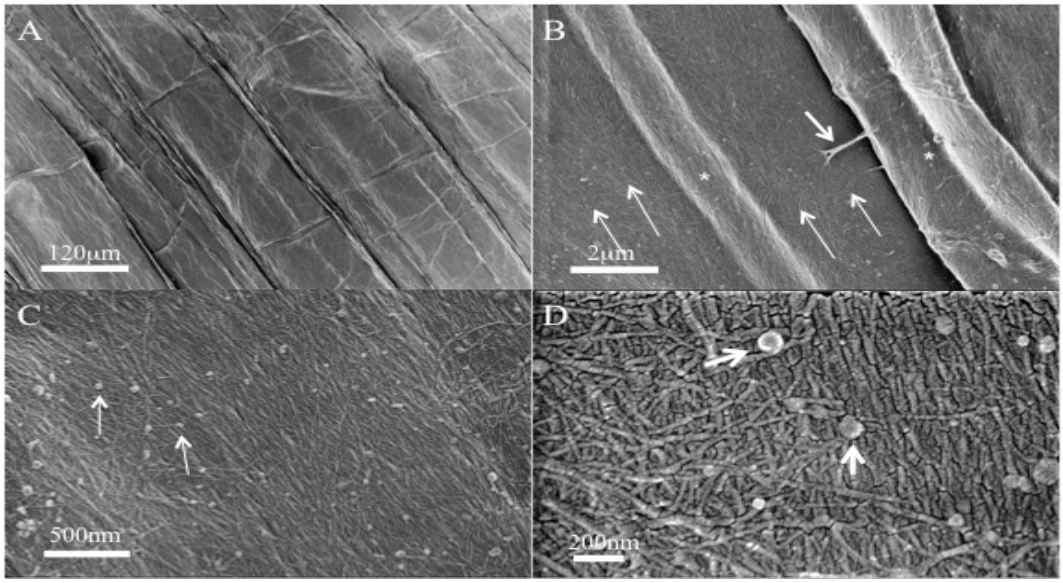

Figure 14. Chitin Nanofiber Organization in Tymbal Membrane of the Periodic Cicada. *Magicicada septendecim.*

A) low magnification SEM of the tymbal membrane surface after the extraction of protein and lipids. A similar pattern of rib structures is clear preserved (arrows), scale bar 120□m; B) higher magnification SEM micrograph of a rib from a tymbal membrane chitin preparation, a disorganized matrix of nano-chitin is found both on the ribs (asterisks) and the inter-rib surfaces (thin arrows), occasionally thicker chitin fibers extend from the rib to the inter-rib surface (thick arrow), scale bar 2□m; C) At higher magnifcations round chitin balls litter the surface of the tymbal chitin surface (thin arrows), scale bar 500nm; D) detail of the 50-100nm chitin balls (thick arrows) on the surface of the tymbal membrane, scale bar 200nm.

3.6.5 Local Variation in Chitin Nano Fiber Organization

Chitin nanofiber organized can be locally complex. Within the socket region of a dorsal thoracic bristle from the periodic cicada, we observed several distinct patterns of chitin nanofibers (Figure 15A). The outer rim of the bristle socket as a cross-linked, even arrangement of chitin nanofibers (Figure 15B); we observed highly aligned fibers along the length of the bristle (Figure 15C); and within the bristle socket we observe a network of thicker chitin nanofibers (Figure 15D).

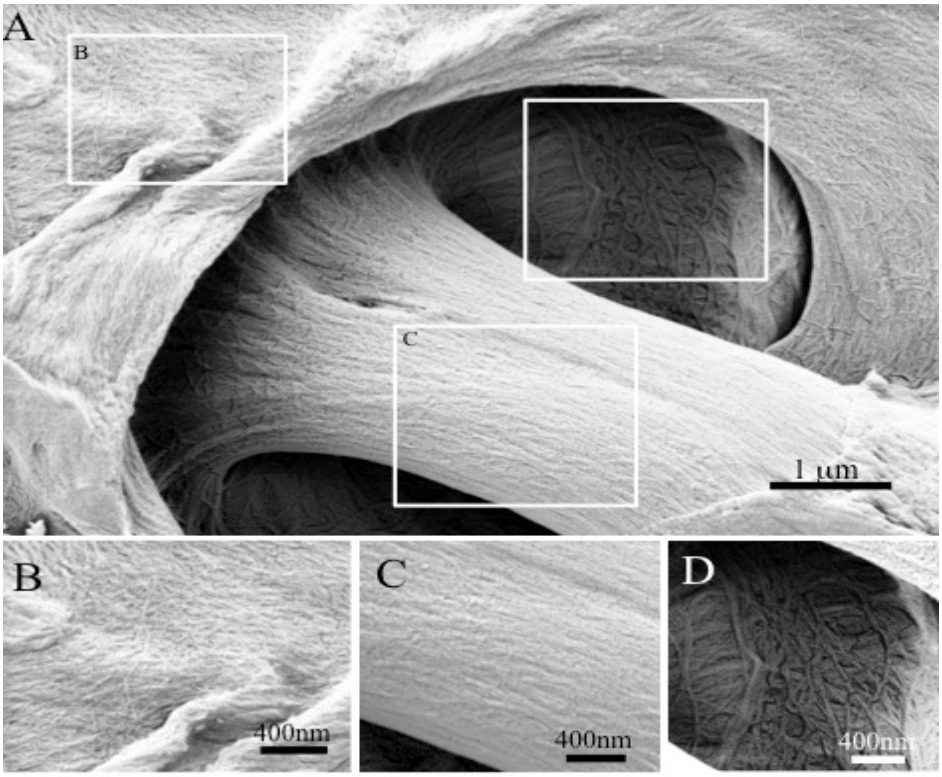

Figure 15. Local Variation of Chitin Nanofiber Organization in Dorsal Thoracic Bristle.

A) An SEM micrograph of a dorsal thoracic bristle in socket after in situ cuticle chitin preparation; inset show different local organizations of surface chitin nanofibers; scale bar 1mm; B) a detail of the lip of the socket region exhibiting a matted meshwork of chitin nanofibers, scale bar 400nm; C) chitin in the bristle proper showing alignment of the fibers along the length of the bristle, scale bare 400nm; D) inside the socket chitin nanofibers are thicker and have a more woven appearance, scale bar 400nm.

3.6.6 Chitin Nanofibers Organization in Insects and Arthropods

To determine whether this technique could be used to study smaller insects or other arthropods such as crustaceans, we used it to determine the in situ organization of chitin nanofibers in the fruit fly Drosophila melanogaster, a tiny insect several millimeters long, and the Atlantic brown shrimp, *Farfantepenaeus aztecus.* We found that the technique worked regardless of the size of the organism. We found that the wing of *Drosophila melanogaster* had a virtually identical pattern of nanoscale chitin as the wing of the period cicada and the sub-wing of the Dog day cicada (Figure 16A).

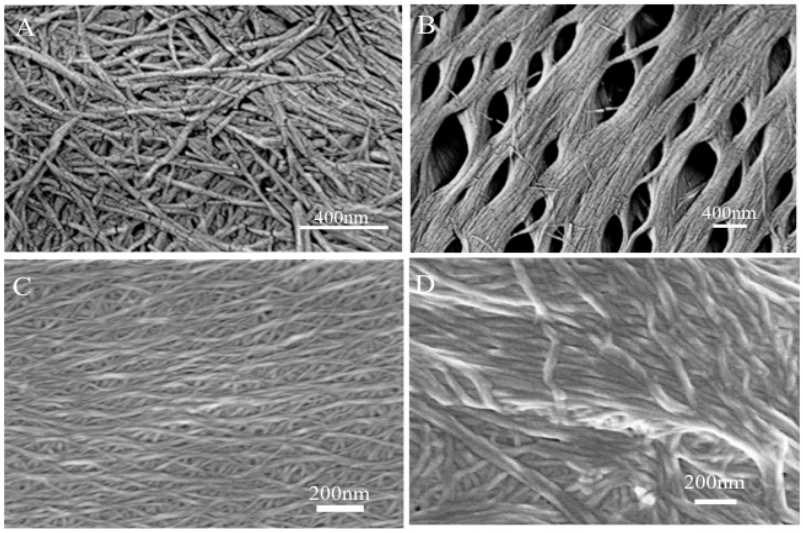

Figure 16. Nanoscale Chitin Organization in the Wing of the Fruit Fly

Drosophila Melanogasterand the head of the atlanitic brown shrimp (Farfantepenaeus Aztecus).A) 20nm chitin nanofibers organization in the wing of the fruit fly Drosophila melanogaster shows a similar network to that found in the wings of cicada, scale bar 400nm; B) Chitin nanofibers in the shrimp head has a similar woven pattern to that of the head and thorax of the cicada, large holes separate the woven chitin fibers (arrows); scale bar 400nm. C) nanoscale Chitin organization from the dorsal thorax of the fruit sly exhibiting a tight weave or chitin nanofibers, scale bar 200nm; D) nanoscale chitin organization from the dorsal thorax of a fruit fly homozygous mutant for the chitin binding protein CPR51A show a thicker chitin fibers and reduced organization, scale bar 200nm.

Moreover, the head of the shrimp *Farfantepenaeus aztecus* exhibited morphology similar to the head of the periodic cicada, showing thick braids of chitin nanofibers that are interspersed with oval voids, although the number of these voids is larger in the shrimp (Figure 16B, arrow). We also used this opportunity to examine the several strains

of Drosophila that were mutant for genes that encoded putative cuticle binding proteins. In this small candidate gene screen we found that one, Cpr51A, expressed a disrupted nano-chitin morphology in the dorsal thorax of the fly (Figure 16D). Wild type fruit flies, express a chitin nanofibers organization in the dorsal thorax (Figure 16C) that is similar to that observed in the periodic cicada (Figure 10A). In the dorsal thorax of the fruit fly, the chitin nanofibers are woven into a loose braid (Figure 16C), in flies homozygous for Cpr51A, the fibers are thicker and are less organized (Figure 16D).

3.7 Discussion

Insect and arthropods cuticles exhibit a broad range of micro-and macro-scale morphologies, in this manuscript this morphological diversity extents into the nanoscale [152, 154-157]. In this paper, we have developed a simple technique that enables the characterization of nanoscale chitin fiber organization within the cuticle of insects and arthropods using SEM. Specifically, we examined nanoscale chitin organization in the periodic cicada *Magicicada septendecim* has a wide range of morphology that is particular to the tissue where is it found. We have shown that the chitin purified in this manner maintains its chemical integrity while preserving important spatial and positional information regarding the nanoscale organization and structure of chitin nanofibers. The 20nm self-assembled chitin nanofibers also has a wide range of morphologies ranging from organized into loosely woven mats in insect wings and sensory organs, but is highly organized in other structures such as the leg, thorax and head. Moreover, we have also examined nanoscale chitin organization in other insects and the crustacean *Farfantepe-*

naeus aztecus and shown that there are in some cases similar ordering of chitin nanofibers which suggests a common role. Our results suggest that the assembly of chitin nanofibers is controlled in a tissue dependent fashion and may reflect or indicate specific mechanical and/or physical properties required of these anatomical structures. Although, nanoscale structure affect the mechanical properties of the cuticle remains to be tested but given the wide range of these properties in both cuticles and in purified chitin may be defined in part due to nanoscale structure.

Using this technique, we are also able to identify two new chitin based structures in the epicuticle. The surface of some wings of cicada like the dog day cicada, *Tibicens tibicens* have an arrays of high aspect ratio nanocones; while other cicadas like the periodic cicada *Magicicada septendecim* wings with smaller less prominent nanoscale features. These nanoscale structures endow the surface of the wing with additional properties such as superhydrophobicity, self-cleaning, broad band antireflection and even antimicrobial activity [152-154, 158-161]. While, the epicuticle of most insects is a waxy layer and we have shown that in addition to this wax is a separate layer that is distinct and separate of nanostructured chitin that serves as the scaffold for more superficial wax and lipid layers (Figure12A). The connection between the highly randomly arranged deeper layer of procuticle chitin is weak and disrupted during the protein/lipid extraction process which suggests that this layer is generated and secreted in a separate step during the wing formation. We also found a new nanostructured surface on the epicuticle of the noise making tymbal membrane (Figures 13 and 14). The tymbal membrane is the noise generating organ of the cicada and the ribbed disc-shapped structure is composed of chitin

with bands of the elastic cuticle protien RESILIN[162]. We found a net-like pattern of material on the surface of the tymbal membrane that is punctuated with 400nm nanoscale knobs structure. In a fashion, similar to the nanocones on the dog day cicada, these nano knobs have a core composed of 100nm chitin nano-balls. Both the nanocones of certain cicada wings and nanoknob of the tymbal membrane may represent specialized epitcuticle features that use chitin scaffolds to maintain and stability their structure.

Cuticular components are secreted from the underlying epithelial cell layer as a liquid crystal matrix and are deposited into an assembly zone where chitin nanofibers and specific proteins self-assemble into regularly arranged fibrils[163-165]. Within this assembly zone, nanofibers of the chitin polysaccharide are arranged into crystalline bundles that are characterized by anti-paralleled hydrogen bonds between sugar chains [19, 166]. The interaction of specific chitin-binding proteins with chitin determines most the properties of a cuticle, e.g hardness, flexibility, elasticity [19, 20, 24, 167-170]. The rubber-like chitin-binding protein RESILIN is the cuticular component of the tendons of certain insect's legs responsible of storing mechanical energy needed for jumping and play roles in flexibility in dragon and damsel fly wings[169, 171-174].The hallmark of most cuticle proteins is the presence of a chitin binding domain, the most common being the Rebin and Reddiford (R&R) domain [20, 24, 174-176]. Several hundred putative chitin binding proteins that have been identified by genome analysis of insects and other arthropods [177], however, the manner in which this binding domain interacts with chitin nanofibers and/or chitin crystallites, the nature of protein-protein interactions within the cuticle, as well as the manner in which chitin nanofibers are organized to confer specific functions

remains unclear. Some chitin binding proteins organize chitin into elaborate structures. In the peritrophic membrane of the insect midgut, chitin organizes a hexagonal lattice laced with ~10nm nanopores that appear to function as sizing filters for food particle [28, 178].

The thorax is a critical component of the indirect flight physiology of the fly and its nanoscale chitin organization is especially well organized. In the thorax of wild type adult fly, the 20nm chitin nanofibers are woven into a highly-organized structure (Figure 10A) which is orthogonal to the long axis of the wing. We have found one mutant that changes this organization; thoraxes mutant for Cuticle Protein 51A (Cpr51A) expressed disorganized chitin nanofibers as well as an increase in the thickness of individual chitin based fibers (Figure 10B). The implication of this result is that CPR51A is both preventing the bundling of thick chitin fibers, as well as being required for the organizing a woven chitin nanofibers material. Furthermore, the affects that this disorganized chitin in Cpr51A mutants have on larger scale mechanics such as movement or flight remains undescribed as well. We believe that there are other genes that encode other cuticle proteins will be involved in other aspects of weaving nanochitin and those altering the pattern of the woven nanochitin will change the mechanical properties of the thorax.

The insect cuticle is similar to modern composite materials such as resin/fiberglass, however, the major difference is that within the insect cuticle the resin, i.e. the proteins/lipid matrix, actively controls and organize the fibrous component and thereby actively change and control the mechanical and physical properties of the materials. In essence, insect cuticles are a quintessential biological smart composite material. By

understanding the process of cuticle formation and the interaction between specific cuticle proteins and chitin, we will be able to develop smart resins that can organize or reorganize nanofiber matrixes in other systems, however this has been problematic due to the issues with the the characterization of nanoscale chitin organization within the cuticle.

CHAPTER IV

FABRICATION OF BIOMIMETIC NANOCONES (BNC'S) ONTO CHITIN NANO FIBER SCAFFOLDS IN-SITU VIA SELF-ASSEMBLY

4.1 Introduction

In this study, I describe an eco-friendly method for extracting and purifying chitin *in-situ* from a whole cicada along with demonstrating a procedure by which we replicate the Biomimetic nanocones (BNC's) structure of the cicada wing using our prepared chitin scaffolds. I analysed the structure of Dog-day (DD) and Brood II (BII) cicada, which possess cones and honey comb structure. I used BII prepared chitin scaffold as a substrate to mimic DD nanocones. Have characterized the structural morphology of these BNC's using FE-SEM and structural confirmation of the polymer scaffold using FT-IR. Further studied the interaction of these BNC's with mammalian cells which shows that these chitin scaffolds display extraordinarily diverse morphologies for biomedical applications. This information provides insight into the mechanisms that are essential for *in-vitro* nanoscale manipulation of chitin in hydrogels and other synthetic biomaterials.

Biopolymers, chitin is mechanically stable but biodegradable, nontoxic, and physiologically inert which makes then very unique compared to other polymers [30]. Despite these desirable properties, artificial bioinspired mimetic composites based on

chitin nanofibers have been difficult to produce due to chitin's insolubility in most aqueous and organic solvents [32]. Here, we report the green process of fabricating chitin nanocones following the protocol of extracting chitin from insect based on authors previous work [179] and mimic the native structures found in insect cuticles that have a diverse array of material properties and a great deal of potential in various biomedical applications [1, 81, 180]. Despite these desirable properties, artificial bioinspired mimictic composites based on chitin nanofibers have been difficult to produce due to chitin's insolubility in most organic solvents [32, 181]. But, following our previous method of extracting chitin nanofibers from both DD and BII cicada, we can overcome the problem of using harmful solvents to dissolve chitin and maintain the innate structure of the chitin assembly. The authors report the successful replication of self-assembled BNC's of chitin for the first time to the best of our knowledge. We used BII chitin scaffold as a substrate to create BNC's that replicate the DD cones by creating a self-assembled monolayer of PS nano-beads onto extracted chitin scaffold to form patterned, bio-mimicked nanocones that could be a potential material for various biomedical applications.

4.2 Materials and Methods

4.2.1 Cicada Species Used in this Study

Insect cuticles for these experiments were from the periodic 17-year cicada BII - *Magicicada septendecim* and the annual DD - *Tibicens tibicens* cicada collected locally in Greensboro, North Carolina.

4.2.2 Cuticle Chitin Preparation

The BII and DD species of cicada wings are dissected carefully and washed three times in dH_2O and then followed the protocol based on the authors previous research work [179]. Further, following our previous method [179] the dissected wing samples, after the extracted chitin, are further dehydrated in an ethanol series 20%, 50% 70% 84%, 90%, 95% for 10-15 minutes and into 100% ethanol overnight and then allowed the solvent to evaporate.

4.2.3 Fabrication of NNC's of Chitin

Polystyrene nano-spheres (Polybead carboxylate, 380 nm) were purchased from Polysciences, Inc. Beads arrived in 2.5% w/v aqueous suspension. The NNC's were fabricated onto BII prepared chitin scaffold to mimic the cone structure of DD cicada using 380 nm beads. CL [59] technique is applied to form nano-patterned surfaces based on the colloid–colloid and colloid–substrate interactions. The PS nanobeads are selfassembled and monolayered onto the extracted chitin scaffold of BII wing. These beads are received on the chitin scaffold through air-water interface and etched using south bay technology model PC-2000 plasma cleaner. A schematic representation of the fabrication process is shown in figure 17.

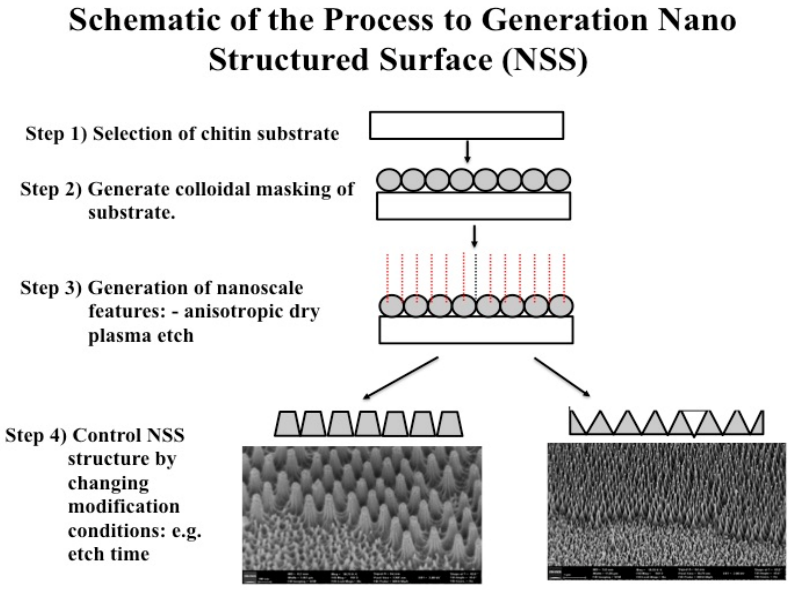

Figure 17. Schematic of Generating Nano-Structured Surfaces (NSS)

4.2.4 SEM (Scanning Electron-Microscopy)

Sample preparation and imaging for morphology study: The samples of the native cicada BII and DD wings, the chitin extracted prepared wing and the BNC's surfaces were washed 3-4 times in dH2O. After drying, the samples had a 4-nm thickness of gold layer applied using a Leica EM ACE200 with a real-time thickness monitoring quartz crystal microbalance (QCM). The scanning electron micrographs were obtained using a Zeiss Auriga FIB/SEM. Scale bars were added using ImageJ software.

4.2.5 Freeze Fracture Analyses

The DD wing sample is cleaned properly in DI water and then submerged the sample in liquid nitrogen until equilibration occurs. Once the equilibrium is reached the

sample is smashed or hit quickly in order to cause fracture using a small hammer and then SEM analysis is done.

4.2.6 FTIR Analysis

FT-IR (Fourier transform infrared spectroscopy), model 670 IR Varian is used to confirm the presence of polystyrene nanobeads masked on to chitin scaffold of BII. Separate spectrums were taken for prepared chitin, polystyrene nanobeads and chitin scaffolds with mololayers polystyrene nanobeads.

4.2.7 Confocal Studies

MDCK cells were grown on either plain wing or etched wing surfaces for seven days at 37°C with 5% CO_2. Following the culture period cells were washed twice with PBS, then fixed for 30 minutes in 4% paraformaldehyde. Fixed cells were washed and then permeablized in 1x PBT (PBS with 1% BSA, 0.1% Triton X) for one hour. Following permeabilaztion, cells were incubated with a mouse anti-human E-Cadherin antibody at 1:500 dilutions in PBT overnight at 4°C. Unbound primary antibody was removed by washing, followed by 2 hours of staining with goat anti-mouse Cy3 labeled secondary antibody. Finally, cells were stained with Phalloidin-AF488 and DAPI for four hours and thirty minutes, respectively. Stained cells were mounted in Permount and imaged using a Zeiss Spinning Disc Confocal Microscope.

4.3 Results

The main objective of this study is to develop a simple and rapid method of mimicking native nano structures of cicada using its prepared wing as a substrate. We used insect wings for chitin extraction specifically the periodic 17 year cicada BII collected locally in Greensboro, North Carolina during the June 2013 emergence, the annual DD cicada collected locally in Greensboro, North Carolina during the summer of 2013, Extraction and purification of chitin scaffold from native DD and BII wing is done based on authors previous work explaining the crystallinity and structural bond through XRD (X-ray diffraction) and FT-IR (Fourier transformer infrared spectroscopy) [179]. Recent experiments have demonstrated that chitin hydrogel formation can result in different chitin morphologies using HFIP as a solvent [182]. We have generated a simple and fast technique that enables the preservation of nanoscale chitin structure in the context of gross anatomy and preserve the innate assembled chitin. This results in a clear, structurally intact and preserved native assembly of chitin exoskeleton (compare Figure 18A and 18B) and also, the SEM image of native DD wing and prepared wing structure (compare Figure 18C and 18D).

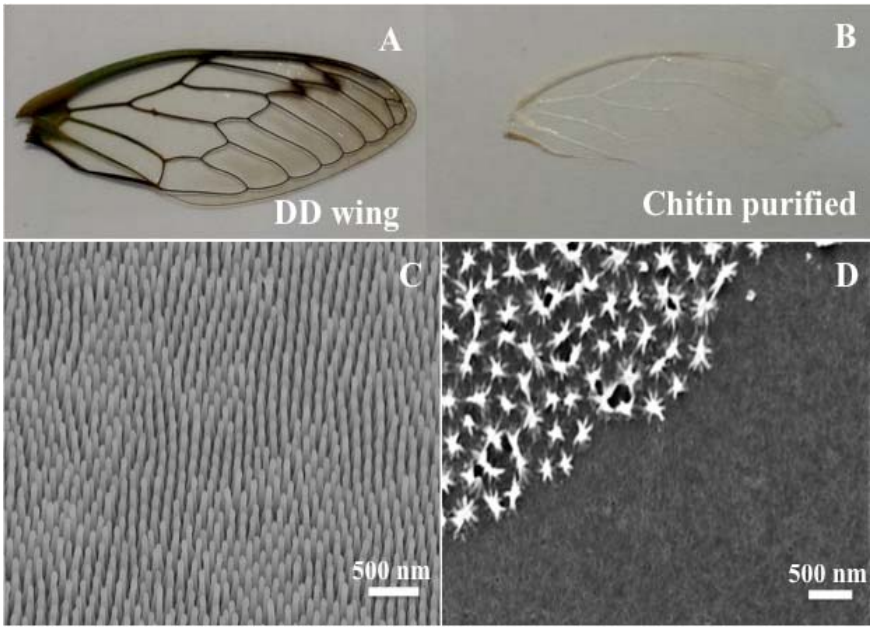

Figure 18. The SEM Image of Native DD Wing and Prepared Wing Structure.
The image of (A) Native DD cicada wing (B) Prepared chitin scaffold from native DD wing and SEM image of (C) Cone structure of native Dog-Day cicada wing and (D) Prepared wing scaffold with very thin layer closely bound to chitin scaffold.

The chitin within the cuticle displays a purity that is comparable to commercial available chitin samples. Similarly, BII native wing and prepared wing morphologies (compare Figure 19A and 19B) and also, the SEM image of native BII wing and prepared wing structure (compare Figure 19C and 19D).

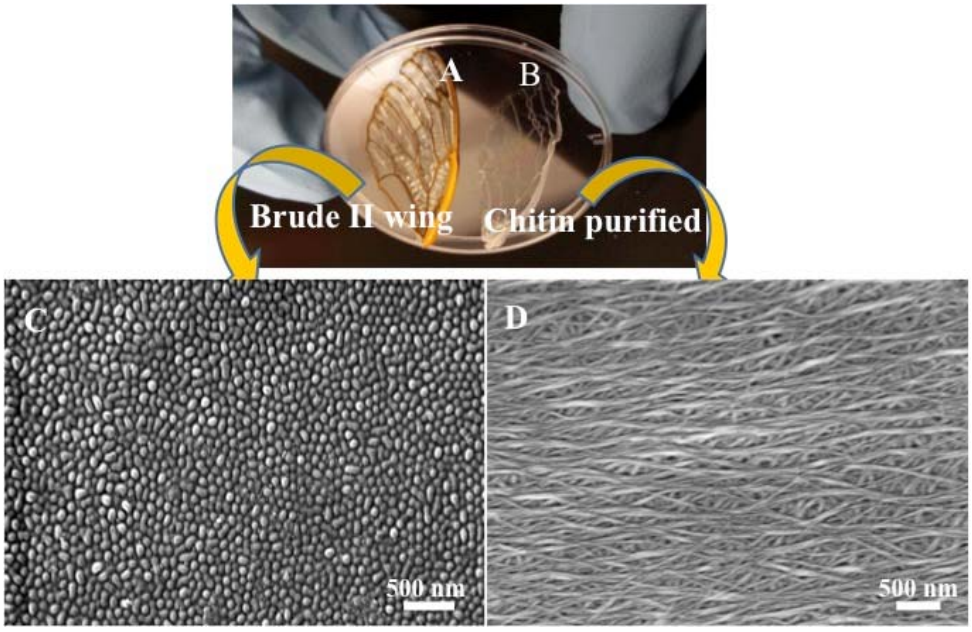

Figure 19. The SEM Image of Native BII Wing and Prepared Wing Structure. The image of (A) Native brood II cicada wing (B) Prepared chitin scaffold from native brood II wing and SEM image of (C) Cone structure of native Brude II cicada wing and (D) Prepared chitin scaffold

The DD wing has this unique cone like morphology which plays a great role in wettability and antimicrobial/fungal activity [180] but the prepared wing still possed a layer of tangible at the macroscopic level during the chitin preparation and the BII wing has a honey comb like structure [179] but the prepared wing does not possess any extra layer as DD wing, which makes it easy to use BII prepared wing as a substrate for masking PS beads to mimic the unique BNC like structure of DD cicada wing.

To understand the internal structure of DD cicada wing for mimicking its cone structure, freeze fracture (FF), which is a unique process that provides the planar view of structural organization through electron microscope is performed. This method is been followed by researchers to analyze the internal structure [183]. Since, this technique helps

to produce cross-sections of DD wing samples. We took a complete DD wing cross-sectioned and the structural morphology of the wing is shown in figure 20, which provides an approximation of PS size to replicate the BNC's on to BII prepared wing.

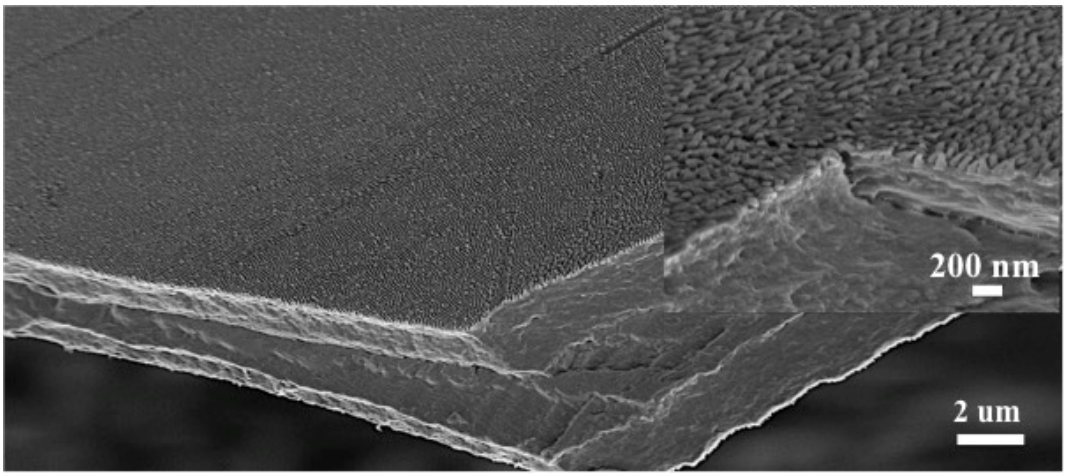

Figure 20. Cross-Section of DD Wing After FF of the Sample in SEM

The FTIR analysis of chitin, polystyrene nanobeads and polystyrene nano beads masked onto chitin The characteristic transmission peaks that represent the amide bonds of chitin amide I ($\nu_{C=O}$) at 1660 and 1627, Amide II (ν_{C-N}) at 1558 and amide III (ν_{C-N}) at 1312; the amide absorbance at 1660/ 627 demonstrate differences in hydrogen bonding within the chitin show that the chitin present is alpha and the transmission peaks between 3102 to 3400 cm^{-1} also show a pattern similar to alpha chitin with strong transmission for hydroxyl groups ($_{OH}$) at 3479 and 3448 and amines ($^{as}_{NH}$ and $^{s}_{NH)}$ respectively [179] and further the transmission peak for polystyrene beads are 1600 to 1400 cc bond stretching vibration and 1250 to 900 shows the presence of aromatic CH deformation vibration and

the combined peak of both chitin with polystyrene nanobead transmission peak is absorbed to provide an insight of masked substrate as shown in figure 21.

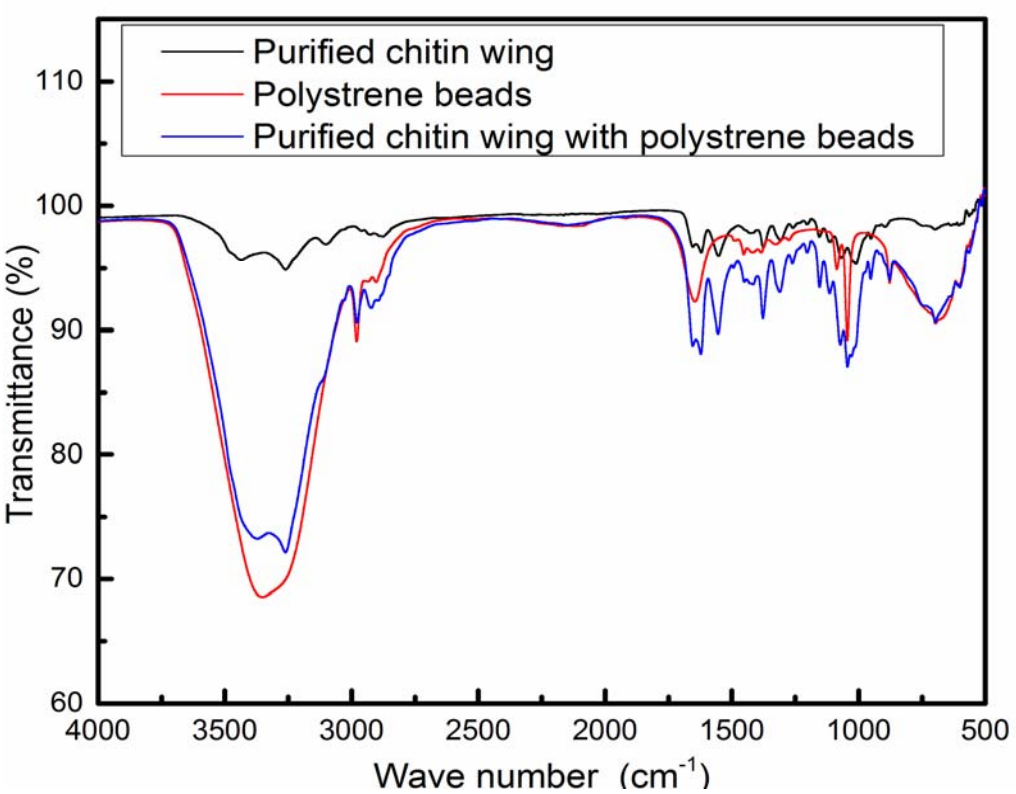

Figure 21. Shows The FT-IR Peaks of Purified Chitin Wing, Polystyrene Beads, Polystyrene Beads on Brude II Chitin Scaffold

4.3.1 Fabrication of BNC's onto BII Prepared Chitin Scaffold

The chitin scaffold extracted from BII is used as a substrate to mask the polystyrene nanobeads and etched to form chitin nanocones that forms the native nanocones of DD cicada wings. Polystyrene nano-spheres with diameters 380 nm were centrifugedand re-suspended in equal parts water and ethanol at 5% w/v. 22 mm^2 cover glass substrates were cleaned and rendered hydrophilic via oxygen plasma cleaning using a South Bay

Technology Model PC-2000 plasma cleaner. Instrument and operating specifications are as follows: RF 13.56 MHz capacitively coupled plasma (CCP) operated at forward power 75-100W with a chamber pressure 180-200mT for 30 sec exposure times. A small volume, 10-15 uL of bead suspension, was applied to a clean glass substrate and allowed to fully wet at which point it was then slowly immersed at a shallow angle (20-30^{o}) relative to the water surface into a 100-mm diameter glass Petri dish three-quarters filled with deionized water. The bead suspension diffuses across the water surface and forms a loosely ordered monolayer at the air/water interface. A small volume 4-6 uL of 2% w/v dodecylsodiumsulfate (SDS) is gently applied to the surface away from the film, driving the beads into a stable hexagonally close-packed monolayer. The film can be removed from the water surface by essentially reversing the process of loading, i.e. slowly submerging, at a shallow angle (20-30^{o}), a clean hydrophilic "receiving" BII substrate underneath the film and delicately scooping and withdrawing it from the surface. For this technique specifically, the wettability of the receiving substrate must be emphasized, as it is particularly important for film removal and quality.

Further, using the south bay technology model PC-2000 unit mentioned previously and oxygen as the process gas, isotropic etching of polymeric substrates was performed. For isotropic (PE), substrates were mounted on the grounded base of the plasma chamber and plasma treated at 100 W forward power and chamber pressure ~ 200 mT for definite exposure times. Mounting the masked substrates directly on the self-biased RF powered electrode allowed anisotropic etching through reactive ion etching (RIE). Process parameters of 100Wforward power ~ -700 V DC bias, and ~ 200 mT chamber pressures were

used for all RIE and 1:30m of exposure times is given for formation of cones structures. The mimicked cones are around 200 -300 nm in size which resembles the size of DD wings as shown below in figure 22.

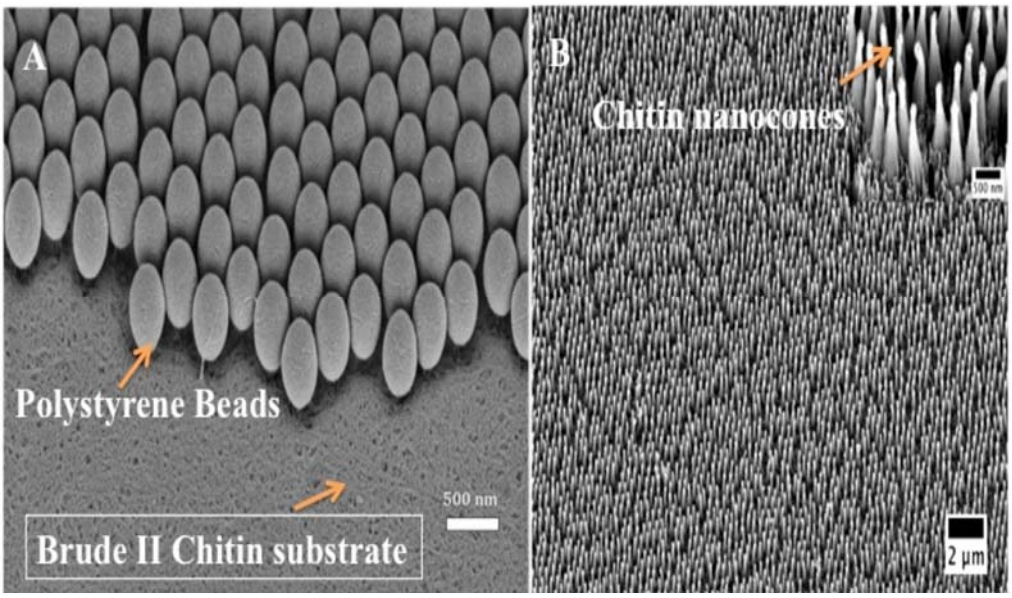

Figure 22. Shows (A) The Self-Assembled Polystyrene Nano Beads on Chitin Scaffold and (B) Biomimetic Chitin Nanocones.

4.3.2 Confocal Studies

Based on our previous work exploring the potential of cicada wings on its wettability and antimicrobial activity, in this work we explored the potential of these fabricated BNC's in tissue engineering, we studied the cell proliferation of MDCK cells which were seven days cultured onto plastic surface as a control, on mimicked BNC's.

Cells grown on plain wings failed to develop the normal epithelial sheets characteristic of MDCK cells grown on tissue culture plastic. Instead, the epithelium formed was disorganized and patchy (figure 23).

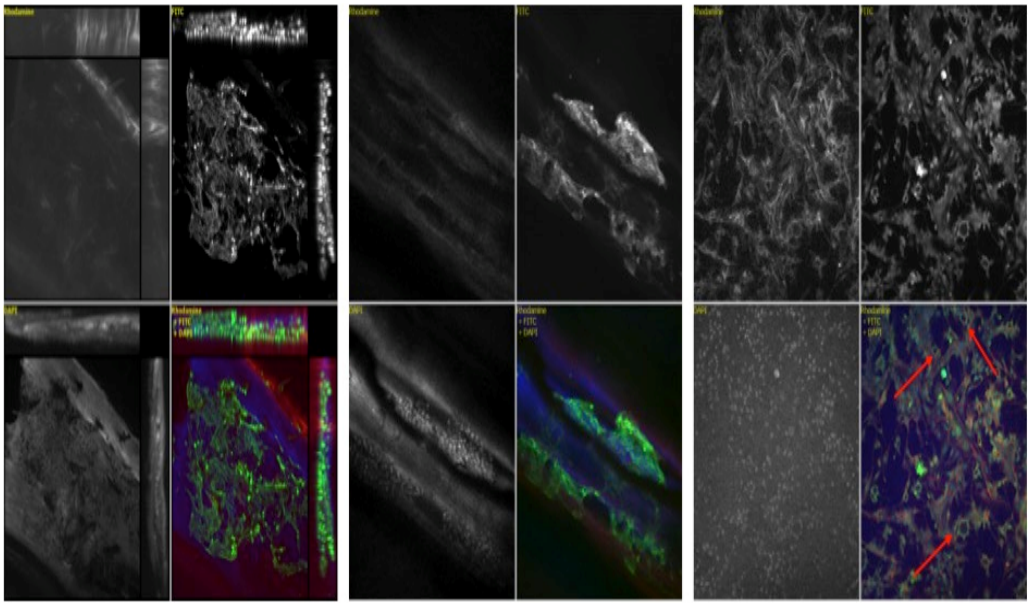

Figure 23. Mdck Cells were Grown for Seven Days on Unmodified Chitin Surfaces. Cells are Stained for E-Cadherin (Rhodamine), Actin (Fitc) and Dna (Dapi). Red Arrows Indicate Tubule-Like Structures.

Tubule-like structures were also observed; however, it is unclear whether these structures were the result of cell growth around protrusions from the wing surface or may be indicative of tubule formation. Cells grown on the etched wing showed highly unusual morphology. Cells appeared spindle shaped with long cytoplasmic projections not normally observed in MDCK cells grown on tissue culture plastic (figure 24).

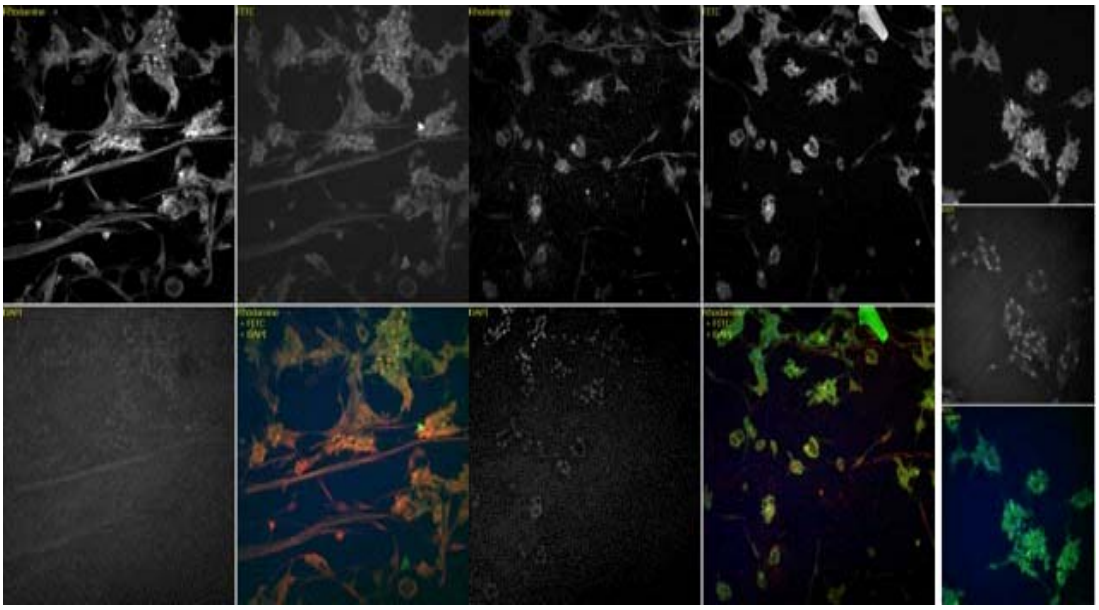

Figure 24. MDCK Cells were Grown for Seven Days on Etched Chitin Surfaces. Cells are Stained for E-Cadherin (Rhodamine), Actin (FITC) and DNA (DAPI).

Epithelium growth was not observed, with cells instead forming disorganized clumps of small numbers of cells. Actin and cadherin organization were both abnormal. Several instances of what appeared to be cell motive membrane extensions were observed, possibly indicating an epithelial–to- mesenchymal transition (Figure 25).

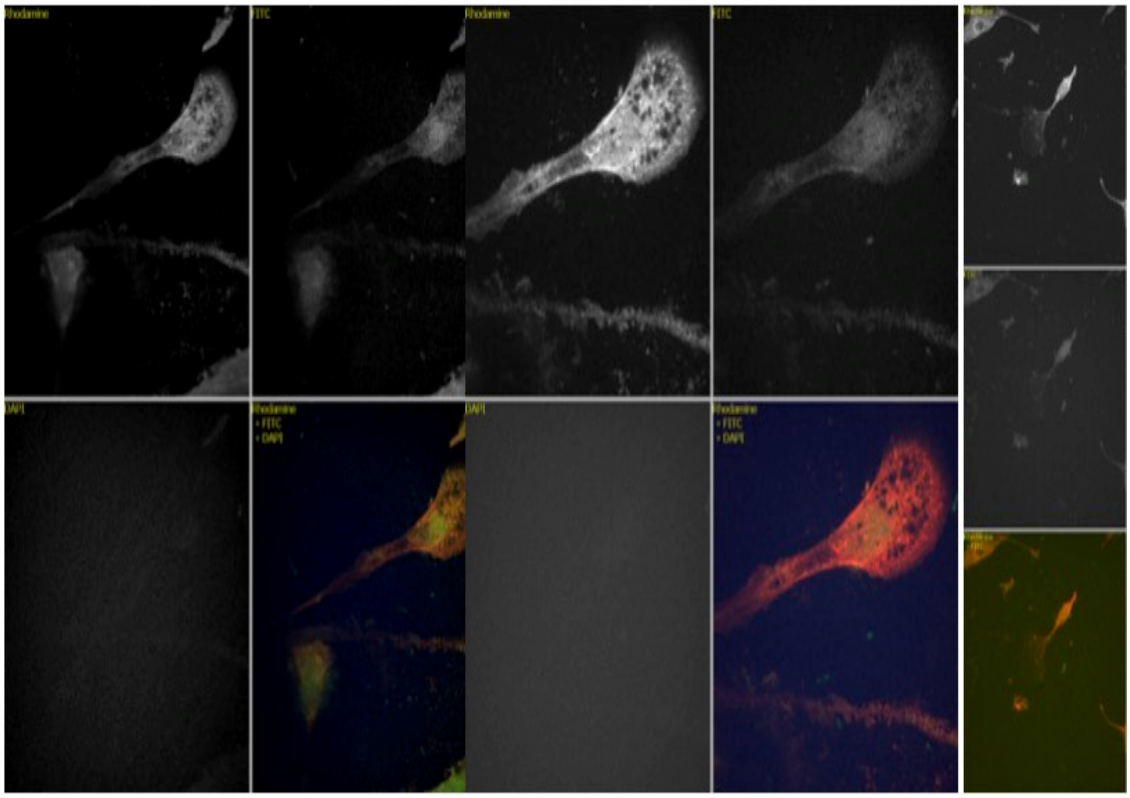

Figure 25. Migratory Cell From Epithelial–To- Mesenchymal Transition.

The surface of the etched wing also appeared to cause cell membrane "deposition", wherein portions of the cell membrane where found to be left behind a migrating cell (Figure 26).

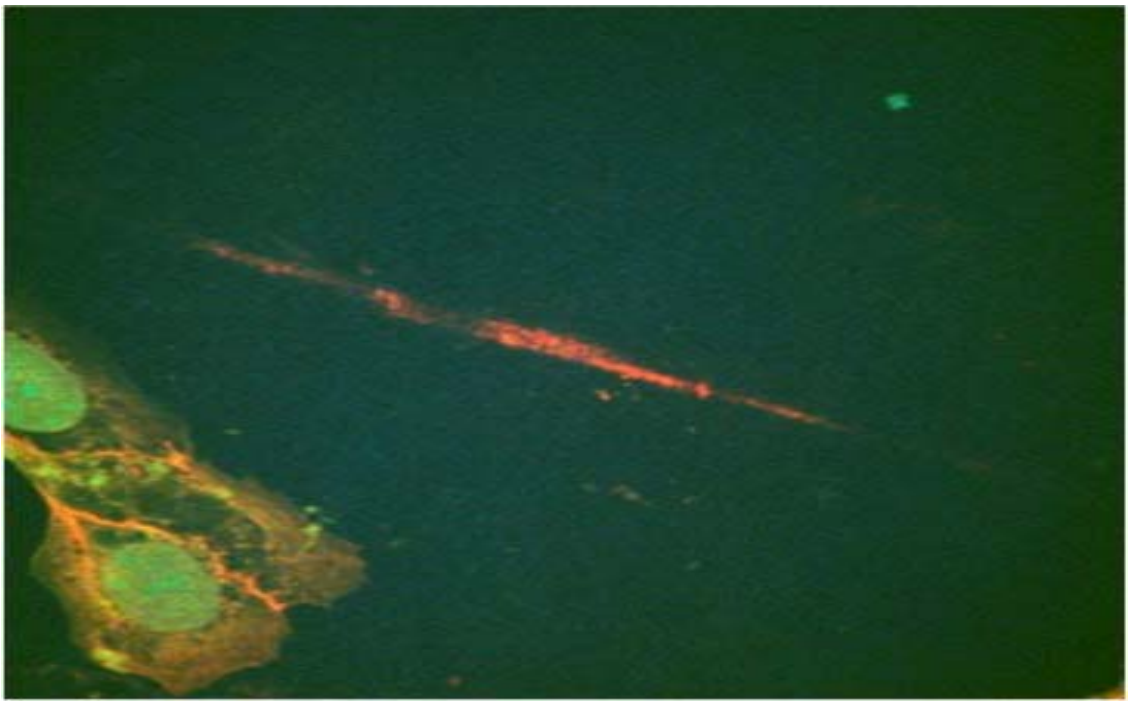

Figure 26. Deposited Cell Membrane Clearly Visible Following Culture on Etched Chitin Surface.

This may be a result of stronger adhesion forces between the ECM binding proteins and the surface than the ECM binding proteins and the cytoskeleton.

4.4 Discussion

The application of polymeric nanomaterial and its nanomimetic process through various nanotechnological approaches plays a vital role in the area of biomedical research. This process of fabrication and growing owing to its capability for producing nanostructures that are able to mimic natural existing structural surfaces which has a great potential in various applications. Few aspects that should be focused in regenerative medicine are the formation of desired scaffold structure, identification and creation of

proper signaling systems or cues to generate self-healing potentiality of endogenous stem cells; developing efficient targeting systems for stem cell therapies, creating standard microenvironment. Finally, still many nanotechnological applications are currently at the concept stage and will require much more basic research before they can be commercialized.

CHAPTER V

CHITIN AND CHITOSAN BASED SYNTHESIS OF SILVER NANOPARTICLES/NANOWIRES ITS MECHANISM AND POTENTIAL APPLICATIONS

5.1 Introduction

Many researchers are working on synthesis of nanosized inorganic/organic materials and their composites to explore new applications. There is an increasing interest in developing nanodevices, which could be used in numerous physical, biological and medical applications [184-186]. Ag (Silver) nanoparticles play an important role in wide variety of applications. Ag nano filters are used in air conditioners to make the outgoing air free from bacteria. Ag based nanocompounds are used to purify water and to reduce the pollutants [187, 188]. Nanocomposites are temperature and corrosion resistant. Nano clothes, either Ag nanoparticles coated or mixed in the fibres, are under development. Ag nanoparticles are more prominent as compared to other metal nanoparticles like Au, Cu etc. because of their wide applications in catalysis [184], contrast agent [189], surface enhanced raman scattering [190, 191], and their antibacterial properties [192, 193]. These wide applications have attracted the attention of scientists to produce them by different methods. The most common mode of synthesis is the chemical route by reducing silver nitrate using sodium borohydride as follows [194, 195]:

$AgNO_3 + NaBH_4 \rightarrow Ag + ½\ H_2 + ½\ B_2H_6 + NaNO_3$

Usually, through this method of synthesis of Ag nanoparticles, the size of Ag as small as 12±2 nm. The plasmon absorbance is around 400 nm and the peak full width at half maximum (FWHM) is 50-70 nm. The absorption of borohydride plays an important role in stabilizing growing nanoparticles by providing particle surface charge. Later in the reaction too much sodium hydroxide increases the overall ionic strength and the particles get aggregated. Therefore, other authors have used polyvinylpyrrolidone to control their size. Due to large positive retention of potential of Ag nanoparticle, oxidation due to stable aqueous and alcoholic suspension is thermodynamically unfavourable without the aid of capping agents. Aggregation can be inhibited by the thick electric double layer,that forms around the metal particles in low- ionic- strength suspension. For high ionic strength of organic phase suspension, capping agents such as self-assembled monolayers [196], surfactants [197, 198], polymer and dendrimers [199-202] are employed to protect the particles from aggregation. Nanoparticles produced by chemical reduction method are mostly non-uniform in size which add variability in their properties. Controlling the particle size has been a necessity to drive out the desired properties. Many authors have reported methods for selection of size and shape of nanoparticles for an efficient control over many physical and chemical properties [190, 203].

Most of them have used chemical methods for capping to control their size. For the last few years biological methods gained an edge over the above methods due to their being environment friendly, cheaper, fast and less time consuming. During the prepara-

tion of silver nanoparticles (AgNPs) and silver nanowires (AgNWs) stabilizers are one kind of major agent that should be present and they play an important role in controlling the formation of nanoparticles, as well as their dispersion stability. Polymers are often used as particle stabilizers due to the fact that they are effective in preventing agglomeration and precipitation of the particles. This is important in synthesizing nanoparticles with nanocomposites, including photochemical [204], Chemical [205], microwave assisted [206, 207], sonochemical and radiochemical [208] assisted synthesis of Ag nanoparticles are been carried out.

I report the green synthesis of AgNPs and AgNWs using chitosan/chitin based polymer as both reducing and stabilizing agent and without using any toxic chemicals. Chitosan / chitin is a polysaccharide that occurs naturally. They are investigated as a natural cationic biopolymer because of its known excellent biocompatibility, biodegradability, nontoxicity, bioactivity, and multifunctional groups from years of research. It is also extensively being studied for food packaging film, bone substitutes, artificial skin,biomedical applications and pH sensitive drug delivery among others due to a number of great properties it possesses [32, 179].

5.2 Materials and Methods

5.2.1 Chitosan and Chitin Sample Preparation

The chitosan polymer (molecular weight: 150,000, 1.5% w/v), acetic acid, sodium hydroxide (NaOH) and NaCl were purchased from Sigma-Aldrich (USA), and used as received without further purification. The BII and DD species of cicada wings are dis-

sected carefully and washed three times in dH_2O and then followed the protocol based on the authors previous research work [179]. Further, following our previous method [179] the dissected wing samples, after the extracted chitin, are further dehydrated in an ethanol series 20%, 50% 70% 84%, 90%, 95% for 10-15 minutes and into 100% ethanol over-night and then allowed the solvent to evaporate.

5.2.2 Synthesis of Silver Nanoparticle/Nanowires Through Chitosan Polymer

$AgNO_3$ (>99 %) was purchased from Sigma Aldrich chemicals and its solution of 10^{-2}M was prepared. Chitosan (0.5 g, dissolved in 10 mL of 1% v/v acetic acid solution) and 0.2M NaCl in 5mL solution is added drop by drop. Mixtures of chitosan and $AgNO_3$ solution were prepared with a ratio of 1:5 (by volume). The mixed sample solutions were kept for ultra-sonication for 3-4 h for formation of monodispersed nanoparticles. Further, the samples were drop casted to make films and analyzed for various analytical character-izations.

5.2.3 Synthesis of Silver Nanoparticle/Nanowires

The chitin extracted from the DD species of cicada wings is used as a source of chitin and the $AgNO_3$ (>99 %) solution of 10^{-2}M is prepared. Chitosan (0.5 g, dissolved in 10 mL of 1% v/v acetic acid solution) and 0.2M NaCl in 5mL solution is added drop by drop on to the chitin wing sample and the sample were kept for ultra-sonication for 3-4 h for formation of monodispersed nanoparticles. Further, the sample is analyzed for various analytical characterizations.

5.3 Characterization Techniques

It is well known that a characteristic absorption peak for Ag nanoparticles appear around 400 -550 nm of the optical range due to surface plasmon resonance [209, 210]. This absorption identifies the formation of Ag nanoparticles in a colloidal solution of chitosan. The optical absorptions of chitosan and mixtures of colloidal solution of $AgNO_3$ (sample solutions) were evaluated in 10 mm optical path length quartz cuvettes of the UV vis spectrophotometer.

To get the size of the synthesized Ag nanoparticles transmission electron microscope (TEM) is used. For getting the results, the copper grid was plasma treated and a drop of sample solution was kept on a copper grid and dried under a vacuum drier, before scanning the sample under TEM.

Morphology including shape and size of nanoparticles, was viewed under Scanning electron microscope (SEM). Sample preparation and imaging for morphology study: The samples are placed on SEM sample pug. After drying, the samples had a 4 nm thickness of gold layer applied using a Leica EM ACE200 with a real time thickness monitoring quartz crystal microbalance (QCM). The scanning electron micrographs were obtained using a Zeiss Auriga FIB/SEM. Scale bars were added using ImageJ software.

5.4 Results and Discussion

The colloidal solutions of the mixture of $AgNo_3$ and chitosan, and the schematic of the interaction of silver ions with NH_3^+ group of the chitosan interacts as shown in figure 27.

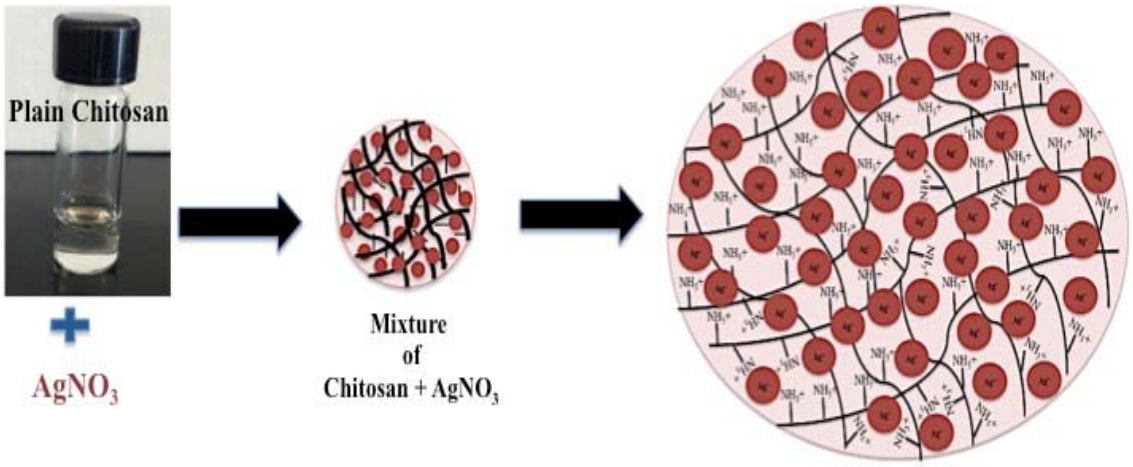

Figure 27. Chitosan and Agno$_3$ Mixture and Schematic of the Ionized Agno$_3$ in Chitosan Matrix

Further, the change in colour of the solution mixture of AgNo$_3$ and chitosan forming pinkish colour as an indication of Ag nanoparticle synthesis and the schematic of how the amine group stabilizes the formation of Ag nanoparticle. The change form opaque chitosan to pinkish occurs by adding the $AgNO_3$ solution into the solution, indicates the presence of Ag nanoparticles as shown in figure 28. This provides an insite on how the formation of the nanoparticles occurs during the series of reactions.

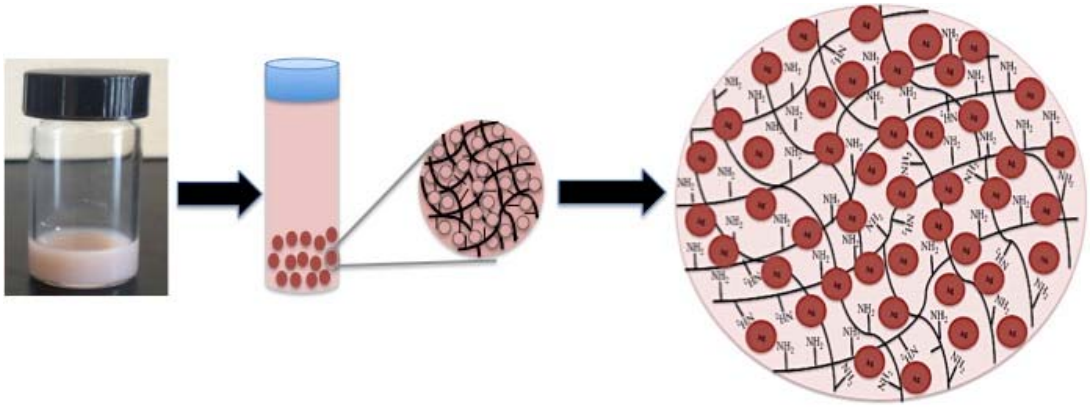

Figure 28. Ag Nanoparticle Formation and the Schematic of Stabilization of Ag Nanoparticles in Chitosan Matrix

5.4.1 UV–Visible Spectroscopy Analysis

The samples were analyzed by UV-vis spectrophotometer to confirm the presence of Ag nanoparticles. The absorption spectra recorded through UV–visible is quite sensitive and provides the confirmation of the formation of silver nanoparticles because of the fact that silver nanoparticles exhibit an intense absorption peak due to surface plasmon resonance (SPR). Figure 29 shows the UV–vis spectra of silver nanoparticles prepared with chitosan and silver nitrate. The spectra exhibit an absorption band in the range of 400–530 nm, a typical plasmon resonance band of silver nanoparticles. The efficiency of nanoparticle synthesis with chitosan and silver nitrate is due to an enhancement in the oxidation of hydroxyl groups of chitosan by silver ions.

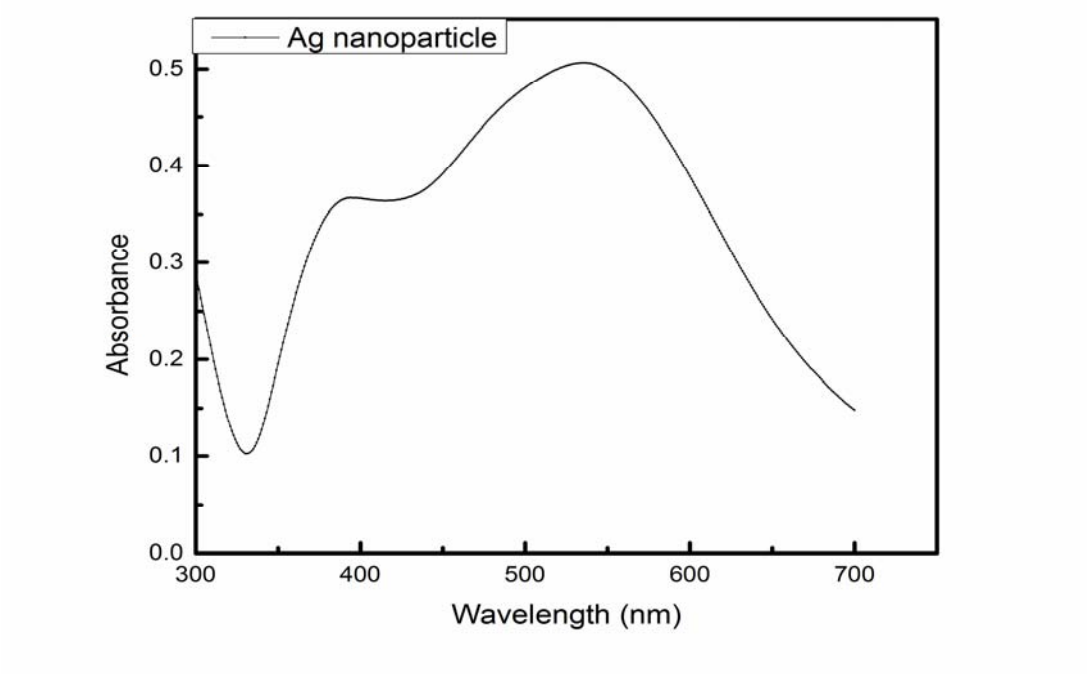

Figure 29. UV–Visible Absorption Spectra of Silver Nanoparticles Stabilized In Chitosan

The graphs of absorbance vs wavelength (nm) are shown in Figure.26. It was noted that the intensity increases with increase of time of reaction kinetics. Peak maxima, at 410 nm and 510 nm, with broadening were observed for sample solutions respectively. The broadening and shifting of the peak maxima for sample solution over time may be due to inhomogeneous shape and size of the Ag nanoparticles at the initial stages of chemical reaction.

5.4.2 DLS (Dynamic Light Scattering) Analysis

Particle size, concentration and distribution are important factors to reflect the mechanism of particle formation. Particle size and distribution were determined by DLS

(Dynamic Light Scattering). figure 30. shows the graphs of volume (%) vs size (d.nm) and figure 31. Shows the graphs of intensity (%) vs size (d.nm). It is observed that the particles are monodisperesed as it is represented by having single peak and lesser PDI (polydisperesity index). The average particle size is around 50-100 nm, which is indicating a comparable population of Ag nanoparticles around this size.

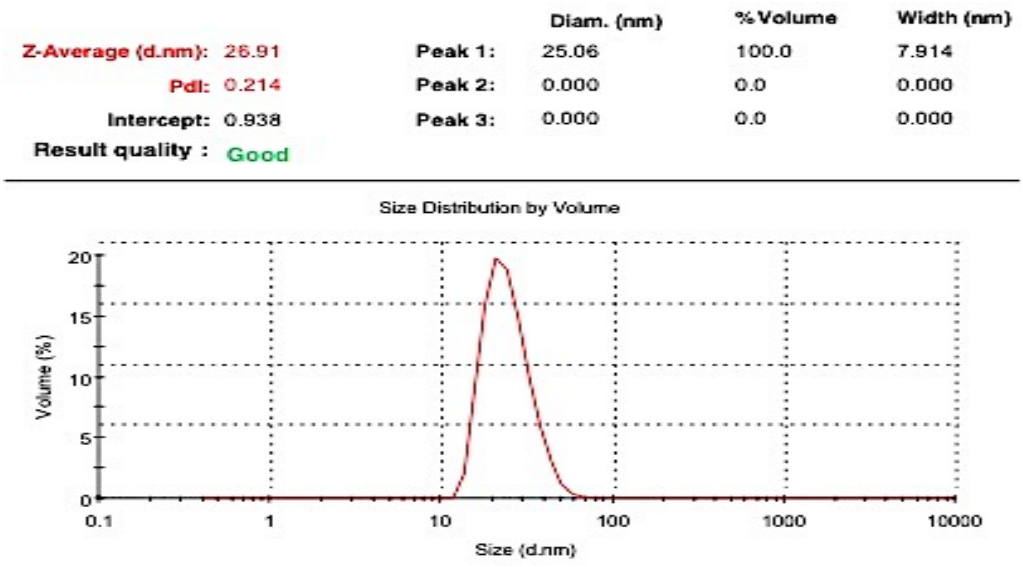

Figure 30. DLS Graphs of Size (D.Nm) Vs Volume (%) for Ag Nanoparticle in Chitosan Sample Solutions

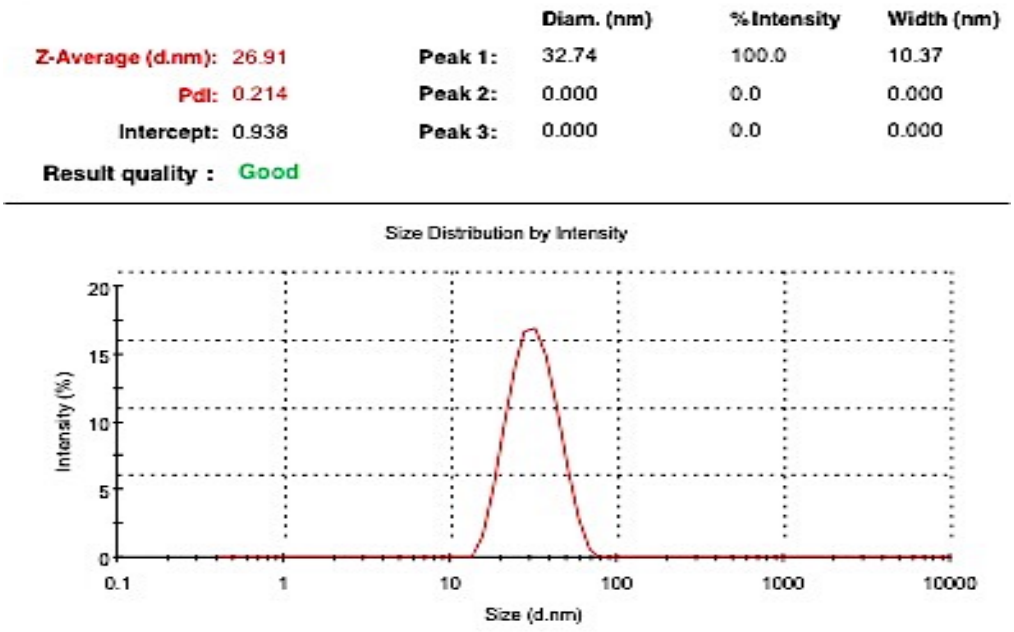

Figure 31. DLS Graphs of Size (D.Nm) Vs Intensity (%) for Ag Nanoparticle in Chitosan Sample Solutions

5.4.3 Fourier Transform Infrared Spectroscopy Analysis (FTIR)

The FTIR spectrum of chitin and chitosan with silver nanoparticles stabilized are studied to understand the structural bonding of Ag nanoparticle. The spectra of α- chitin display a series of narrow absorption bands, typical of crystalline polysaccharide samples. The IR spectrum was collected to compare and contrast the quality of chitin obtained. The presence of characteristic transmission peaks for vibrational information at hydroxyl bonds 3479 and 3426, amines 3290 and 3106 The C=O stretching region of the amide moiety, between 1700 and 1500 cm−1 yields the signature of α- chitin. For α-chitin, the amide I band is split into two components at 1660 and 1630 cm−1 (due to the influence of hydrogen bonding or the presence of an enol form of the amide moiety [211,

212]. whereas for β-chitin it is at 1630 cm−1. at 1,635 cm-1, representing chitin–CONH2 and –NH2 groups, which indicated the attachment of silver to nitrogen atom.The amide II band is observed in both chitin allomorphs: at 1558 cm−1 for α-chitin and 1562 cm−1 for β-chitin [211]. Another characteristic marker is the CH deformation of the β-glycosidic bond. This band shifts from 895 cm−1 in α-chitin. These IR spectra demonstrate that the in situ chitin preparation results in an alpha type chitin as shown in figure 3.

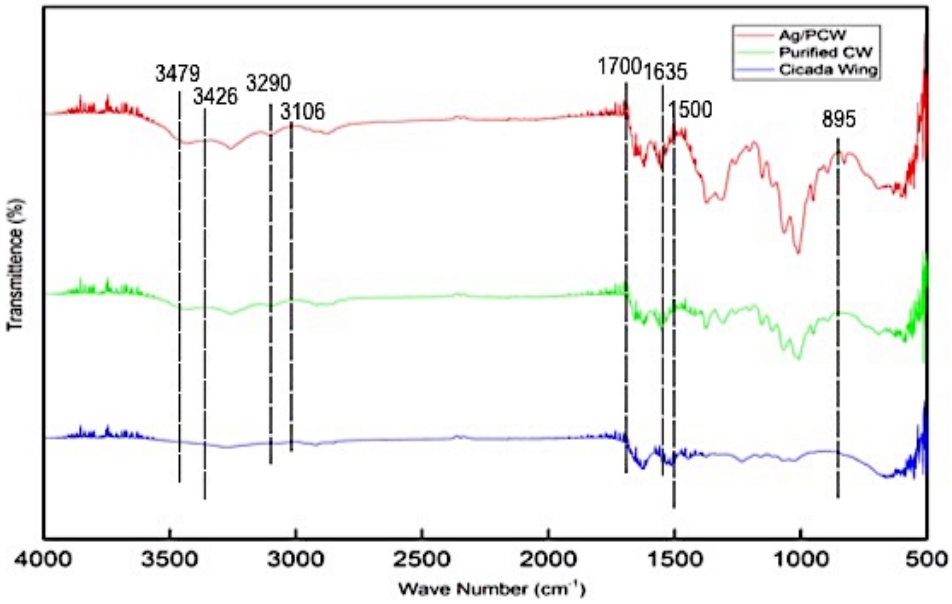

Figure 32. FTIR Analysis of Cicada Wing (CW), Purified CW and Ag Embedded Chitin Wing

The FTIR spectrum of chitosan and silver nanoparticles stabilized in Chitin.The presence of characteristic transmission peaks for vibrational information at hydroxyl bonds 3479 and 3426 cm^{-1}, amines 3290 and 3106 cm^{-1}. The C=O stretching region of the amide moiety, between 1700 and 1500 cm^{-1} yields the signature of α- chitin. At 1,635

cm^{-1}, representing chitin–CONH2 and –NH2 groups, which indicated the attachment of silver to nitrogen atom causing increase in peak and at 895 cm^{-1} is the CH deformation of the β-glycosidic bond.

The Fourier transform infrared spectrum of chitosan (Figure 33) shows vibration bands at 3447 and 3294 cm−1 due to overlapping of O–H and amine N–H stretching bands. 1657 and 1584 cm−1 for N–H bending; and 1,374 cm^{-1} of the C-H group of the primary alcoholic group in chitin. The amino group has a characteristic absorption band in the region of 3,400–3,500 cm^{-1},which is masked by the broad spectrum band from the –OH group. The absorption band at 1,657 cm^{-1} is attributed to the N–H bending group of chitosan. In the FTIR spectrum of silver nanoparticle stabilized in chitosan, the absorption bands at 1,657 cm^{-1} and 1584 cm^{-1} which representing chitosan –NH2 groups is disappeared and a new band appeared at 1,600 cm^{-1} is formed which indicated the attachment of silver to nitrogen atom [86] . The variation in the shape and peak positions of the –NH2 and –OH at 3,447 cm^{-1} occurred because of contribution toward the reduction and stabilization process.

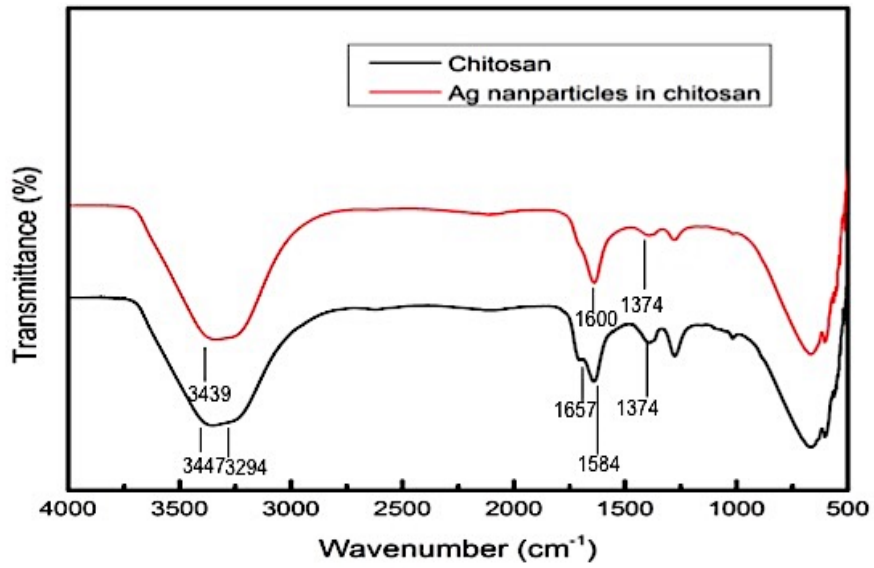

Figure 33. FTIR Spectra of Silver Nanoparticles Stabilized in Chitosan and Pure Chitosan

5.4.4 TEM (Transmission Electron Microscopy) Analysis of Silver Nanoparticles Stabilized in Chitosan

TEM image of silver nanoparticles are shown in figure 34. The particles were cubical in shape (dark) and distributed in smaller and bigger size zones. It was noted that the nanoparticles are having striations, which indicated the presence of crystallinity in the synthesized Ag nanoparticles. The size of the particles is around 30-60 nm.

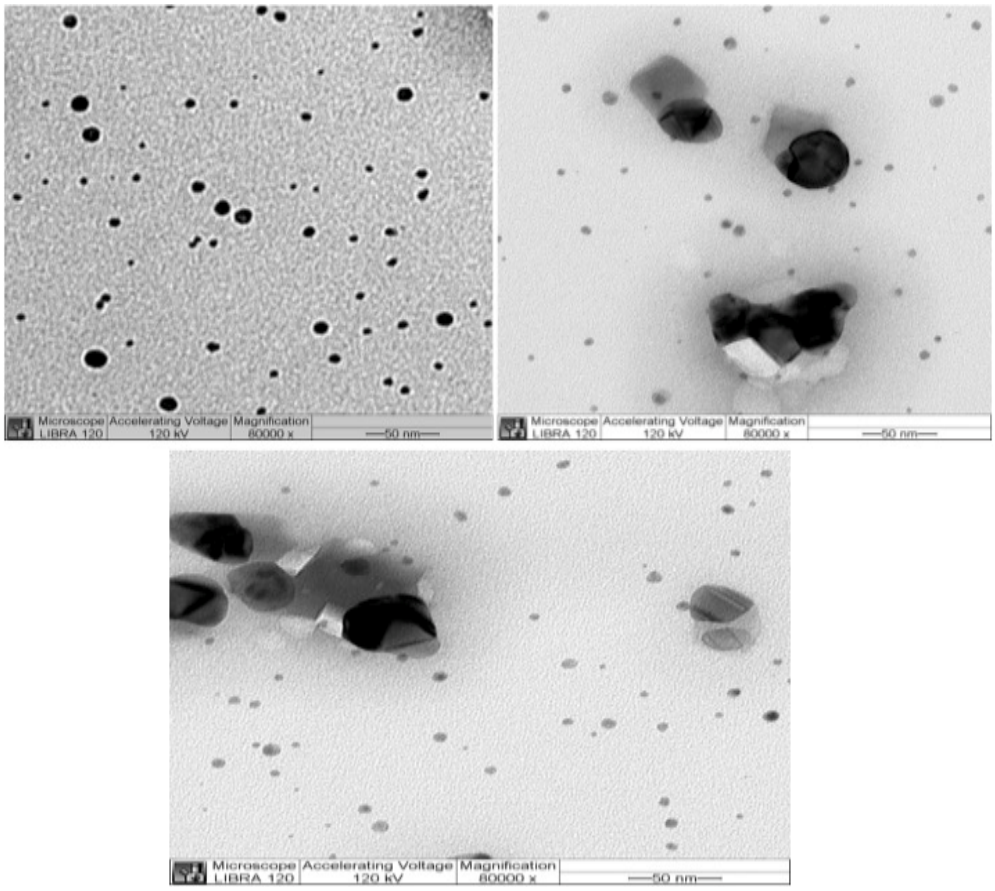

Figure 34. TEM Image of Silver Nanoparticles Stabilized in Chitosan

5.4.5 SEM (Scanning Electron Microscopy) Analysis

In order to reveal the structure of the nanoparticles/nanowires and their surroundings, they were examined under SEM. Figure 35. shows the plain chitosan, AgNPs embedded chitosan and AgNWs. It is found that the AgNWs are nucleated and grow through the chitosan film and also to verify the formation of AgNWs through the film, the chitosan film is masked with monolayer polystyrene nanobeads (400nm), the AgNWs formation through the chitosan film by forcing the beads out indicates the bottom-up for-

mation of Ag nanowires. Further the EDAX (Energy Dispersive Spectroscopy) of the sample is taken to show the presence AgNWs.

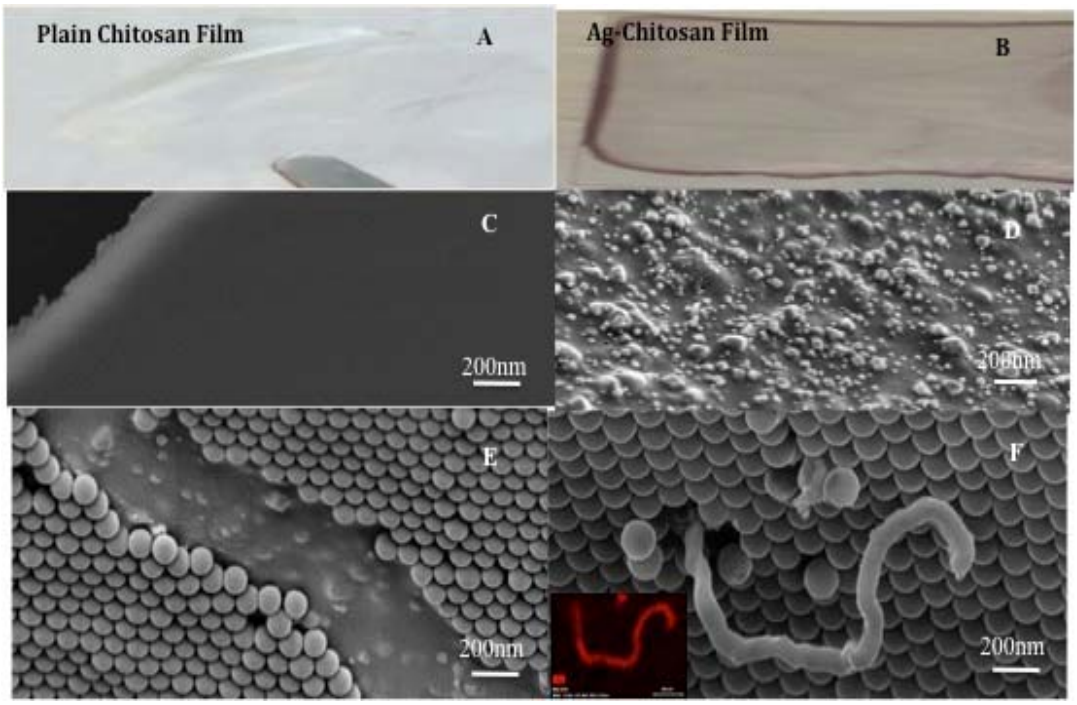

Figure 35. Shows the Optical and SEM Image of Chitosan and Ag Embedded Chitosan and Formation of Ag Nanowires

(A) Chitosan plain film, (B) AgNP embedded Chitosan film, (C) SEM image of plain chitosan film (D) SEM image of AgNP embedded chitosan film, (E) SEM image of polystyrene masked on AgNP embedded film and (F) AgNW emerging from the masked film and top left shows the EDAX of the AgNW.

Similarly, the SEM analysis on chitin is performed. The optical image of the purification of the cicada wing to chitin and the metallization of the Ag nanoparticle and the formation of the AgNWs through the purified chitin wing and the EDAX analysis is done

to prove the presence of metallic AgNWs and AgNps formation on the purified chitin sample as shown in figure 36.

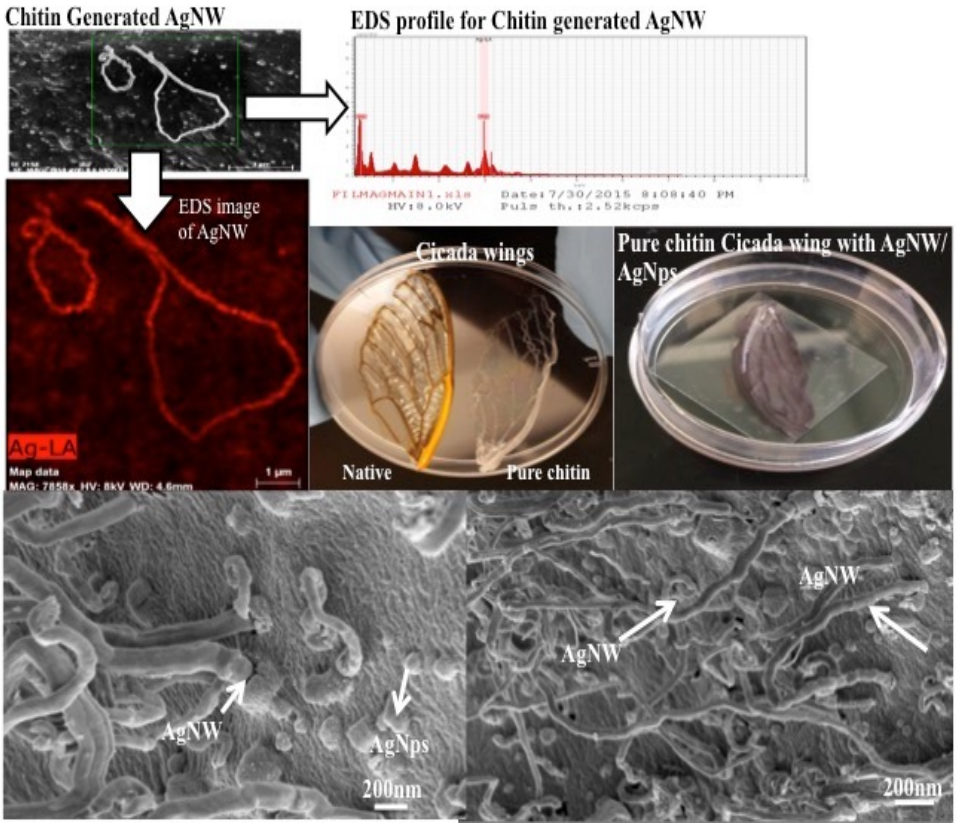

Figure 36. Chitin Synthesis of Silver Nanoparticles (Agnp) and Silver Nanowires (Agnw)

5.4.6 SurPASS Surface Charge Density Analysis

Characterization of the surface charge density of chitin with Ag nanoparti-cle/nanowires conductimetric titration. The suspension samples were titrated with 0.05 M NaOH. and 4 ml of 0.05 M HCI which assures an excess of H^+ in the suspension. The surface charge at solid/liquid interface determines the electrostatic interaction between

the solid surface and dissolved components in the liquid phase. It is therefore indicative for any changes relating to the solid surface and represents an important parameter for surface material characterization. Here the chitin wing sample with Ag nanoparticles were analyzed, the surface charge is related to the zeta potential at the solid/liquid interface, which arises from the motion of the liquid phase relative to solid surface. It shows that the surface of the chitin/Ag shows more acidic with increase in zeta potential and the isoelectric point (IEP) is observed around ~ 6.7 which indicates that the overall sample surface is more or less inert or mild acidic and in the case of chitosan since the dissolving process requires acetic acid its surface charge is mild acidic too. Below, shows the table and the plot chitin /Ag surface to understand the IEP of the sample.

Table 4. Surpass – Surface Charge Potential Analysis of Chitin/Ag

Titration Source	Solute	Concentration [g/l]	Titration Vol [ml]	Measuring Step Parameter Set	pH	Conductivity [mS/m]	Cell Resistance [KOhm]	ζ [mV]	ζ Stdev	Elapsed Time [min]
TU1	NaOH(aq)	2	0.1	Z_R200_180_P200I_20	5.516132917	16.85160333	351.2015917	22.47770891	0.015154663	3.29135
TU1	NaOH(aq)	2	0.4	Z_R200_180_P200I_20	5.552943	16.87917167	352.6914333	21.84644353	0.152270258	6.573866667
TU1	NaOH(aq)	2	0.9	Z_R200_180_P200I_20						
TU1	NaOH(aq)	2	5	Z_R200_180_P200I_20	6.687476833	16.90227667	398.186825	0.024577135	0.933054388	9.89095
TU1	NaOH(aq)	2	15	Z_R200_180_P200I_20	9.047354667	17.20902533	462.8770833	-23.72311882	0.403083846	13.24235

The graph of chitin /Ag surface is ploted based on the above result and the isoelectric point (IEP) is observed around ~ 6.7 which indicates that the overall sample surface is more or less inert or mild acidic which is shown in figure 37.

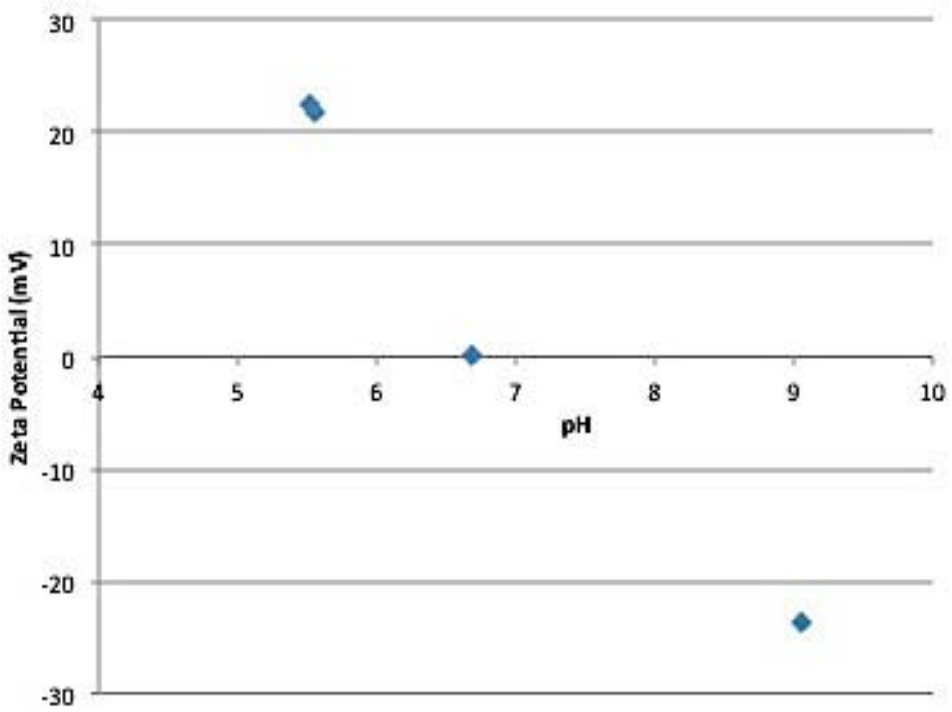

Figure 37. Surpass Graph of Surface Charge Potential Analysis of Chitin/Ag

5.5 Discussions

It is well known that chemical reduction is a common method for preparing nano-particles. For example, sodium borohydride solution is used for nucleation of Ag nano-particles as follows:

$$AgNO_3 + NaBH_4 \rightarrow Ag + 1/2\ H_2 + 1/2\ B_2H_6 + NaNO_3$$

In the above reaction, it is the electrostatic force among the Ag nanoparticles, which keep them suspended in the colloidal solution. As the reaction proceeds, more borohydride layers are formed around them and particles grow in size. Some authors have used PVA (Polyvinyl alcohol) and other polymers for stabilization of nanoparticles. In the present investigation, Ag nanoparticles are reduced by chitosan and chitin biopolymer with its amine group and also the self-assembling polymer acts as a stabilizing agent, which provides the dual purpose for the formation of the Ag nanoparticles.

5.5.1 Formation of Colloidal Particles

The colloids in liquid are charged particles. These particles acquire charge through the composition of colloidal material. As soon as they are exposed to liquid, ions of opposite charges accumulate around them. The accumulation of ions leads to formation of electric double layer. The ions move under the phenomena of brownian motion and form a dynamic double layer around them which is loosely bound. Stability of colloids can be increased by increasing the stearic repulsion (hindrance), which occurs by adsorption of some layers of different materials on colloidal particle. Adsorption of organic molecules on inorganic colloidal particle e.g., Ag nanoparticle, is possible to reduce the attractive forces by addition of adsorbed layers. Consequently, the effective size of the particle changes, which helps them to stay at a larger distance due to reduction of the attractive interaction.

In this process, the biosynthesis of the Ag nanoparticles is formed by self-assembling of the chitosan/chitin biopolymer during the reduction process. Charge trans-

fer takes place from the amine groups present in the biopolymer, resulting in the nucleation of Ag nanoparticles. Further,this is followed by condensation, surface reduction and electrostatic stabilization by oxalic acid molecule layer as shown in the schematic figure 38.

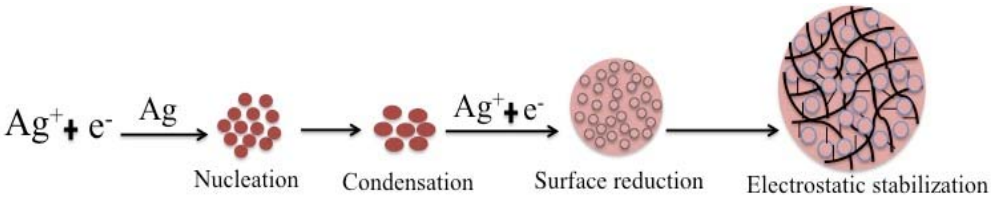

Figure 38. Schematic Representation of Nucleation, Condensation, Surface Reduction and Electrostatic Stabilization of Ag Nanoparticle

Chitosan/chitin polymer have the amine and acetylamine functional group,where the acetamide of chitin makes it less soluble in water and more de-acetylated form of chitin is chitosan is soluble in water under mild acidic condition. The structure of the alpha chitin orientation, which creates the socket for the Ag nanoparticles to get stabilized and also grow AgNWs. (shown below), which make them poorly soluble in water but the deacetylated form (chitosan) lacks the acetamide group. Below is the structure of alpha chitin.

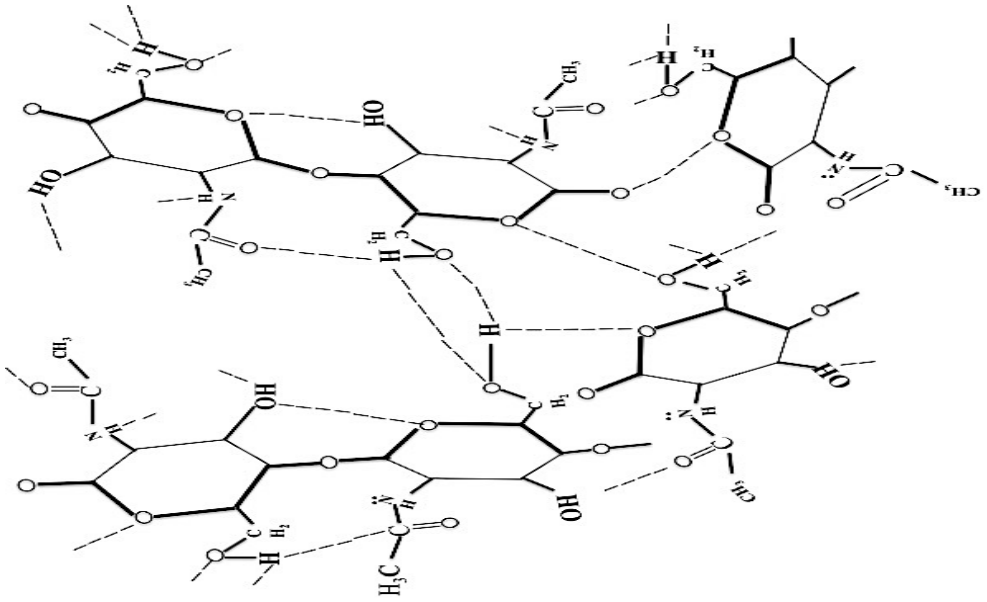

Figure 39. Molecular Structure of Representation of Chitin/Chitosan

On subsequent stages of reaction the above molecules structure of the polymer, get adsorbed to the Ag nanoparticle under influence of coulomb force (electrostatic double layer) resulting in formation of layers of the polymer side chain with the layer of reducing agent, i.e., amines as schematically shown in figure 40.

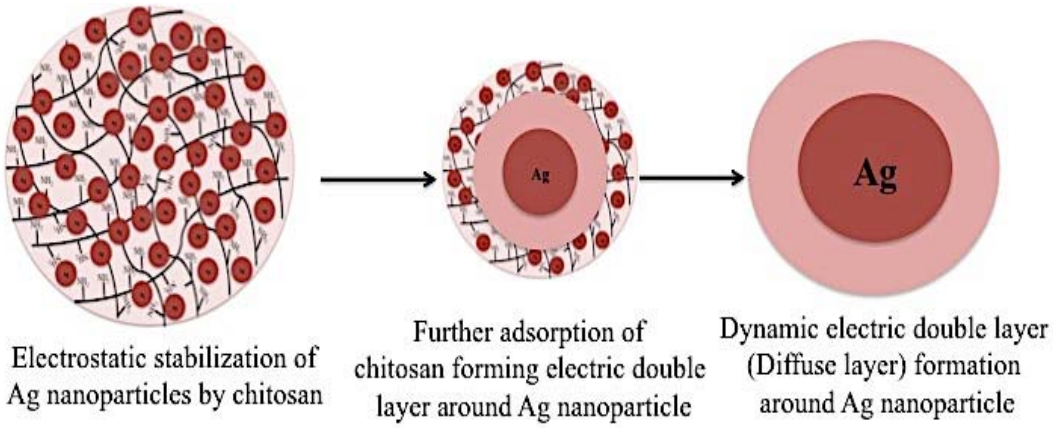

Figure 40. Schematic Representation of Formation of Electric Double Layer and Dynamic Electric Double Layers Around Ag Nanoparticle

In the similar way of the formation of the AgNPs, the formation of the AgNWs arises through the surface of the polymer and the individual AgNPs assembles as a bottom-up proces to form the AgNWs and the structure of the polymer plays a major role in the AgNWs formation at the room temperature as shown in figure 41. The oriented attachment and growth of the Ag NPs can lead to the formation of Ag NW. The structure of the α-chitin orientation and the de-acetylated form chitosan can creates the socket for the Ag NPs to get stabilized and Ag NWs formation could occur based on the crystal orientation.

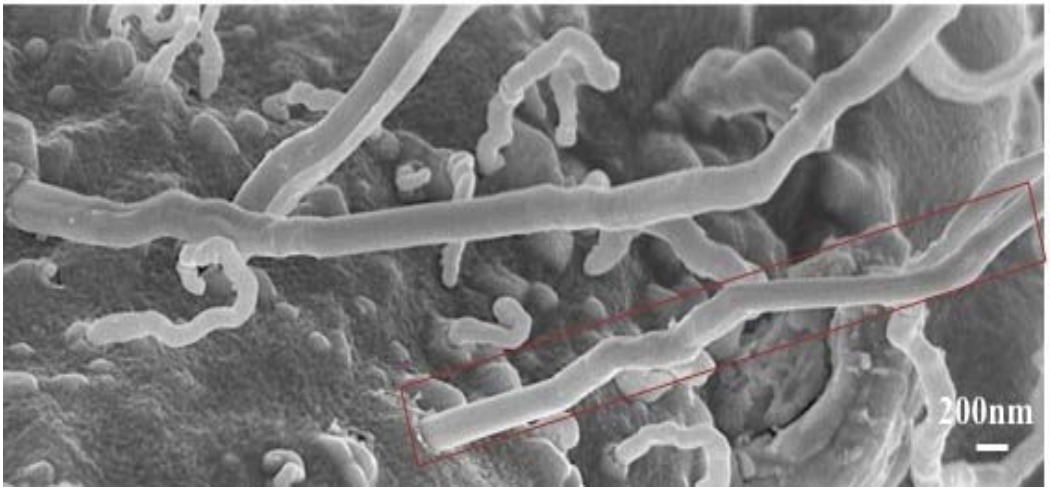

Figure 41. SEM Image of Agnws and the Schematic of Chitosan Mediated Synthesis of Ag Nanowires (Agnws)

The charge distribution of layers of polymer around the electric double layer, and dynamic electric double layers are schematically represented around the Ag nanoparticle (figure 42). There is coulombic force between the electric double layers. Outside this layer there are multiple layers of polymer moieties, due to their adsorption around the electric double layers, forming diffuse layer. The stearic hindrance arose from the variability of molecule structures of the polymer, entangled around the Ag nanoparticles, which enhances their stability.

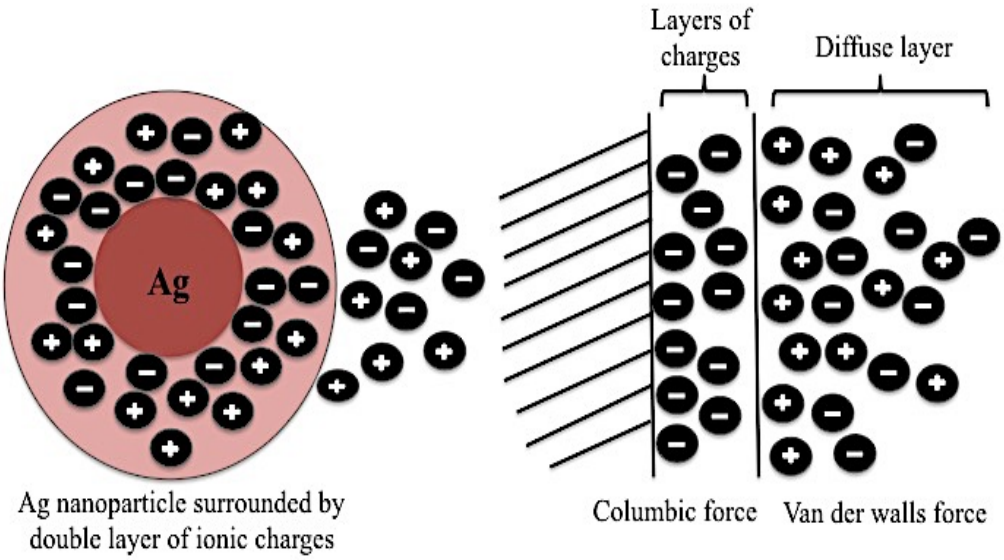

Figure 42. Schematic Representation of the Charges Formed Around Electric Double Layer and Dynamic Electric Double Layer (Diffuse Layer)

5.6 Potential Application Of Chitosan/Ag Nanoparticles as A Biosensor

5.6.1 Biosensor Overview

A biosensor can be defined as a "compact analytical device or unit incorporating a biological or biologically derived sensitive recognition element integrated or associated with a physio-chemical transducer"[213]. There are three main parts of a biosensor: (i) the biological recognition elements that differentiate the target molecules in the presence of various chemicals, (ii) a transducer that converts the biorecognition event into a measurable signal, and (iii) a signal processing system that converts the signal into a readable form [214-216]. The molecular recognition elements include receptors, enzymes, antibodies, nucleic acids, microorganisms and lectins [217-219]. The five principal transducer classes are electrochemical, optical, thermometric, piezoelectric, and magnetic [220,

221]. The majority of the current biosensors are of the electrochemical type, because of their better sensitivity, reproducibility, and easy maintenance as well as their low cost. Electrochemical sensors may be subdivided into potentiometric, amperometric, or conductometric types [222]. One of the key issues in biosensor design is the establishment of a fast electron-transfer between the enzyme active site and the electrochemical transducer that is the communication between the biosensing element or biomolecule and the transducer. The active center of bio-recognition element, like those of most oxidoreductases, is electrically insulated by a protein shell. Because of this glycoprotein shell, the enzyme cannot be oxidized or reduced at an electrode easily or any potential. There are three 'generations' of biosensors: First generation biosensors where the normal product of the reaction diffuses to the transducer and causes the response. Electronic coupling between redox enzymes and electrodes is achieved with the native enzyme co-factor. Second generation biosensors which involve specific 'mediators' between the reaction and the transducer in order to generate improved response. The third generation biosensors where the reaction itself causes the response and no product or mediator diffusion is directly involved. It aims at the direct electron transfer between the native enzyme co-factor and the electrode surface.

5.6.2 Chemicals and Reagents

Gold Electrode, chitosan and, chitosan/Ag and hydrogen peroxide. The supporting electrolyte is phosphate buffer at pH 6.5 were prepared by mixing stock standard solution

of K_2HPO_4 and KH_2PO_4 and adjust the pH with NaOH. All of the solutions were prepared with deionized (DI) water.

5.6.3 Apparatus

The electrochemical measurements were performed using conventional three electrode system consisting of a platinum wire counter electrode, Ag/AgCl (saturated KCl) reference electrode and a glassy carbon electrode (3 mm diameter) working electrode with electrochemical analyzer/workstation. A platinum wire counter electrode, Ag/AgCl (3 M KCl) reference electrode and gold electrode (GE, diameter 3mm) were inserted into a modified 5–10mL Glass cell as shown in figure 43.

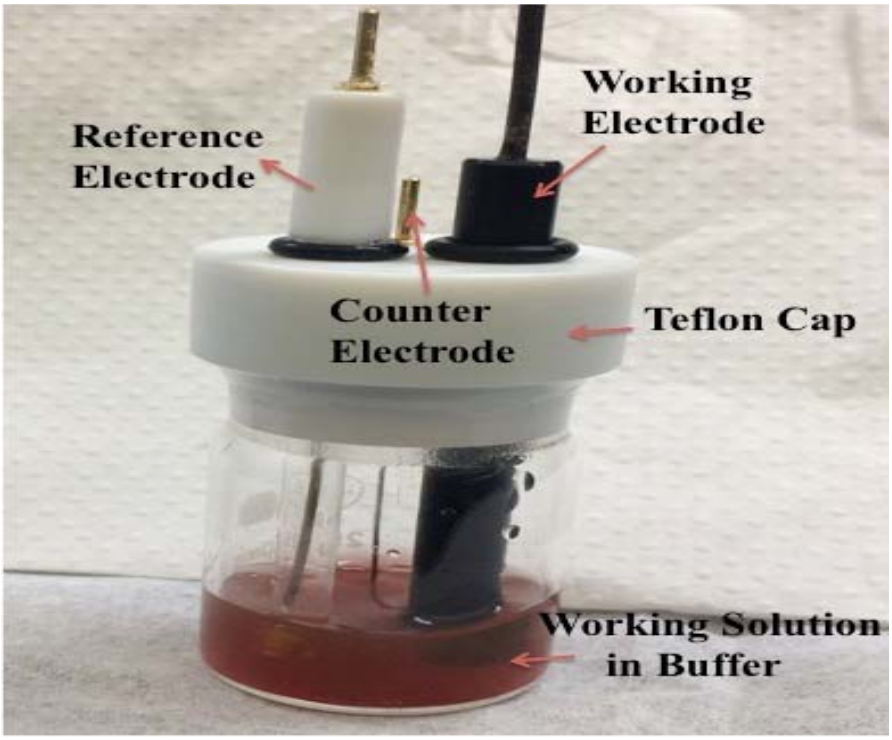

Figure 43. Three Electrode Cell Setup for Electrochemical Workstation

Electrochemical performance was performed on a bio-logic VMP3 electrochemical workstation using a three-electrode testing system with a gold electrode taped with a Ag-chitosan film (diameter of 6 mm) as working electrode, a platinum wire as counter-electrode and Ag/AgCl as the reference electrode in 3 mL of 5 mM PBS (pH 7.0) as the electrolyte solution (an applied voltage of 0.8 V). Note that the CA measurements reach steady-state after 60 seconds. With the increase of H_2O_2 concentration, the current from the CA measurement (Figure 44) increases.

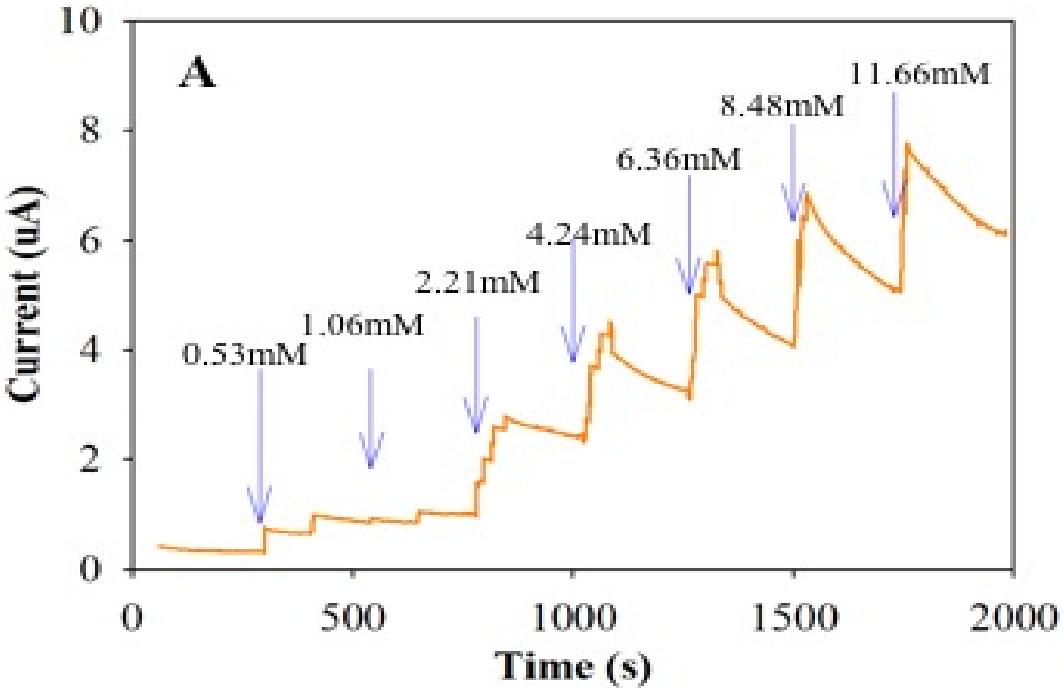

Figure 44. A. Chronoamperometry (CA) Measurements with an Applied Voltage of 0.8V with Addition of Different Concentration of H_2O_2

Since there is no obvious change between chitosan associated with the addition of different concentration H_2O_2 (control experiment), it could be proposed that the enhanced current is due to the electron transfer between Ag NPs and H_2O_2. After averaging the current over 240s for typical concentration of H_2O_2 as shown in Figure 45.

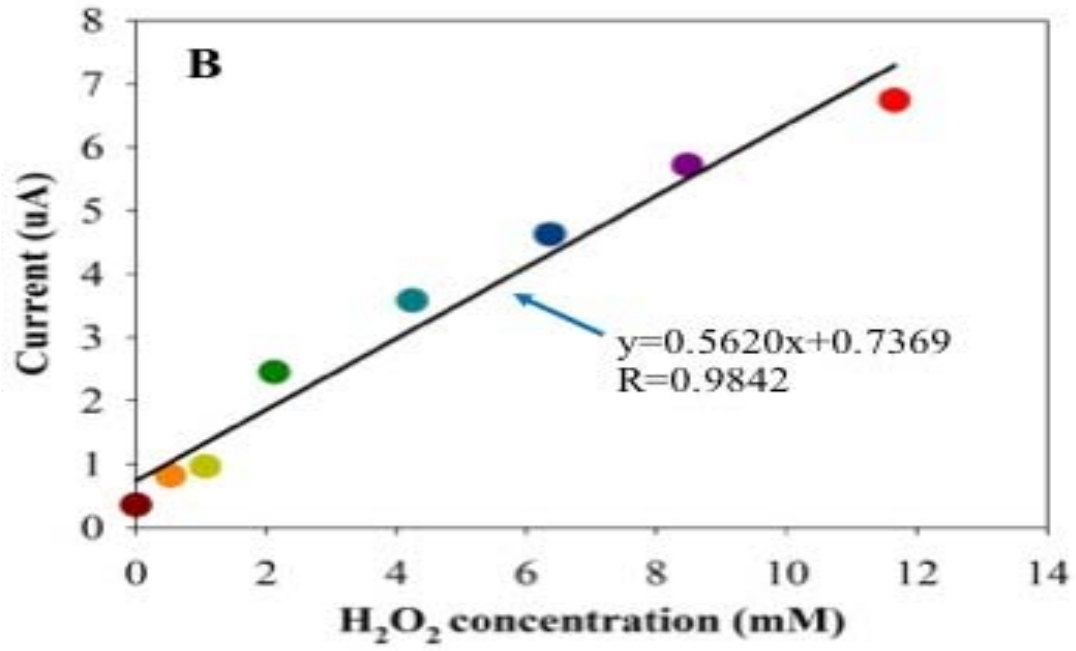

Figure 45. The Calibration Curve for the CA Measurements

The linear relationship between Ag-chitosan film and H_2O_2 concentration from 0.53 mM to 11.66 mM (R=0.9842) with a limit of detection of 94.3 uM estimated by a signal-to-noise of 3 (3*standard error of 5 trials of blank sample/slope). This sensitive response is due to the high conductivity and good electrocatalytic activity of Ag-chitosan film, indicating its potential application as the H_2O_2 sensor.

CHAPTER VI

CONCLUSION

Polymer nanomaterial's in biomedical research has the potential to create a paradigm shift in the healthcare systems of tomorrow by evolving efficient targeting systems for various therapies. This multidisciplinary approach will help to create a unique 'smart polymeric' biomaterial that can mimic the natural occurring materials. The nature itself have established a number of unique materials that combines many inspiring properties such as bio-metallization, miniaturization, hierarchical organization and unique mechanical properties and show various functions from the micro to nanoscale level of organization. In this work, I analyzed and understood the insect cuticle composition and alignment to modern composite polymeric materials, however, the major difference is that within the insect cuticle the resin, i.e. the proteins/lipid matrix, actively controls and organize the fibrous component and thereby actively change and control the mechanical and physical properties of the materials. In essence, insect cuticles are a quintessential biological smart composite material. By understanding the process of cuticle formation and the interaction between specific cuticle proteins and chitin, I am able to develop smart resins that can organize or reorganize nanofiber matrixes in other systems, however this has been problematic due to the issues with the the characterization of nanoscale

chitin organization within the cuticle. To overcome the limitations, I have developed a simple technique to extract chitin form insect cuticles like cicada that enables the characterization of nanoscale chitin fiber organization within the cuticle of insects and arthropods using SEM. I have shown that the chitin purified in this manner maintains its chemical integrity while preserving important spatial and positional information regarding the nanoscale organization and structure of chitin nanofibers.

Moving into the technological aspects, I have successfully fabricated and replicated the bioinspired nanocones that DD cicadas possess. The chitin scaffold of BII wing is used as a substrate and without destroying its innate structure by following our previous *insitu* protocol as mention. The PS colloidal beads templates were assembled orderly onto prepared BII wings forming a monolayer. The chitin scaffold extracted from BII is used as a substrate to mask the polystyrene nanobeads and etched to form chitin biomemitic-nanocones that is similar to DD cicada wings. The mimicked cones are around 200 -300 nm in size which resembles the size of DD wings. The internal and structural morphology of mimicked BNC's with the beads onto and etched wings are shown and cells studies were carried to know the biocompatibility of these BNC's.

Further, the bio-metallization process on the chitin/chitosan were performed and mimicked based on how the nature does. The chitin/chitosan polymers have this unique property of bio-metallizing various metal precursors and the investigation of formation of Ag nanoparticles onto this surface and synthesizing the Ag nanoparticles and Ag nanowires *in-situ* by understanding its mechanism of formation. The samples were characterized and investigated using various analytical techniques to understand the structural

functionality; morphology of the polymer material and synthesized AgNPs and AgNWs and further the bio-metallized chitin/chitosan polymer is being analyzed for potential bio-sensing application.

REFERENCES

1. Rakkiyappan, C., et al., *Nanomaterials: Tissue Regeneration*, in *Encyclopedia of Biomedical Polymers and Polymeric Biomaterials*. 2015, Taylor & Francis. p. 5379-5392.
2. He, X., et al., *An Electrically and Mechanically Autonomic Self-healing Hybrid Hydrogel with Tough and Thermoplastic Properties.* ACS Appl Mater Interfaces, 2017.
3. Kretlow, J.D. and A.G. Mikos, *Review: mineralization of synthetic polymer scaffolds for bone tissue engineering.* Tissue Eng, 2007. **13**(5): p. 927-38.
4. Li, Y., Y. Xiao, and C. Liu, *The Horizon of Materiobiology: A Perspective on Material-Guided Cell Behaviors and Tissue Engineering.* Chem Rev, 2017. **117**(5): p. 4376-4421.
5. Chen, P.-Y., et al., *Structure and mechanical properties of selected biological materials.* Journal of the Mechanical Behavior of Biomedical Materials, 2008. **1**(3): p. 208-226.
6. Meyers, M.A., J. McKittrick, and P.-Y. Chen, *Structural biological materials: critical mechanics-materials connections.* science, 2013. **339**(6121): p. 773-779.
7. Lomakin, J., et al., *Mechanical properties of the beetle elytron, a biological composite material.* Biomacromolecules, 2010. **12**(2): p. 321-335.
8. Vincent, J.F., *Arthropod cuticle: a natural composite shell system.* Composites Part A: Applied Science and Manufacturing, 2002. **33**(10): p. 1311-1315.
9. Chen, P.-Y., et al., *Structure and mechanical properties of crab exoskeletons.* Acta Biomaterialia, 2008. **4**(3): p. 587-596.
10. Mayer, G., *Rigid biological systems as models for synthetic composites.* Science, 2005. **310**(5751): p. 1144-1147.
11. Munch, E., et al., *Tough, bio-inspired hybrid materials.* Science, 2008. **322**(5907): p. 1516-1520.
12. Studart, A.R., *Towards High□Performance Bioinspired Composites.* Advanced Materials, 2012. **24**(37): p. 5024-5044.
13. Khoushab, F. and M. Yamabhai, *Chitin research revisited.* Marine drugs, 2010. **8**(7): p. 1988-2012.
14. Jayakumar, R., et al., *Biomedical applications of chitin and chitosan based nanomaterials—A short review.* Carbohydrate Polymers, 2010. **82**(2): p. 227-232.
15. Andersen, S.O., *Regional differences in degree of resilin cross-linking in the desert locust, Schistocerca gregaria.* Insect Biochem Mol Biol, 2004. **34**(5): p. 459-66.
16. Beament, J.W., *The water relations of insect cuticle.* Biol Rev Camb Philos Soc, 1961. **36**: p. 281-320.

17. Galbreath, R.A., *Water balance across the cuticle of a soil insect.* J Exp Biol, 1975. **62**(1): p. 115-20.
18. Neumann, D. and D. Woermann, *Physical conditions for trapping air by a microtrichia-covered insect cuticle during temporary submersion.* Naturwissenschaften, 2009. **96**(8): p. 933-41.
19. Vincent, J.F. and U.G. Wegst, *Design and mechanical properties of insect cuticle.* Arthropod Struct Dev, 2004. **33**(3): p. 187-99.
20. Willis, J.H. and S. Muthukrishnan, *Insect Cuticle. Foreword.* Insect Biochem Mol Biol, 2010. **40**(3): p. 165.
21. Wigglesworth, V.B., *The insect cuticle.* Biol Rev Camb Philos Soc, 1948. **23**(4): p. 408-51.
22. Muller, M., et al., *Micromechanical properties of consecutive layers in specialized insect cuticle: the gula of Pachnoda marginata (Coleoptera, Scarabaeidae) and the infrared sensilla of Melanophila acuminata (Coleoptera, Buprestidae).* J Exp Biol, 2008. **211**(Pt 16): p. 2576-83.
23. Brzozowska, A.M., et al., *Biomimicking micropatterned surfaces and their effect on marine biofouling.* Langmuir, 2014. **30**(30): p. 9165-9175.
24. Hamodrakas, S.J., J.H. Willis, and V.A. Iconomidou, *A structural model of the chitin-binding domain of cuticle proteins.* Insect Biochem Mol Biol, 2002. **32**(11): p. 1577-83.
25. Klocke, D. and H. Schmitz, *Water as a major modulator of the mechanical properties of insect cuticle.* Acta Biomater, 2011. **7**(7): p. 2935-2942.
26. Rolandi, M. and R. Rolandi, *Self-assembled chitin nanofibers and applications.* Advances in colloid and interface science, 2014. **207**: p. 216-222.
27. Devenport, M., H. Fujioka, and M. Jacobs-Lorena, *Storage and secretion of the peritrophic matrix protein Ag-Aper1 and trypsin in the midgut of Anopheles gambiae.* Insect Mol Biol, 2004. **13**(4): p. 349-58.
28. Wang, P. and R.R. Granados, *Molecular structure of the peritrophic membrane (PM): identification of potential PM target sites for insect control.* Arch Insect Biochem Physiol, 2001. **47**(2): p. 110-8.
29. Campbell, P.M., et al., *Proteomic analysis of the peritrophic matrix from the gut of the caterpillar, Helicoverpa armigera.* Insect Biochem Mol Biol, 2008. **38**(10): p. 950-8.
30. Muzzarelli, R. and C. Muzzarelli, *Chitosan chemistry: Relevance to the biomedical sciences*, in *Polysaccharides I*. 2005, Springer. p. 151-209.
31. Vincent, J.F. and U.G. Wegst, *Design and mechanical properties of insect cuticle.* Arthropod Structure & Development, 2004. **33**(3): p. 187-199.
32. Rinaudo, M., *Chitin and chitosan: properties and applications.* Progress in polymer science, 2006. **31**(7): p. 603-632.
33. Jin, J., et al., *A Biomimetic Composite from Solution Self□Assembly of Chitin Nanofibers in a Silk Fibroin Matrix.* Advanced Materials, 2013. **25**(32): p. 4482-4487.

34. Fernandez, J.G. and D.E. Ingber, *Unexpected strength and toughness in chitosan□fibroin laminates inspired by insect cuticle.* Advanced materials, 2012. **24**(4): p. 480-484.
35. Jayakumar, R., et al., *Novel chitin and chitosan nanofibers in biomedical applications.* Biotechnology advances, 2010. **28**(1): p. 142-150.
36. Desai, K., et al., *Nanofibrous chitosan non-wovens for filtration applications.* Polymer, 2009. **50**(15): p. 3661-3669.
37. Huang, X.-J., D. Ge, and Z.-K. Xu, *Preparation and characterization of stable chitosan nanofibrous membrane for lipase immobilization.* European Polymer Journal, 2007. **43**(9): p. 3710-3718.
38. Noh, H.K., et al., *Electrospinning of chitin nanofibers: degradation behavior and cellular response to normal human keratinocytes and fibroblasts.* Biomaterials, 2006. **27**(21): p. 3934-3944.
39. Jiang, H., et al., *Preparation and characterization of ibuprofen-loaded poly (lactide-co-glycolide)/poly (ethylene glycol)-g-chitosan electrospun membranes.* Journal of Biomaterials Science, Polymer Edition, 2004. **15**(3): p. 279-296.
40. Zhang, K., et al., *Solid-state spectroscopic characterization of α-chitins deacetylated in homogeneous solutions.* The journal of physical chemistry B, 2012. **116**(15): p. 4584-4592.
41. Sadasivam, M., et al., *Self-assembled liposomal nanoparticles in photodynamic therapy.* Eur J Nanomed, 2013. **5**(3).
42. Castelletto, V., et al., *Self-Assembly and Anti-Amyloid Cytotoxicity Activity of Amyloid beta Peptide Derivatives.* Sci Rep, 2017. **7**: p. 43637.
43. Hwang, S., E. Kim, and J. Kwak, *Electrochemical detection of DNA hybridization using biometallization.* Anal Chem, 2005. **77**(2): p. 579-84.
44. Guo, P., *RNA nanotechnology: engineering, assembly and applications in detection, gene delivery and therapy.* J Nanosci Nanotechnol, 2005. **5**(12): p. 1964-82.
45. Kurland, N.E., et al., *Self-assembly mechanisms of silk protein nanostructures on two-dimensional surfaces.* Soft Matter, 2012. **8**(18): p. 4952-4959.
46. Chen, Y. and G. Liang, *Enzymatic self-assembly of nanostructures for theranostics.* Theranostics, 2012. **2**(2): p. 139-47.
47. Blin, J.L. and M. Imperor-Clerc, *Mechanism of self-assembly in the synthesis of silica mesoporous materials: in situ studies by X-ray and neutron scattering.* Chem Soc Rev, 2012.
48. Lee, W., et al., *Dynamic self-assembly and control of microfluidic particle crystals.* Proc Natl Acad Sci U S A, 2010. **107**(52): p. 22413-8.
49. Gooding, J.J., et al., *Self-Assembled Monolayers into the 21st Century: Recent Advances and Applications.* Electroanalysis, 2003. **15**(2): p. 81-96.
50. Silva, J.M., et al., *Tuning cell adhesive properties via layer-by-layer assembly of chitosan and alginate.* Acta Biomater, 2017. **51**: p. 279-293.

51. Senaratne, W., L. Andruzzi, and C.K. Ober, *Self-assembled monolayers and polymer brushes in biotechnology: current applications and future perspectives.* Biomacromolecules, 2005. **6**(5): p. 2427-48.
52. Tang, Z., et al., *Biomedical Applications of Layer-by-Layer Assembly: From Biomimetics to Tissue Engineering.* Advanced Materials, 2006. **18**(24): p. 3203-3224.
53. Iler, R.K., *Multilayers of colloidal particles.* Journal of Colloid and Interface Science, 1966. **21**(6): p. 569-594.
54. Decher, G., J.D. Hong, and J. Schmitt, *Buildup of ultrathin multilayer films by a self-assembly process: III. Consecutively alternating adsorption of anionic and cationic polyelectrolytes on charged surfaces.* Thin Solid Films, 1992. **210,Äì211, Part 2**(0): p. 831-835.
55. Lu, Y., et al., *pH-Induced antireflection coatings derived from hydrogen-bonding-directed multilayer films.* Langmuir, 2010. **26**(22): p. 17749-55.
56. Seo, J., et al., *Covalently bonded layer-by-layer assembly of multifunctional thin films based on activated esters.* Langmuir, 2010. **26**(3): p. 1830-6.
57. Wang, F., et al., *Halogen bonding as a new driving force for layer-by-layer assembly.* Langmuir, 2007. **23**(19): p. 9540-2.
58. Matsusaki, M., et al., *Layer-by-layer assembly through weak interactions and their biomedical applications.* Adv Mater, 2012. **24**(4): p. 454-74.
59. Berry, C.C., et al., *The interaction of human bone marrow cells with nanotopographical features in three dimensional constructs.* J Biomed Mater Res A, 2006. **79**(2): p. 431-9.
60. He, X., Y. Wang, and G. Wu, *Layer-by-layer assembly of type I collagen and chondroitin sulfate on aminolyzed PU for potential cartilage tissue engineering application.* Applied Surface Science, 2012. **258**(24): p. 9918-9925.
61. Gaudiere, F., et al., *Mechano-chemical control of cell behaviour by elastomer templates coated with biomimetic Layer-by-Layer nanofilms.* Soft Matter, 2012. **8**(32): p. 8327-8337.
62. Catros, S., et al., *Layer-by-layer tissue microfabrication supports cell proliferation in vitro and in vivo.* Tissue Eng Part C Methods, 2012. **18**(1): p. 62-70.
63. Engel, E., et al., *Nanotechnology in regenerative medicine: the materials side.* Trends Biotechnol, 2008. **26**(1): p. 39-47.
64. Reheem, A.M.A., M.I.A.A. Maksoud, and A.H. Ashour, *Surface modification and metallization of polycarbonate using low energy ion beam.* Radiation Physics and Chemistry, 2016. **125**: p. 171-175.
65. Vasina, A., et al., *Interaction of polypropylene with sputtered and evaporated au nanolayers.* Polymer Engineering & Science, 2013. **53**(11): p. 2270-2275.
66. Ren, D.F., et al., *[Effect of ceramic thickness and resin cement shades on final color of heat-pressed ceramic veneers].* Zhonghua Kou Qiang Yi Xue Za Zhi, 2017. **52**(2): p. 109-113.

67. Krasowska, M., et al., *Structure-diffusion relationship of polymer membranes with different texture.* Phys Rev E, 2017. **95**(1-1): p. 012155.
68. Moura, D., et al., *Chitosan nanocomposites based on distinct inorganic fillers for biomedical applications.* Sci Technol Adv Mater, 2016. **17**(1): p. 626-643.
69. Martino, S., et al., *Stem cell-biomaterial interactions for regenerative medicine.* Biotechnol Adv, 2012. **30**(1): p. 338-51.
70. Armentano, I., et al., *Novel poly(L-lactide) PLLA/SWNTs nanocomposites for biomedical applications: material characterization and biocompatibility evaluation.* J Biomater Sci Polym Ed, 2011. **22**(4-6): p. 541-56.
71. Wei, J., et al., *New Insight into the Synthesis of Large-Pore Ordered Mesoporous Materials.* J Am Chem Soc, 2017.
72. Zhu, L., et al., *Supramolecular Gel-Templated In Situ Synthesis and Assembly of CdS Quantum Dots Gels.* Nanoscale Res Lett, 2017. **12**(1): p. 30.
73. Zhang, Q., et al., *Facile synthesis, microstructure and photophysical properties of core-shell nanostructured (SiCN)/BN nanocomposites.* Sci Rep, 2017. **7**: p. 39866.
74. Raja, M.A., et al., *Synthesis and evaluation of pH-sensitive, self-assembled chitosan-based nanoparticles as efficient doxorubicin carriers.* J Biomater Appl, 2017: p. 885328216681184.
75. Ahmadizadegan, H., *Surface modification of TiO2 nanoparticles with biodegradable nanocellolose and synthesis of novel polyimide/cellulose/TiO2 membrane.* J Colloid Interface Sci, 2016. **491**: p. 390-400.
76. Tian, Q., et al., *Monodisperse raspberry-like multihollow polymer/Ag nanocomposite microspheres for rapid catalytic degradation of methylene blue.* J Colloid Interface Sci, 2016. **491**: p. 294-304.
77. Macocinschi, D., et al., *Polyurethane–extracellular matrix/silver bionanocomposites for urinary catheters.* Journal of Bioactive and Compatible Polymers, 2015. **30**(1): p. 99-113.
78. Soliman, G.M., *Nanoparticles as safe and effective delivery systems of antifungal agents: Achievements and challenges.* Int J Pharm, 2017.
79. Ndikau, M., et al., *Green Synthesis and Characterization of Silver Nanoparticles Using Citrullus lanatus Fruit Rind Extract.* Int J Anal Chem, 2017. **2017**: p. 8108504.
80. Fievet, F., et al., *Homogeneous and heterogeneous nucleations in the polyol process for the preparation of micron and submicron size metal particles.* Solid State Ionics, 1989. **32–33, Part 1**: p. 198-205.
81. Jayakumar, R., et al., *Biomaterials based on chitin and chitosan in wound dressing applications.* Biotechnol Adv, 2011. **29**(3): p. 322-37.
82. Xia, Y., et al., *Shape-Controlled Synthesis of Metal Nanocrystals: Simple Chemistry Meets Complex Physics?* Angewandte Chemie (International ed. in English), 2009. **48**(1): p. 60-103.

83. Korte, K.E., S.E. Skrabalak, and Y. Xia, *Rapid synthesis of silver nanowires through a CuCl- or CuCl2-mediated polyol process.* Journal of Materials Chemistry, 2008. **18**(4): p. 437-441.
84. TANG, X., et al., *Roles of Chloride Anions in the Shape Evolution of Anisotropic Silver Nanostructures in Poly(vinylpyrrolidone) (PVP)-Assisted Polyol Process*. Vol. 82. 2009, Tokyo, JAPON: Chemical Society of Japan. 9.
85. Calderon-Jimenez, B., et al., *Silver Nanoparticles: Technological Advances, Societal Impacts, and Metrological Challenges.* Front Chem, 2017. **5**: p. 6.
86. Venkatesham, M., et al., *A novel green one-step synthesis of silver nanoparticles using chitosan: catalytic activity and antimicrobial studies.* Applied Nanoscience, 2014. **4**(1): p. 113-119.
87. Logaranjan, K., et al., *Shape- and Size-Controlled Synthesis of Silver Nanoparticles Using Aloe vera Plant Extract and Their Antimicrobial Activity.* Nanoscale Res Lett, 2016. **11**(1): p. 520.
88. Won, S., et al., *Co-operative transitions of responsive-polymer coated gold nanoparticles; precision tuning and direct evidence for co-operative aggregation.* J Mater Chem B Mater Biol Med, 2016. **4**(34): p. 5673-5682.
89. Jendrzej, S., et al., *How Size Determines the Value of Gold - Economic Aspects of Wet Chemical and Laser-Based Metal Colloid Synthesis.* Chemphyschem, 2017.
90. Pena-Gonzalez, C.E., et al., *Gold nanoparticles stabilized by cationic carbosilane dendrons: synthesis and biological properties.* Dalton Trans, 2017.
91. Burrows, N.D., et al., *Understanding the Seed-Mediated Growth of Gold Nanorods through a Fractional Factorial Design of Experiments.* Langmuir, 2017. **33**(8): p. 1891-1907.
92. Jana, N.R., L. Gearheart, and C.J. Murphy, *Wet chemical synthesis of silver nanorods and nanowires of controllable aspect ratio.* Chemical Communications, 2001(7): p. 617-618.
93. Pietrobon, B., M. McEachran, and V. Kitaev, *Synthesis of size-controlled faceted pentagonal silver nanorods with tunable plasmonic properties and self-assembly of these nanorods.* ACS Nano, 2009. **3**(1): p. 21-6.
94. Stamplecoskie, K.G. and J.C. Scaiano, *Light emitting diode irradiation can control the morphology and optical properties of silver nanoparticles.* J Am Chem Soc, 2010. **132**(6): p. 1825-7.
95. Liu, Z., et al., *Size-controlled synthesis and growth mechanism of monodisperse tellurium nanorods by a surfactant-assisted method.* Langmuir, 2004. **20**(1): p. 214-8.
96. Kereselidze, Z., et al., *Gold nanostar synthesis with a silver seed mediated growth method.* J Vis Exp, 2012(59).
97. Niu, K., et al., *Chelating-Template-Assisted in Situ Encapsulation of Zinc Ferrite Inside Silica Mesopores for Enhanced Gas-Sensing Characteristics.* ACS Appl Mater Interfaces, 2016. **8**(37): p. 24682-91.

98. Niu, K., et al., *Fabrication and photoluminescent properties of ZnO/mesoporous silica composites templated by a chelating surfactant.* Langmuir, 2011. **27**(22): p. 13820-7.
99. Niu, K., et al., *Chelating template-induced encapsulation of NiO cluster in mesoporous silica via anionic surfactant-templated route.* J Colloid Interface Sci, 2011. **362**(1): p. 74-80.
100. Dorozhkin, S., *Nanodimensional and Nanocrystalline Apatites and Other Calcium Orthophosphates in Biomedical Engineering, Biology and Medicine.* Materials, 2009. **2**(4): p. 1975-2045.
101. Wopenka, B. and J.D. Pasteris, *A mineralogical perspective on the apatite in bone.* Materials Science and Engineering: C, 2005. **25**(2): p. 131-143.
102. Kay, S., et al., *Nanostructured polymer/nanophase ceramic composites enhance osteoblast and chondrocyte adhesion.* Tissue Eng, 2002. **8**(5): p. 753-61.
103. Zhou, H. and J. Lee, *Nanoscale hydroxyapatite particles for bone tissue engineering.* Acta Biomater, 2011. **7**(7): p. 2769-81.
104. Redey, S.A., et al., *Behavior of human osteoblastic cells on stoichiometric hydroxyapatite and type A carbonate apatite: role of surface energy.* J Biomed Mater Res, 2000. **50**(3): p. 353-64.
105. Dvir, T., et al., *Nanotechnological strategies for engineering complex tissues.* Nat Nanotechnol, 2011. **6**(1): p. 13-22.
106. Wei, J. and Y. Li, *Tissue engineering scaffold material of nano-apatite crystals and polyamide composite.* European Polymer Journal, 2004. **40**(3): p. 509-515.
107. Zhang, P., et al., *In vivo mineralization and osteogenesis of nanocomposite scaffold of poly(lactide-co-glycolide) and hydroxyapatite surface-grafted with poly(L-lactide).* Biomaterials, 2009. **30**(1): p. 58-70.
108. Ma, P.X., *Biomimetic materials for tissue engineering.* Adv Drug Deliv Rev, 2008. **60**(2): p. 184-98.
109. Verma, S., A.J. Domb, and N. Kumar, *Nanomaterials for regenerative medicine.* Nanomedicine (Lond), 2011. **6**(1): p. 157-81.
110. Gloria, A., R. De Santis, and L. Ambrosio, *Polymer-based composite scaffolds for tissue engineering.* J Appl Biomater Biomech, 2010. **8**(2): p. 57-67.
111. Jagur□Grodzinski, J., *Polymers for tissue engineering, medical devices, and regenerative medicine. Concise general review of recent studies.* Polymers for advanced technologies, 2006. **17**(6): p. 395-418.
112. Mistry, A.S., A.G. Mikos, and J.A. Jansen, *Degradation and biocompatibility of a poly(propylene fumarate)-based/alumoxane nanocomposite for bone tissue engineering.* J Biomed Mater Res A, 2007. **83**(4): p. 940-53.
113. Mistry, A.S., et al., *In vivo bone biocompatibility and degradation of porous fumarate-based polymer/alumoxane nanocomposites for bone tissue engineering.* J Biomed Mater Res A, 2010. **92**(2): p. 451-62.
114. Mistry, A.S., et al., *Fabrication and in vitro degradation of porous fumarate-based polymer/alumoxane nanocomposite scaffolds for bone tissue engineering.* J Biomed Mater Res A, 2009. **89**(1): p. 68-79.

115. Derakhshan, A.A. and L. Rajabi, *ChemInform Abstract: Applications of Carboxylate-Alumoxane Nanostructures.* ChemInform, 2012. **43**(35): p. no-no.
116. Delabarde, C., et al., *Biodegradable polylactide/hydroxyapatite nanocomposite foam scaffolds for bone tissue engineering applications.* J Mater Sci Mater Med, 2012. **23**(6): p. 1371-85.
117. Poursamar, S.A., M. Azami, and M. Mozafari, *Controllable synthesis and characterization of porous polyvinyl alcohol/hydroxyapatite nanocomposite scaffolds via an in situ colloidal technique.* Colloids Surf B Biointerfaces, 2011. **84**(2): p. 310-6.
118. Eosoly, S., et al., *Selective laser sintering of hydroxyapatite/poly-epsilon-caprolactone scaffolds.* Acta Biomater, 2010. **6**(7): p. 2511-7.
119. Mondrinos, M.J., et al., *Porogen-based solid freeform fabrication of polycaprolactone-calcium phosphate scaffolds for tissue engineering.* Biomaterials, 2006. **27**(25): p. 4399-408.
120. McCullen, S.D., et al., *Electrospun composite poly(L-lactic acid)/tricalcium phosphate scaffolds induce proliferation and osteogenic differentiation of human adipose-derived stem cells.* Biomed Mater, 2009. **4**(3): p. 035002.
121. Pitukmanorom, P., T.-H. Yong, and J.Y. Ying, *Tunable Release of Proteins with Polymer–Inorganic Nanocomposite Microspheres.* Advanced Materials, 2008. **20**(18): p. 3504-3509.
122. Pek, Y.S., A.C. Wan, and J.Y. Ying, *The effect of matrix stiffness on mesenchymal stem cell differentiation in a 3D thixotropic gel.* Biomaterials, 2010. **31**(3): p. 385-91.
123. Calandrelli, L., et al., *Development and performance analysis of PCL/silica nanocomposites for bone regeneration.* J Mater Sci Mater Med, 2010. **21**(11): p. 2923-36.
124. Yan, S., et al., *Apatite-forming ability of bioactive poly(l-lactic acid)/grafted silica nanocomposites in simulated body fluid.* Colloids Surf B Biointerfaces, 2011. **86**(1): p. 218-24.
125. Gaharwar, A.K., et al., *Assessment of using laponite cross-linked poly(ethylene oxide) for controlled cell adhesion and mineralization.* Acta Biomater, 2011. **7**(2): p. 568-77.
126. Gaharwar, A.K., et al., *Transparent, elastomeric and tough hydrogels from poly(ethylene glycol) and silicate nanoparticles.* Acta Biomater, 2011. **7**(12): p. 4139-48.
127. Dou, Y., C. Wu, and J. Chang, *Preparation, mechanical property and cytocompatibility of poly(l-lactic acid)/calcium silicate nanocomposites with controllable distribution of calcium silicate nanowires.* Acta Biomater, 2012. **8**(11): p. 4139-50.
128. Jose, M.V., et al., *Aligned PLGA/HA nanofibrous nanocomposite scaffolds for bone tissue engineering.* Acta Biomater, 2009. **5**(1): p. 305-15.
129. Gee, A.O., et al., *Fabrication and evaluation of biomimetic-synthetic nanofibrous composites for soft tissue regeneration.* Cell Tissue Res, 2012. **347**(3): p. 803-13.

130. Lee, J.Y., et al., *Polypyrrole-coated electrospun PLGA nanofibers for neural tissue applications.* Biomaterials, 2009. **30**(26): p. 4325-35.
131. Kuo, Y.C. and C.F. Yeh, *Effect of surface-modified collagen on the adhesion, biocompatibility and differentiation of bone marrow stromal cells in poly(lactide-co-glycolide)/chitosan scaffolds.* Colloids Surf B Biointerfaces, 2011. **82**(2): p. 624-31.
132. Shen, H., et al., *Ciliary neurotrophic factor-coated polylactic-polyglycolic acid chitosan nerve conduit promotes peripheral nerve regeneration in canine tibial nerve defect repair.* J Biomed Mater Res B Appl Biomater, 2010. **95**(1): p. 161-70.
133. Han, J., et al., *Co-electrospun blends of PLGA, gelatin, and elastin as potential nonthrombogenic scaffolds for vascular tissue engineering.* Biomacromolecules, 2011. **12**(2): p. 399-408.
134. Koepsell, L., et al., *Electrospun nanofibrous polycaprolactone scaffolds for tissue engineering of annulus fibrosus.* Macromol Biosci, 2011. **11**(3): p. 391-9.
135. Ghasemi-Mobarakeh, L., et al., *Electrospun poly(epsilon-caprolactone)/gelatin nanofibrous scaffolds for nerve tissue engineering.* Biomaterials, 2008. **29**(34): p. 4532-9.
136. Jin, G., M.P. Prabhakaran, and S. Ramakrishna, *Stem cell differentiation to epidermal lineages on electrospun nanofibrous substrates for skin tissue engineering.* Acta Biomater, 2011. **7**(8): p. 3113-22.
137. Zhao, Y., et al., *Nanofibrous scaffold from self-assembly of beta-sheet peptides containing phenylalanine for controlled release.* J Control Release, 2010. **142**(3): p. 354-60.
138. Guo, J., et al., *Self-assembling peptide nanofiber scaffold promotes the reconstruction of acutely injured brain.* Nanomedicine, 2009. **5**(3): p. 345-51.
139. Guo, J., et al., *Reknitting the injured spinal cord by self-assembling peptide nanofiber scaffold.* Nanomedicine, 2007. **3**(4): p. 311-21.
140. Hamada, K., et al., *Spatial distribution of mineralized bone matrix produced by marrow mesenchymal stem cells in self-assembling peptide hydrogel scaffold.* J Biomed Mater Res A, 2008. **84**(1): p. 128-36.
141. Zhang, F., et al., *Designer self-assembling peptide scaffold stimulates pre-osteoblast attachment, spreading and proliferation.* J Mater Sci Mater Med, 2009. **20**(7): p. 1475-81.
142. Sargeant, T.D., et al., *Mineralization of peptide amphiphile nanofibers and its effect on the differentiation of human mesenchymal stem cells.* Acta Biomater, 2012. **8**(7): p. 2456-65.
143. Sargeant, T.D., et al., *Hybrid bone implants: self-assembly of peptide amphiphile nanofibers within porous titanium.* Biomaterials, 2008. **29**(2): p. 161-71.
144. Ghanaati, S., et al., *Dynamic in vivo biocompatibility of angiogenic peptide amphiphile nanofibers.* Biomaterials, 2009. **30**(31): p. 6202-12.

145. Zhao, J., et al., *Fabrication and in vivo osteogenesis of biomimetic poly(propylene carbonate) scaffold with nanofibrous chitosan network in macropores for bone tissue engineering.* J Mater Sci Mater Med, 2012. **23**(2): p. 517-25.
146. Sun, C., et al., *Development of channeled nanofibrous scaffolds for oriented tissue engineering.* Macromol Biosci, 2012. **12**(6): p. 761-9.
147. Locke, M., *Pore Canals and Related Structures in Insect Cuticle.* Journal of Biophysical and Biochemical Cytology, 1961. **10**(4): p. 589-&.
148. Kaya, M., T. Baran, and M. Karaarslan, *A new method for fast chitin extraction from shells of crab, crayfish and shrimp.* Nat Prod Res, 2015. **29**(15): p. 1477-80.
149. Kaur, S. and G.S. Dhillon, *Recent trends in biological extraction of chitin from marine shell wastes: a review.* Crit Rev Biotechnol, 2015. **35**(1): p. 44-61.
150. Kaur, S. and G.S. Dhillon, *The versatile biopolymer chitosan: potential sources, evaluation of extraction methods and applications.* Crit Rev Microbiol, 2014. **40**(2): p. 155-75.
151. Ca´rdenas, G., Cabrera,Gustavo, Taboada, Edelio, Miranda, S. Patricia, *Chitin Characterization by SEM, FTIR, XRD, and 13C Cross Polarization/Mass Angle Spinning NMR.* Journal of Applied Polymer Science, 2004. **93**: p. 1876-1885.
152. Sun, M., et al., *Wetting properties on nanostructured surfaces of cicada wings.* Journal of Experimental Biology, 2009. **212**(19): p. 3148-55.
153. Ivanova, E.P., et al., *Natural bactericidal surfaces: mechanical rupture of Pseudomonas aeruginosa cells by cicada wings.* Small, 2012. **8**(16): p. 2489-94.
154. Nowlin, K., et al., *Adhesion-dependent rupturing of Saccharomyces cerevisiae on biological antimicrobial nanostructured surfaces.* J R Soc Interface, 2015. **12**(102): p. 20140999.
155. Boseman, A., et al., *Ultrastructural analysis of wild type and mutant Drosophila melanogaster using helium ion microscopy.* Micron, 2013. **51**: p. 26-35.
156. Watson, G.S., B.W. Cribb, and J.A. Watson, *How micro/nanoarchitecture facilitates anti-wetting: an elegant hierarchical design on the termite wing.* Acs Nano, 2010. **4**(1): p. 129-36.
157. Watson, J.A., et al., *A Dual Layer Hair Array of the Brown Lacewing: Repelling Water at Different Length Scales.* Biophys J, 2011. **100**(4): p. 1149-1155.
158. Wisdom, K.M., et al., *Self-cleaning of superhydrophobic surfaces by self-propelled jumping condensate.* Proc Natl Acad Sci U S A, 2013. **110**(20): p. 7992-7.
159. Hasan, J., et al., *Selective bactericidal activity of nanopatterned superhydrophobic cicada Psaltoda claripennis wing surfaces.* Appl Microbiol Biotechnol, 2013. **97**(20): p. 9257-62.
160. Park, K.C., et al., *Nanotextured Silica Surfaces with Robust Superhydrophobicity and Omnidirectional Broadband Supertransmissivity.* Acs Nano, 2012. **6**(5): p. 3789-3799.
161. Sun, M., et al., *A study of the anti-reflection efficiency of natural nano-arrays of varying sizes.* Bioinspir Biomim, 2011. **6**(2): p. 026003.

162. Young, D. and H. Bennet-Clark, *The role of the tymbal in cicada sound production.* J Exp Biol, 1995. **198**(Pt 4): p. 1001-20.
163. Wolfgang, W.J., D. Fristrom, and J.W. Fristrom, *An assembly zone antigen of the insect cuticle.* Tissue Cell, 1987. **19**(6): p. 827-38.
164. Yoon, C.S., K. Hirosawa, and E. Suzuki, *Corneal lens secretion in newly emerged Drosophila melanogaster examined by electron microscope autoradiography.* J Electron Microsc (Tokyo), 1997. **46**(3): p. 243-6.
165. Gangishetti, U., et al., *Effects of benzoylphenylurea on chitin synthesis and orientation in the cuticle of the Drosophila larva.* Eur J Cell Biol, 2009. **88**(3): p. 167-80.
166. Neville, A.C., D.A. Parry, and J. Woodhead-Galloway, *The chitin crystallite in arthropod cuticle.* J Cell Sci, 1976. **21**(1): p. 73-82.
167. Charles, J.P., *The regulation of expression of insect cuticle protein genes.* Insect Biochem Mol Biol, 2010. **40**(3): p. 205-13.
168. Papandreou, N.C., et al., *A possible structural model of members of the CPF family of cuticular proteins implicating binding to components other than chitin.* J Insect Physiol, 2010. **56**(10): p. 1420-6.
169. Donoughe, S., et al., *Resilin in dragonfly and damselfly wings and its implications for wing flexibility.* J Morphol, 2011.
170. Li, L., et al., *Tunable mechanical stability and deformation response of a resilin-based elastomer.* Biomacromolecules, 2011. **12**(6): p. 2302-10.
171. Appel, E. and S.N. Gorb, *Resilin-bearing wing vein joints in the dragonfly Epiophlebia superstes.* Bioinspir Biomim, 2011. **6**(4): p. 046006.
172. Andersen, S.O., *Studies on resilin-like gene products in insects.* Insect Biochem Mol Biol, 2010. **40**(7): p. 541-51.
173. Charati, M.B., et al., *Hydrophilic elastomeric biomaterials based on resilin-like polypeptides.* Soft Matter, 2009. **5**(18): p. 3412-3416.
174. Iconomidou, V.A., J.H. Willis, and S.J. Hamodrakas, *Unique features of the structural model of 'hard' cuticle proteins: implications for chitin-protein interactions and cross-linking in cuticle.* Insect Biochem Mol Biol, 2005. **35**(6): p. 553-60.
175. Cornman, R.S. and J.H. Willis, *Annotation and analysis of low-complexity protein families of Anopheles gambiae that are associated with cuticle.* Insect Mol Biol, 2009. **18**(5): p. 607-22.
176. Cornman, R.S., et al., *Annotation and analysis of a large cuticular protein family with the R&R Consensus in Anopheles gambiae.* BMC Genomics, 2008. **9**: p. 22.
177. Willis, J.H., *Structural cuticular proteins from arthropods: annotation, nomenclature, and sequence characteristics in the genomics era.* Insect Biochem Mol Biol, 2010. **40**(3): p. 189-204.
178. Hegedus, D., et al., *New insights into peritrophic matrix synthesis, architecture, and function.* Annu Rev Entomol, 2009. **54**: p. 285-302.
179. Chandran, R., et al., *SEM characterization of anatomical variation in chitin organization in insect and arthropod cuticles.* Micron, 2016. **82**: p. 74-85.

180. Nowlin, K., et al., *Adhesion-dependent rupturing of Saccharomyces cerevisiae on biological antimicrobial nanostructured surfaces.* Journal of The Royal Society Interface, 2015. **12**(102): p. 20140999.
181. Zhong, C., et al., *A facile bottom-up route to self-assembled biogenic chitin nanofibers.* Soft Matter, 2010. **6**(21): p. 5298-5301.
182. Rolandi, M. and R. Rolandi, *Self-assembled chitin nanofibers and applications.* Adv Colloid Interface Sci, 2014. **207**: p. 216-22.
183. Severs, N.J., *Freeze-fracture electron microscopy.* Nat Protoc, 2007. **2**(3): p. 547-76.
184. Kamal, T., et al., *Synthesis and catalytic properties of silver nanoparticles supported on porous cellulose acetate sheets and wet-spun fibers.* Carbohydr Polym, 2017. **157**: p. 294-302.
185. Forestier, F., et al., *Effect of nanoparticle-bound ampicillin on the survival of Listeria monocytogenes in mouse peritoneal macrophages.* J Antimicrob Chemother, 1992. **30**(2): p. 173-9.
186. El-Kassas, H.Y. and M.G. Ghobrial, *Biosynthesis of metal nanoparticles using three marine plant species: anti-algal efficiencies against "Oscillatoria simplicissima".* Environ Sci Pollut Res Int, 2017.
187. Leudjo Taka, A., K. Pillay, and X. Yangkou Mbianda, *Nanosponge cyclodextrin polyurethanes and their modification with nanomaterials for the removal of pollutants from waste water: A review.* Carbohydr Polym, 2017. **159**: p. 94-107.
188. Zhao, Y., et al., *Titanium tetrachloride for silver nanoparticle-humic acid composite contaminant removal in coagulation-ultrafiltration hybrid process: floc property and membrane fouling.* Environ Sci Pollut Res Int, 2016.
189. Orza, A., et al., *A nanocomposite of Au-AgI core/shell dimer as a dual-modality contrast agent for x-ray computed tomography and photoacoustic imaging.* Med Phys, 2016. **43**(1): p. 589.
190. Cao, J., D. Zhao, and Q. Mao, *A highly reproducible and sensitive fiber SERS probe fabricated by direct synthesis of closely packed AgNPs on the silanized fiber taper.* Analyst, 2017.
191. Sergiienko, S., et al., *Nanoparticle-nanoparticle vs. nanoparticle-substrate hot spot contributions to the SERS signal: studying Raman labelled monomers, dimers and trimers.* Phys Chem Chem Phys, 2017.
192. Venugopal, A., et al., *Incorporation of silver nanoparticles on the surface of orthodontic microimplants to achieve antimicrobial properties.* Korean J Orthod, 2017. **47**(1): p. 3-10.
193. Gomaa, E.Z., *Silver nanoparticles as an antimicrobial agent: A case study on Staphylococcus aureus and Escherichia coli as models for Gram-positive and Gram-negative bacteria.* J Gen Appl Microbiol, 2017.
194. Singh, R., S. Magesh, and C. Rakkiyappan, *Formation of fenugreek (Trigonella foenum-graecum) extract mediated Ag nanoparticles: mechanism and applications.* Int J Bioeng Sci Technol, 2011. **2**(3): p. 64-73.

195. Singh, R., S. Magesh, and C. Rakkiyappan, *Ginger (Zingiber officinale) root extract: a source of silver nanoparticles and their application.* Int. J. Bio-Eng. Sci. Technol, 2011. **2**(3): p. 75-80.
196. Li, X., et al., *Self-assembled metal colloid films: two approaches for preparing new SERS active substrates.* Langmuir, 2004. **20**(4): p. 1298-304.
197. Yalcinkaya, E.E., et al., *Cellulose nanocrystals as templates for cetyltrimethylammonium bromide mediated synthesis of Ag nanoparticles and their novel use in PLA films.* Carbohydr Polym, 2017. **157**: p. 1557-1567.
198. Siddiq, A.M., et al., *Effect of gemini surfactant (16-6-16) on the synthesis of silver nanoparticles: A facile approach for antibacterial application.* Enzyme Microb Technol, 2016. **95**: p. 118-127.
199. Narayanan, K.B. and S.S. Han, *Highly selective and quantitative colorimetric detection of mercury(II) ions by carrageenan-functionalized Ag/AgCl nanoparticles.* Carbohydr Polym, 2017. **160**: p. 90-96.
200. Tyliszczak, B., A. Drabczyk, and S. Kudlacik, *Comparison of Hydrogels Based on Commercial Chitosan and Beetosan(R) Containing Nanosilver.* Molecules, 2016. **22**(1).
201. Levi-Polyachenko, N., et al., *Chitosan wound dressing with hexagonal silver nanoparticles for hyperthermia and enhanced delivery of small molecules.* Colloids Surf B Biointerfaces, 2016. **142**: p. 315-24.
202. Majidi, M.R., et al., *Synthesis of dendritic silver nanostructures supported by graphene nanosheets and its application for highly sensitive detection of diazepam.* Mater Sci Eng C Mater Biol Appl, 2015. **57**: p. 257-64.
203. Dai, L., et al., *Silver nanoparticles-containing dual-function hydrogels based on a guar gum-sodium borohydride system.* Sci Rep, 2016. **6**: p. 36497.
204. Cao, Y., et al., *Thiolate-Mediated Photoinduced Synthesis of Ultrafine Ag2 S Quantum Dots from Silver Nanoparticles.* Angew Chem Int Ed Engl, 2016. **55**(48): p. 14952-14957.
205. Liu, L., et al., *One-step synthesis of Ag/AgCl/GO composite: A photocatalyst of extraordinary photoactivity and stability.* J Colloid Interface Sci, 2016. **493**: p. 281-287.
206. Kreder, K.J. and A. Manthiram, *Metal nanofoams via a facile microwave-assisted solvothermal process.* Chem Commun (Camb), 2017. **53**(5): p. 865-868.
207. Mishra, S.K. and S. Kannan, *Microwave Synthesis of Chitosan Capped Silver-Dysprosium Bimetallic Nanoparticles: A Potential Nanotheranosis Device.* Langmuir, 2016. **32**(51): p. 13687-13696.
208. Acar Bozkurt, P., *Sonochemical green synthesis of Ag/graphene nanocomposite.* Ultrason Sonochem, 2017. **35**(Pt A): p. 397-404.
209. Kumar, B., et al., *Green synthesis of silver nanoparticles using Andean blackberry fruit extract.* Saudi J Biol Sci, 2017. **24**(1): p. 45-50.
210. Kharat, S.N. and V.D. Mendhulkar, *"Synthesis, characterization and studies on antioxidant activity of silver nanoparticles using Elephantopus scaber leaf extract".* Mater Sci Eng C Mater Biol Appl, 2016. **62**: p. 719-24.

211. Brunner, E., et al., *Chitin-based scaffolds are an integral part of the skeleton of the marine demosponge Ianthella basta.* J Struct Biol, 2009. **168**(3): p. 539-47.
212. Focher, B., et al., *Structural differences between chitin polymorphs and their precipitates from solutions—evidence from CP-MAS 13C-NMR, FT-IR and FT-Raman spectroscopy.* Carbohydrate Polymers, 1992. **17**(2): p. 97-102.
213. Turner, A.P., *Tech.Sight. Biochemistry. Biosensors--sense and sensitivity.* Science, 2000. **290**(5495): p. 1315-7.
214. Clark, L.C., Jr. and C. Lyons, *Electrode systems for continuous monitoring in cardiovascular surgery.* Ann N Y Acad Sci, 1962. **102**: p. 29-45.
215. Hoshino, T., S. Sekiguchi, and H. Muguruma, *Amperometric biosensor based on multilayer containing carbon nanotube, plasma-polymerized film, electron transfer mediator phenothiazine, and glucose dehydrogenase.* Bioelectrochemistry, 2012. **84**: p. 1-5.
216. Kase, Y. and H. Muguruma, *Amperometric glucose biosensor based on mediated electron transfer between immobilized glucose oxidase and plasma-polymerized thin film of dimethylaminomethylferrocene on sputtered gold electrode.* Anal Sci, 2004. **20**(8): p. 1143-6.
217. Iqbal, S.S., et al., *A review of molecular recognition technologies for detection of biological threat agents.* Biosens Bioelectron, 2000. **15**(11-12): p. 549-78.
218. Hinman, S.S. and Q. Cheng, *Bioinspired Assemblies and Plasmonic Interfaces for Electrochemical Biosensing.* J Electroanal Chem (Lausanne), 2016. **781**: p. 136-146.
219. Lan, L., et al., *Recent sadvances in nanomaterial-based biosensors for antibiotics detection.* Biosens Bioelectron, 2017. **91**: p. 504-514.
220. Newman, J.D. and A.P. Turner, *Biosensors: principles and practice.* Essays Biochem, 1992. **27**: p. 147-59.
221. Pearson, J.E., A. Gill, and P. Vadgama, *Analytical aspects of biosensors.* Ann Clin Biochem, 2000. **37 (Pt 2)**: p. 119-45.
222. Habermuller, K., M. Mosbach, and W. Schuhmann, *Electron-transfer mechanisms in amperometric biosensors.* Fresenius J Anal Chem, 2000. **366**(6-7): p. 560-8.